THE UNIVERSITY *of* EDINBURGH

Understanding and predicting global leaf phenology using satellite observations of vegetation

Silvia Caldararu

THE UNIVERSITY
of EDINBURGH

Thesis submitted in fulfilment of the requirements
for the degree of Doctor of Philosophy to the
University of Edinburgh — February 2013

Declaration

I declare that this thesis has been composed solely by myself and that it has not been submitted, either in whole or in part, in any previous application for a degree. Except where otherwise acknowledged, the work presented is entirely my own.

Silvia Caldararu

February 2013

Abstract

Leaf phenology refers to the timing of leaf life cycle events and is essential to our understanding of the earth system as it impacts the terrestrial carbon and water cycles and indirectly global climate through changes in surface roughness and albedo. Traditionally, leaf phenology is described as a response to higher temperatures in spring and lower temperatures in autumn for temperate regions. With the advent of carbon ecosystem models however, we need a better representation of seasonal cycles, one that is able to explain phenology in different areas around the globe, including tropical regions, and has the capacity to predict phenology under future climates. We propose a global phenology model based on the hypothesis that phenology is a strategy through which plants reach optimal carbon assimilation. We fit this 14 parameter model to five years of space borne data of leaf area index using a Bayesian fitting algorithm and we use it to simulate leaf seasonal cycles across the globe. We explain the observed increase in leaf area over the Amazon basin during the dry season through an increase in available direct solar radiation. Seasonal cycles in dry tropical areas are explained by the variation in water availability, while phenology at higher latitudes is driven by changes in temperature and daylength. We explore the hypothesis that phenological traits can be explained at the biome (plant functional group) level and we show that some characteristics can only be explained at the species level due to local factors such as water and nutrient availability. We anticipate that our work

can be incorporated into larger earth system models and used to predict future phenological patterns.

Acknowledgements

First of all I would like to thank my two supervisors, Paul Palmer and Drew Purves, for all the support they gave me and for everything they taught me. Also thank you to Matthew Smith for giving me the opportunity to do new and exciting science right to the end of my PhD. A big thank you to everyone in the Earth Observation and Modelling Group (affectionately known as the Palmer Group) at the University of Edinburgh and the Computational Science group at Microsoft Research who have been of great help to my work and who have also become great friends.

I need to thank Microsoft Research for providing the funding without which all our great scientific ideas can never become real.

A big thank you to my family for supporting me in all my career decisions so far, I'm sure having two scientists parents had something to do with where I am today. Also thank you to my little brother for well, being. I'd like to take this opportunity to ask to be put in his thesis acknowledgements when he gets to this stage. You know I'm the first one to get here just because I have the age advantage! Thank you to Richard Nair for letting me talk through all my scientific ideas when I needed it. I of course need to mention everyone in the Crew Attic for the great working (or not working?) environment. In particular, thank you to Dr. A. Anthony Bloom for always being ready to argue about wacky

scientific ideas. Also, together with Stephen Carr, James Howie and Oliver Sus, for showing me that you don't need to be a grown up to do a PhD, all through the rubber band wars of 2009 and other adventures. Thank you to Nancy Burns for showing me how little I really know by repeatedly asking 'simple' questions that I never knew how to answer. Also worth of mention is His Majesty the King of Austria, Dr. Siegfried Gonzi for being a constant reminder that I'm not the weirdest person around.

Contents

List of Tables

List of Figures

Chapter 1

Introduction

1.1 A brief history of phenology

The term phenology refers to the timing of cyclic biological events, such as the date of budburst, flowering or bird migration. Historically, phenological dates have been observed since ancient times, mostly for agricultural purposes and to mark festival dates, such as the date of first cherry blossom in Japan, which is currently the longest phenological record, dating back to the 9th century AD (Aono and Kazui, 2008). Later, more detailed observations were made by individuals as a hobby and we possess long term records of spring dates in Europe, recorded by the same family over several generations, such as the Marsham and White records (White, 1789; Marsham, 1789). In the late 19th century phenology became more focused as a scientific study and the Royal Meteorological Society formed a phenological committee (Clark, 1936), with similar studies taking place elsewhere in Europe (Defila and Clot, 2001). At this time, the existing records were studied more closely and related to meteorological observations, with a view towards scientific understanding (Margary, 1926, 1927).

As the issue of global climate change became more important (IPCC, 2001a) it became obvious that phenology plays an important role in understanding the current and future effects of global warming on terrestrial ecosystems and the carbon cycle through changes in spring and autumn dates and growing season length.

1.2 Leaf phenology and climate change

Spring phenology is believed to be triggered by temperature and the first formal relation was established in 1753 by French physicist Rene de Reaumur (Reaumur, 1753), who stated that the date of leaf budburst is determined by the number of days with a temperature above a certain threshold, a model known as growing degree days which is still widely used today. In relation to the observed and projected climate change and increase in temperature, it has become apparent that temperate phenology will be affected, most likely by an advance in spring budburst (IPCC, 2001b; Sparks and Menzel, 2002). Analyses of the existing phenological records observe an advance of spring by approximately 2 days per decade (Parmesan and Yohe, 2003; Menzel *et al.*, 2006). However, the biological triggers for budburst are more complex than a simple linear relation with spring temperatures. Whilst the simplest phenological models use the degree day parametrisation, variations include chilling requirements and photoperiod (Korner and Basler, 2010). A model that takes into account chilling stipulates that trees require a given number of days with temperatures below a certain threshold before leaf out, in order to prevent any budburst occurring after warm periods in winter (Chuine and Cour, 1999; Hanninen, 1990; Linkosalo, 2000). Such a chilling requirement could lead to a negative effect of warming on spring phenology, as warmer winters can delay budburst (Linkosalo, 2000). Another type of constraint on leafing date is daylength, known as photoperiod, so that leaf out occurs only

after daylength has exceed a given number of hours. Such a constraint would imply that budburst cannot start indefinitely early even when triggered by very high temperatures, as photoperiod has a fixed date (Korner and Basler, 2010). Existing ecosystem models describe vegetation phenology using a combination of these parametrisations, as summarised in Table 1.1.

The change in autumn phenology has been less intensively studied (Sparks and Menzel, 2002) and is thus less clear, as some studies show that leaf senescence is strictly triggered by day length (Keskitalo *et al.*, 2005), while others show that the trigger is related to the lower temperatures in autumn or a combination of the two factors (Hänninen *et al.*, 1990). The second explanation would lead to a later autumn and hence a longer growing season under global warming, as shown by Menzel (2000).

The impact of climate change on leaf phenology is of interest because of more than phenology itself, as the leaf area, which is directly determined by the start of the growing season, is an essential driver for terrestrial carbon assimilation and other biosphere-atmosphere exchanges, as well as a factor in global climate through changes in albedo and surface roughness (Schwartz, 1992; Hogg *et al.*, 2000). Early studies have shown an increase in CO_2 uptake in response to an observed increase in the length of the growing season (Myneni *et al.*, 1997) and further studies have shown a substantial increase in carbon assimilation of 5.9 g Cm^{-2} for each additional day of growing season (Baldocchi and Wilson, 2001). However, the exact response of the terrestrial carbon cycle to a longer growing season is still unclear, as higher temperatures can also affect other ecosystem processes. For example, warmer autumns can lead to higher respiration rates and hence a lower net carbon uptake at the end of the growing season (Piao *et al.*, 2008). This effect could be further heightened by the fact that leaf photosynthetic capacity declines in autumn despite the higher temperatures (Bauerle *et al.*, 2012). Higher temperatures can also affect drought conditions (Kljun *et al.*, 2006), which would

Table 1.1: Phenology parametrisations in existing vegetation models. Adapted from Richardson *et al.* (2013).

Model	Leaf onset	Control on LAI	Leaf offset	Reference
BEPS	Satellite	Satellite	Satellite	Ju *et al.* (2006)
Biome-BGC	GDD and radiation sum	Dynamic C allocation	Daylength and low temperature	Thornton *et al.* (2002)
IBIS	Temperature threshold	GDD and dynamic C	Prescribed	El Maayar *et al.* (2002)
CN-CLASS	C balance	C balance	Daylength and low temperature	Arain *et al.* (2006)
Ecosys	Hours above T threshold	Dynamic C allocation	Hours below T threshold	Grant *et al.* (2009)
JULES	Chilling T dependency	Optimal LAI	Chilling T dependency	Clark *et al.* (2011)
LPJ	GDD	GDD	Leaf longevity	Sitch *et al.* (2003)
ORCHIDEE	GDD and chilling	Dynamic C allocation	Decreasing T and T threshold	Krinner *et al.* (2005)
SiBCASA	Prescribed	Prescribed	Prescribed	Schaefer *et al.* (2008)

imply a lower productivity, and nutrient availability (Richardson *et al.*, 2009), leading to reduced assimilation. Increases in temperature can also affect the maximum leaf area, thus increasing carbon uptake (Jolly *et al.*, 2004).

Understanding the effect rising temperatures might have on ecosystem primary production requires an extension of phenological measurements and models, as the date of budburst is no longer sufficient for understanding large scale carbon uptake. While the concept of start of the growing season is the same, the scale of the observations changes, both spatially, extending from species to the landscape (Morisette *et al.*, 2008) and temporally, as the entire seasonal cycle needs to be monitored. Such phenological observations are focused more on photosynthetic activity (Gu *et al.*, 2003) and can be extended to boreal forests which retain leaves throughout the year but only resume photosynthetic activity in spring, as well as tropical forests which retain both leaves and photosynthetic activity all year.

1.3 Leaf phenology in tropical regions

Traditionally, leaf phenology research concerns itself with temperate deciduous species both because of the location of the first observations and because of the ease of measurement. Species in tropical regions also exhibit leaf seasonality, most commonly related to seasonal changes in precipitation, as this climate is often characterised by a wet and a dry season, where the wet season can be more or less severe depending on location. Tropical phenological behaviour is often not as straightforward as that observed at higher latitudes. While some strictly deciduous species will shed all their leaves during the dry periods, others will keep part or all their leaves (Borchert, 1994). Also, not all individuals of the same species will produce new leaves at the same time, although synchronous flushing is common in drier areas (Lieberman and Lieberman, 1984). Leaf flushing

is not always directly correlated to precipitation, indicating that there is a further trigger behind tropical phenology.

Several studies have observed leaf flushing before the start of the wet season in various areas of the world (e.g. Australia, Williams *et al.* (1997) and Central America, Reich and Borchert (1982)). These studies attribute this phenomenon to a rehydration of the trees immediately after leaf shedding, which provides the necessary water for the production of new leaves. Another hypothesis suggests that this is a strategy meant to protect young leaves from herbivory by the larger insect population in the wet season (Aide, 1992), but this hypothesis does not include an environmental cue for leaf flushing.

As has been recently highlighted in the literature (Myneni *et al.*, 2007; Hutyra *et al.*, 2007), , tropical forests considered evergreen also show leaf seasonality even if not as dramatic as that in other regions. Ground observations of litterfall in these regions show an increase in leaf fall during the dry season (Malhado *et al.*, 2009; Chave *et al.*, 2010) suggesting a water limitation. Remote-sensing (Myneni *et al.*, 2007; Huete *et al.*, 2006) and carbon flux studies (Hutyra *et al.*, 2007) show an increase in leaf area and carbon uptake during the dry season, perhaps in response to an increase in direct light. The seasonality of such wet tropical forests can be complicated even more by the presence of flooded areas, as flooding can act as a stress factor, causing leaf shedding (Schöngart *et al.*, 2002), but this phenomenon is restricted to forests located on the floodplains.

1.4 Phenological measurements

The simplest phenological measurement is the eye-witness observation, often of the first day of budburst or flower (see Section 1.1). Whilst such records provide some information on long term trends, they are often unreliable and hard to

confront with meteorological data. Similar observations of first budburst now exist from botanical gardens and field sites, for one or several species across the globe, in North America (e.g. at Harvard forest (Richardson and OḰeefe, 2009) and Hubbard Brook Experimental Forest (Richardson *et al.*, 2006)) and in Europe through the International Botanical Gardens project, which uses cloned individuals of the same species at various gardens throughout Europe (Menzel, 2000; Chmielewski, 2008), giving a reliable relationship between climate and tree phenology.

Another way to quantify spring response to higher temperatures is by using warming experiments in which plants are artificially exposed to higher temperatures, either for individual plants or at larger plot scales. Pot experiments are often limited to herbaceous species (Beuker, 1994; Sherry *et al.*, 2007). Plot experiments at larger scales can be made using either passive warming through closed- or open-top chambers (Kilpelainen *et al.*, 2006; Walker *et al.*, 2006; Norby *et al.*, 2003; Repo *et al.*, 1996) and night shading (Van Wijk *et al.*, 2004) or active warming through, for example infra-red heaters (Morin *et al.*, 2010). Data from such experiments suffers from certain biases such as unequal day to night warming and unwanted increases in temperature but they nevertheless have the major advantage of a controlled temperature increase on the scale of that predicted for future warming during the experimental period. The majority of these experiments show an advance in spring in response to higher temperatures with a few exceptions which show ambivalent responses (Norby *et al.*, 2003) or no response at all (Jones *et al.*, 1997). The response in autumn senescence dates is more varied, ranging from a later date (Norby *et al.*, 2003) to an early autumn (Kilpelainen *et al.*, 2006) and no observed response (Jones *et al.*, 1997).

However, observations of budburst dates for one species or individual do not offer sufficient information of canopy development. Continuous monitoring can be achieved using optical or radiometric measurements of canopy development at

flux tower sites. The simplest such method is to use digital cameras (Crimmins and Crimmins, 2008; Richardson *et al.*, 2007) which provide information on leaf development. A more quantitative approach is to use vegetation indices based on leaf optical properties and absorbed and reflected photosynthetically active radiation (Moore *et al.*, 1996; Huemmrich *et al.*, 1999) or CO_2 fluxes to determine growing season dates (Gu *et al.*, 2003; Richardson *et al.*, 2010). Such observations do have a very high temporal resolution and are available at a large number of field sites (e.g. the FLUXNET network, Baldocchi *et al.* (2001)), but cannot capture phenological behaviour on regional or global scales (Richardson *et al.*, 2007).

But if the phenological dates are to be incorporated in global studies of the terrestrial carbon cycle, which are often on regional or global scales, what is needed is a much larger, spatially and temporally continuous dataset, which can be obtained by space-borne observations of vegetation.

1.5 Remote sensing of vegetation

Space borne observations of vegetation provide large scale continuous information for phenological studies. Remote sensing data was used as early as the 1970s for atmospheric and meteorological measurements using instruments on board both satellites (Yates, 1970) and aircraft (Hovis *et al.*, 1970), as well as for measuring other environmental variables such as sea surface temperature (Maul and Sidran, 1972) and detection of algal blooms (Strong, 1974). The first satellite instrument to be used for terrestrial vegetation measurements was Landsat 1, launched in 1972, closely followed by Landsat 2 in 1976. The Landsat family of instruments has been used widely for greenness and biomass measurements (Chen and Cihlar, 1996; Goetz and Prince, 1996). The longest standing timeseries of vegetation

indices was derived from the NOAA AVHRR (Advanced Very high Resolution Radiometer) (Goward *et al.*, 1985; Moulin *et al.*, 1997; Myneni *et al.*, 1997; Shabanov *et al.*, 2002). Other satellite platforms that are used for monitoring of vegetation include, but are not limited to, the SPOT (Satellite pour l'Observation de la Terre) VEGETATION, first launched in 1978 followed by another four SPOT satellites with SPOT 6 to be launched in 2012; and the MODIS (Moderate Resolution Imaging Spectroradiometer) on board the Terra and Aqua platforms, launched in 1999 and 2002 respectively. The vegetation index products (see below) that can be obtained from these instruments have a range of temporal and spatial resolutions depending on the particular index and compositing method used; the temporal resolution is generally 10 days to a month while the spatial resolution varies from 30 m to 1° grid cells.

Remote sensing of vegetation is based on the optical properties of leaves, in particular the different absorption in the red (0.6-0.7 μm) and near infrared (0.75-1.35 μm) wavelengths (Tucker, 1979). This difference is caused by the optical properties of chlorophyll, the main photosynthetic pigment, which has its absorption maximum at 0.69 μm. This peak, combined with the lack of absorption in the adjacent near infrared region results in the observed sharp difference (Myneni *et al.*, 1995b). This difference is the basis of various vegetation indices which describe the amount of greenness over a given area. The simplest such indices are the simple ratio (SR) and normalized difference vegetation index (NDVI), which are based on the ratio between the red and near infrared bands. Another widely used index is the enhanced vegetation index (EVI) which includes corrections for atmospheric interference and background soil reflectance (Gao *et al.*, 2000; Liu and Huete, 1995; Kaufman and Tanre, 1992), but this can only be calculated using data from newer instruments (e.g. MODIS) as it requires blue band reflectance (Huete *et al.*, 2002). Less used vegetation measures include indices that have a soil correction factor such as the soil adjusted vegetation

index (Huete, 1988) or the weighted difference vegetation index (Clevers, 1989) or non-linear indices (Pinty and Verstraete, 1992; Jackson, 1983).

Remote sensing of vegetation provides a spatially and temporally continuous record of vegetation, but it nevertheless suffers from a number of error sources. The most important of these is atmospheric interference, as the signal measured by all space borne instruments must necessarily pass through the atmosphere, where radiation in the wavelengths required for vegetation indices can be absorbed or scattered by either clouds or aerosols, leading to retrievals with a much higher uncertainty (Baret and Guyot, 1991; Holben *et al.*, 1986). There are several ways to account for this effect. We can include a correction factor when calculating the vegetation index itself, as is the case with the MODIS EVI and leaf area index products, either using empirical functions or using reflectance in a different band (e.g blue for EVI) (Kaufman and Tanre, 1992). Another way to correct for atmospheric effects is to filter the data and only use cloud free pixels, or pixels with a cloud level lower than a given threshold or to use a smoothing method for the observed time series, smoothing which is often dependent on the specific problem and data set (Reed *et al.*, 1994). One method for doing this is temporal compositing, a technique in which only the best data point in a given period of time are kept (Holben, 1986; Huete *et al.*, 2002). The quality of vegetation indices is also affected by canopy structure through changes in light absorption in the canopy and soil interference, which changes the background reflectance. These effects are often accounted for when calculating the vegetation indices (Justice *et al.*, 1998; Yang *et al.*, 2006). One other factor affecting the quality of remotely sensed data is the presence of snow, which is particularly important in boreal and high altitude regions and can affect the quality of the data by producing unreasonably low values (Beck *et al.*, 2006; Rautiainen *et al.*, 2012). One way to account for these effects is to not use pixels with snow cover. However, snow presence is often hard to identify in forested areas, leading to

further errors (Klein *et al.*, 1998) so that measurements at higher latitudes can often have a poor quality.

While vegetation indices provide relative information on the spatial and temporal variations in vegetation, to obtain further insight into ecosystem functions and to incorporate in ecological models, we need to relate these indices to ecological meaningful variables. The two most commonly used measures of greenness are leaf area index (LAI), the ratio of one sided leaf area to ground area, and the fraction of absorbed photosynthetically active radiation (fAPAR). Both of these have been shown to correlate well with NDVI (Myneni *et al.*, 1995a; Price, 1993) and EVI (Huete *et al.*, 2002). One of the caveats when using NDVI as a measure of leaf area is that it saturates for high LAI values (above 4) such as those observed in moist tropical forests (Asner *et al.*, 2003), an issue which can be partially addressed by using EVI (Huete *et al.*, 1997; Justice *et al.*, 1998). A LAI and fAPAR product was developed using reflectance data from the MODIS instrument, which further improves the determination of LAI by including corrections for soil reflectance and canopy structure (Shabanov *et al.*, 2005; Yang *et al.*, 2006). Other ecosystem measures that can be estimated using vegetation indices include primary productivity and photosynthetic capacity (Sellers *et al.*, 1992; Rahman *et al.*, 2005).

Remotely-sensed vegetation data can be used to study seasonal cycles in both temperate and tropical regions and various methods for determining the start and end of the growing season have been proposed. The simplest method is to specify an arbitrary threshold for the specific vegetation index used as the beginning and end of the vegetated period (Lloyd, 1990; Fischer, 1994) or a threshold based on the ratio between the observed maximum and minimum, a method which is better suited for application across different sites (White *et al.*, 1997). Another method as developed by, for example, Reed *et al.* (1994) and Moulin *et al.* (1997) is to identify the inflection point on a fitted sinusoidal or bell shaped curve.

More recently satellite based data sets have also been used for boreal (Rautiainen *et al.*, 2012) and tropical (Huete *et al.*, 2006; Myneni *et al.*, 2007) systems. (See also Section 1.3). A further step in using remotely sensed data for phenological purposes is to use the data as input for regional and global models that require seasonal vegetation information.

1.6 Models informed by data

As shown above, there is ample evidence that leaf phenology has an important impact on other earth system processes, in particular the global carbon cycle, which is why we need a robust parametrisation of phenological processes. Leaf phenology models were developed as early as the 1700s (Reaumur, 1753) and can include all hypothesised triggers for budburst (see Section 1.2). Such models have necessarily been incorporated into regional and global carbon models to provide information on the start and end of the growing season and consequently the presence or absence or leaves.

An alternative to using a phenology model is to use existing LAI data (or other vegetation indices) to drive the photosynthesis model. Both of these approaches have certain disadvantages. Using existing data as an input provides information on the current phenological behaviour, often at large scales, but lacks any predictive capabilities, especially when confronted with climate change scenarios. On the other hand, using a phenology model would provide information on future changes, but these models are often parametrised based on point measurements often for a single species and increase the uncertainty of the carbon model when applied to larger areas. A third alternative is to use existing phenology data to inform the phenology model and estimate parameters, as used for example by Hanson *et al.* (2004) and Knorr *et al.* (2010).

Informing models with data, a technique known as data assimilation, refers to a family of mathematical procedures intended to optimise given model quantities by minimizing the difference between the model prediction and the data. Data assimilation has been used widely in various areas of environmental science, such as atmospheric science (Daley, 1993.) and hydrology (Beven and Freer, 2001), and more recently to improve ecosystem models and datasets (Canadell *et al.*, 2004; Fox *et al.*, 2009; Friend *et al.*, 2007). A data assimilation system must include a model formulation, a data set and a method to link the two, which is the actual data assimilation procedure. The first step is to formulate a cost function, also known as a likelihood function in some circumstances. Such a function describes the difference between the model and data and includes uncertainties for both quantities. The choice of cost function depends on both model structure and the optimisation algorithm used, as this is the function that will be minimised by the search algorithm (Raupach *et al.*, 2005). The quantities that are optimised by the algorithm can be either model parameter values, which is a particular case of data assimilation known as parameter estimation, or state variables within the model (e.g. carbon pools within ecosystem models) or in some cases prior parameter intervals. The choice of the quantity to be optimised depends on the model structure and the question to be addressed. For simple model formulations, the fitting method used can be as simple as a linear regression, but for more complex models as is often the case with ecological models, we need to choose more powerful search algorithms.

A particular class of search algorithms often used in ecological modelling are Bayesian methods, in particular the Markov Chain Monte Carlo (MCMC) algorithms. Bayesian inference has the advantage that it allows the user to include any prior information they might have on parameters and processes, an advantage which is of particular importance in ecosystem models, where there is always some prior knowledge and realistic parameter ranges. The MCMC

methods are a group of methods in which all iterations form a chain so that any one iteration is only dependent on the previous one in the chain. The first such algorithm, the Metropolis algorithm, was first developed in the 1950s for use in particle physics (Metropolis *et al.*, 1953). In the following years this algorithm was further improved by setting it in a formal mathematical framework and presenting to the general scientific community (Hastings, 1970; Kirkpatrick *et al.*, 1983). The MCMC method was set into a Bayesian framework by Geman and Geman (1984) through the introduction of the Gibbs sampler and then formalised as a statistical procedure (Gelfand and Smith, 1990). Since then, the algorithm has been used widely in a variety of fields including computer science and image processing and physical and biological sciences (Richey, 2010). For a more detailed explanation of the MCMC algorithm and its implementation see chapter 2.

1.7 The carbon optimality hypothesis

The most commonly used phenology models, which include only temperature responses, can describe observed seasonal cycles accurately, but are only empirical representations of phenology and do not include an explanation of phenological processes. This is why when confronted with more complex questions such as the effect of a warmer climate on phenology or impacts on the carbon cycle they often fail to give an accurate answer or result in contradictory conclusions, as outlined in previous sections. A different approach to phenological modelling is to consider a carbon benefit approach. This approach starts from the primary function of the leaf, carbon assimilation, and considers leaf gain and loss processes to be a strategy for achieving optimal carbon assimilation. Kikuzawa (1995) builds a carbon benefit model to predict the leaf habit, whether evergreen or deciduous, based on the relative lengths of the favourable and unfavourable seasons, so that a leaf reaches maximum net carbon gain over its lifetime. Arora and Boer

(2005) describe a carbon based phenology model that is used within a global climate model, where leaf seasonality is driven by environmental factors which affect carbon gain. While still using temperature as the main driver for leaf abscission, these models have the advantage of linking phenological events with photosynthetic capacity. Such a model has the major advantage that it is based on previously known photosynthesis and respiration processes at the leaf and canopy level, making it easy to interpret and incorporate into larger earth system models.

1.8 Outline

In this study I propose a global model of phenology based on mechanistic understanding of leaf gain and loss processes. I fit this model using a Bayesian algorithm to space based data of leaf area index. The thesis is structured as follows:

1. Chapter 2 presents a model of tropical phenology, specifically for the Amazon basin. I explain the observed increase in LAI during the dry season by an increase in solar radiation during the same period. Additional information for this study is included in chapter 3. This paper has been previously published as Caldararu *et al.* (2012).

2. Chapter 4 presents a global phenology model based on the previously described tropical model with additional responses to temperature and soil water. This chapter has been submitted for publication.

3. Chapter 5 discusses a different parametrisation of the model presented in chapter 4 to produce a more general phenology model with better predictive capabilities.

4. Chapter 6 is a discussion of the results presented in the previous chapters and includes a discussion of model and data uncertainty, model predictive capabilities and future applications.

Chapter 2

Inferring Amazon leaf demography from satellite observations of leaf area index

2.1 Introduction

Seasonal and year-to-year variations in leaf area imprint significant spatial and temporal variability on biogeochemical cycles and affect land-surface properties related to climate (Hayden, 1998). For example, the transfer of water from the soil to the atmosphere is mostly via leaves through evapotranspiration, subsequently affecting humidity, air temperature and rainfall (Wilson and Baldocchi,

This work has been published (Caldararu *et al.*, 2013) and the paper is reproduced in Appendix A.

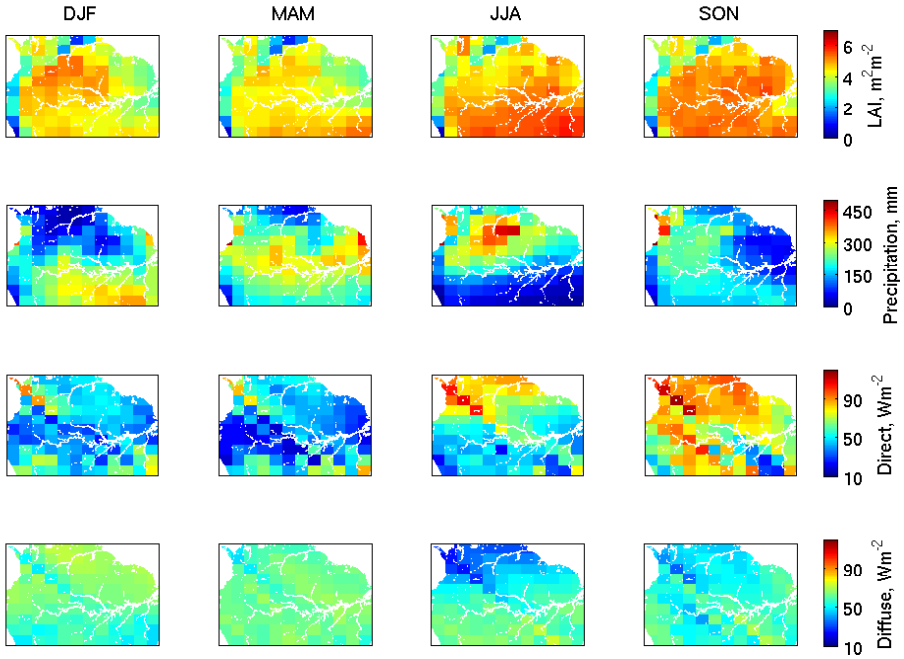

Figure 2.1: From top to bottom: MODIS leaf area index (m^2m^{-2}), WorldClim precipitation (mm) (Hijmans *et al.*, 2005), GEOS-4 direct and diffuse photosynthetically active radiation, PAR (Wm^{-2}) across the study region. The dry season, with precipitation levels of under 100 mm/month, runs generally from July-September, period which coincides with an increase in direct PAR due to a decrease in cloud cover. We can observe that the LAI also peaks during this period, reaching its lowest levels in the wet season.

2000). Similarly, carbon enters vegetated ecosystems through carbon fixation via photosynthesis (White *et al.*, 1999).

Over temperate regions leaf phenology is known to be driven by changes in day length and temperature (Schwartz, 1999), although the relative importance of these determining factors and how they might change with climate is poorly understood (Korner and Basler, 2010). However, the majority of the world's forests retain leaves year round: boreal forests which are dominated by evergreen needle-leaf trees and often mixed with deciduous broadleaf and needle-leaf species; and mesic tropical forests, dominated by evergreen broadleaf species, which are

responsible for the majority of terrestrial carbon fixation (Malhi and Grace, 2000). Observed LAI over these evergreen forests, particularly over the tropics, still show seasonal and year-to-year variations (Myneni *et al.*, 2007), but we lack knowledge about the magnitude, geography, timing, and the processes driving such variation, partly reflecting the difficulty of taking year-round measurements. Consequently many modelling studies assume that tropical leaf area is constant (Cramer *et al.*, 2001; Arora and Boer, 2005).

Space-borne observations of LAI offer the best opportunity to develop a quantitative model of large-scale controls of leaf area by virtue of their frequency and global coverage. We focus our study on the Amazon basin (10°N–10°S, 80°W–50°W). The vegetation in the region is mainly semi-deciduous or evergreen tropical forest, but the species composition varies widely due to the differences in soil type and altitude across the basin (Sombroek *et al.*, 2000). The Amazon basin experiences wet and dry seasons, with the dry season generally running from June-September, with longer and drier periods in the south-eastern regions (Sombroek, 2001). Figure 2.1 shows that the timing of low precipitation coincides with an increase in direct radiation mainly due to a decrease in cloud cover. Levels of diffuse radiation are comparatively constant throughout the year.

Ground-based studies have reported an increase in leaf litterfall during the dry period (Malhado *et al.*, 2009; Chave *et al.*, 2010), but without simultaneous measurements of leaf gain we cannot determine whether the increased litterfall represents a net loss of leaves. Studies using space-borne vegetation data (Myneni *et al.*, 2007; Huete *et al.*, 2006) have reported an increase in greenness during the dry season over the Amazon, even during severe droughts (Saleska *et al.*, 2007), but these drought observations have been disputed (Samanta *et al.*, 2010; Doughty and Goulden, 2008). These observations are consistent with indirect evidence from the seasonal cycle of satellite-observed emission of biogenic trace gases (Barkley *et al.*, 2009). The dry-season increase in leaf area could be explained by soil

moisture dynamics: water is available all year round in the deeper soil layers (Harper *et al.*, 2010), which can be readily accessed by the large rooting depths of Amazonian vegetation (Nepstad *et al.*, 1994; Jipp *et al.*, 1998). Under these circumstances, we expect that light availability is the primary controlling factor for determining changes in leaf area (Wright and Vanschaik, 1994). This implies that trees will carry more leaves in the dry season when direct radiation is greater. To test this idea and to enable predictive modelling of Amazon leaf phenology, we develop a simple leaf phenology model for the Amazon tropical forest. Section 2.3 describes this model, which we fit to MODIS LAI data (section 2.2) to obtain parameter values for the Amazon basin. We discuss our results in section 2.4 and demonstrate how, in principle, our predictions of leaf area and age distribution could impact carbon assimilation using a simple carbon model. We conclude our paper in section 2.5.

2.2 Data sets used

2.2.1 MODIS LAI data

We use leaf area index (LAI) data obtained from the MODIS (Moderate Resolution Imaging Spectroradiometer) instrument aboard the NASA Terra platform. The LAI/fPAR (fraction of absorbed photosynthetically active radiation) product collection 5 (MOD15A2) is available globally at a spatial resolution of 1 km every 8 days for the period 2000–present and has been downloaded from `https://lpdaac.usgs.gov/`. The 8 day temporal resolution is a result of compositing, i.e. assigning the best value for the 8 day period based on maximum fPAR. The data set is split into tiles (10° latitude by 10° longitude at the equator), which cover northern South America and include the Amazon basin. We use tiles h10-12v08 and h10-12v09 for the years 2001 to 2005.

The LAI is calculated using a radiative transfer algorithm (the main algorithm), which uses the red (648 nm) and near-infrared (858 nm) bands. The algorithm uses biome-specific vegetation structure and height, leaf type and soil brightness to obtain LAI values (Yang *et al.*, 2006; Knyazikhin *et al.*, 1997, 1999). In conditions where the main algorithm cannot be applied, a back-up algorithm is used, in which case the LAI value is calculated using an empirical relationship between Normalised Difference Vegetation Index (NDVI) and LAI. The data quality is affected by the presence of cloud, atmospheric aerosol loading and snow cover. Snow cover is not an issue for our study region, but cloud cover can affect the quality of the data, especially during the wet season, while aerosols from biomass burning can interfere with measurements during the dry season. The quality flags provided along with the LAI data offer information on overall data quality, the algorithm used, cloud cover and aerosol presence. Ground validation studies (Cohen *et al.*, 2006) have shown that the back-up algorithm is often unreliable and our analysis of the data over the Amazon region shows that values assigned by the backup algorithm are often unrealistically low, leading to large week-to-week swings in LAI. As a consequence, we remove any LAI values calculated using the back-up algorithm prior to spatial averaging.

LAI retrievals of vegetation often have saturation problems in that LAI becomes insensitive to changes in reflectance. Studies have shown that this was an issue for high-biomass areas for collections 3 and 4, but this has been considerably improved for collection 5 (Yang *et al.*, 2006). Ground based values of LAI in the Amazon basin range from 3.5–6 m^2m^{-2} (Malhado *et al.*, 2009; Aragao *et al.*, 2005; Roberts *et al.*, 1996; Meir *et al.*, 2000), with values of up to 10 m^2m^{-2} registered by some studies (Doughty and Goulden, 2008), with differences arising from the different measurement methods. MODIS LAI values are in the range 2–6 m^2m^{-2}, which provides us with some confidence that there are no major saturation problems.

When relating leaf reflectance measurements to seasonal cycles we must take into account the fact that changes in observed reflectance can also be caused by changes in the number of young leaves, as these have different reflectance properties. This has been advanced as an explanation for the observed seasonal swings over the Amazon basin by several studies (Doughty and Goulden, 2008; Asner and Alencar, 2010; Aragao *et al.*, 2009; Brando *et al.*, 2010). However, the observed seasonal changes in LAI are too large to be attributed to a flush of new leaves only (Samanta *et al.*, 2012).

The study region includes lowland tropical forests, alpine forests, savannas and grasslands. As our study is focused on forests, we use the MODIS landcover product MOD12Q1 to filter non-forested pixels. We use the provided IGBP classification scheme and have retained only pixels in classes 1–5, evergreen needleleaf forest, deciduous needleleaf forests, deciduous broadleaf forest, evergreen broadleaf forest and mixed forest. As there is no way to distinguish between lowland and alpine forests we include both in our analysis.

We reproject the LAI data to an orthogonal projection and average it to the resolution of the GEOS-4 PAR data (2° latitude and 2.5° longitude) and subsequently fit our model at this resolution.

2.2.2 Radiation data

We use photosynthetic active radiation (PAR) fields from assimilated meteorological data products of the Goddard Earth Observing System (GEOS-4) based at the NASA Global Modelling and Assimilation Office (GMAO) (Bey *et al.*, 2001). The temporal resolution of this data is 1 day and the spatial resolution is $2° \times 2.5°$.

2.2.3 Soil moisture data

We use the volumetric soil moisture for 10-200 cm depth from the NCAR/NCEP reanalysis daily average surface flux data set (`http://www.esrl.noaa.gov/psd/data/gridded/data.ncep.reanalysis.surfaceflux.html`) (Kalnay *et al.*, 1996). The data is available at global scales at daily timesteps for the period 1948 to present on a Gaussian grid. We reproject the data onto the orthogonal GEOS-4 grid for model fitting.

2.3 Leaf phenology model

The central assumption of our model is that trees adjust their gains and losses of leaves in order to try to achieve, at any given time, an optimal LAI, which we refer to as the target LAI, LAI_{targ}. The value of LAI_{targ} is determined as the minimum of a light-limited target, LAI_{targ}^{light}, and a water-limited target, LAI_{targ}^{water}. We define LAI_{targ}^{light} such that the bottom layer of leaves receives just enough light to return a positive carbon balance, i.e., receives light at the light compensation point C as derived from Beer's law:

$$LAI_{targ}^{light} = -\frac{1}{\alpha}\ln(\frac{C}{I_0}), \tag{2.1}$$

where I_0 is the incoming PAR at the top of the canopy and α is the light attenuation coefficient applying to Beer's Law, which we have fixed to 0.5 (Section 3.1.1). To recognise the potentially important difference between direct and diffuse light we apply Eq. 2.1 separately for both direct and diffuse PAR, to determine their respective compensation points (C_{direct} and $C_{diffuse}$), and then keep the minimum of the two values. For both diffuse and direct PAR we assume that, in order to avoid sub-optimal responses to very short-term variation in

light, trees calculate the target LAI_{targ}^{light} using an effective I_0, defined as the average over the previous p days. We drive Eq. 2.1 with GEOS-4 reanalysis estimates of incoming PAR (section 2.2.2). We define the water-limited target as $LAI_{targ}^{water} = \beta_1 + \beta_2 W_s$, where W_s is soil moisture (from the NCAR/NCEP Reanalysis, section 2.2.3) and β_1 and β_2 are empirical coefficients (Section 3.1.2)

We assume leaf demography (the gain and loss of leaves of different ages) is determined by the factor limiting LAI_{targ}. If the current LAI is below LAI_{targ} trees add new leaves of age a=0 at a maximum rate $gain_{max}$ to reach LAI_{targ}. If LAI_{targ} is water limited and the current LAI is above LAI_{targ}, to avoid excessive water loss or overheating leaves, trees lose leaves, beginning with the oldest leaves, until they achieve LAI_{targ}. When LAI_{targ} is light limited and LAI is above LAI_{targ}, trees add no new leaves, but do not actively drop leaves. In all of the above cases, leaves are subject to continuous leaf loss according to a mortality rate μ due to leaf ageing that depends only on leaf age a. We define a minimum age, a_{crit} (years), below which we only consider the background loss, e.g. herbivory, branch loss, so that the mortality is $\mu = \exp^{-\mu_0}$. Leaves older than a_{crit} are lost at a faster rate $\mu = exp^{-\mu_1}$ which is caused by leaf ageing. In order to calculate the age-dependent mortality we introduce the concept of leaf cohorts, defined as a group of leaves of the same age. For each cohort $LAI(a, \mathbf{x}, t)$ we apply the mortality rate as:

$$LAI(a, \mathbf{x}, t) = \mu(a) LAI(a - 1, \mathbf{x}, t - 1), \tag{2.2}$$

with the mortality rate μ defined as above. The overall LAI at each time step, $LAI(\mathbf{x}, t)$ is the sum of all leaf cohorts.

Table 2.1: Model parameters

Symbol	Units	Description
C_{direct}	Wm^{-2}	Light compensation point for direct PAR (Eq. 2.1)
$C_{diffuse}$	Wm^{-2}	Light compensation point for diffuse PAR (Eq.2.1)
p	days	Length of time window for average PAR
$gain_{max}$	$\mathrm{m}^2\mathrm{m}^{-2}$	Maximum gain rate for new leaves
a_{crit}	years	Age after which leaves start ageing
μ_0	years^{-1}	Background decay constant
μ_1	years^{-1}	Age-related decay constant

Overall the rate of change of LAI at each location $\mathbf{x}$ and time t (Figure 2.2) is:

$$\frac{d}{dt}(LAI(\mathbf{x},t)) = P(I_0(\mathbf{x},t), LAI(\mathbf{x},t-1)) - L(LAI(\mathbf{x},t), W_s(\mathbf{x},t)), \qquad (2.3)$$

where $P(I_0(\mathbf{x},t), LAI(\mathbf{x},t-1))$ denotes production processes and $L(LAI(\mathbf{x},t)W_s(\mathbf{x},t))$, refers to loss processes due to both the age-related mortality rate and active leaf dropping due to water stress. When integrated over time t, Eq. 2.3 provides, for each location $\mathbf{x}$ and time t, a predicted LAI (Section 3.2.1) given environmental drivers (direct and diffuse PAR, and available soil moisture), and given the value of 9 parameters specific to location $\mathbf{x}$: $C_{direct}, C_{diffuse}, p, gain_{max}, a_{crit}, \mu_0, \mu_1, \beta_1, \beta_2$ (Table 2.1). Initial parameter estimates (not shown) estimated that $LAI_{targ}^{light} < LAI_{targ}^{water}$ for nearly all locations at nearly all times, such that the fit to data was not statistically improved by considering water limitation of leaf area so that we can set $LAI_{targ} = LAI_{targ}^{light}$; consequently we do not discuss soil moisture further.

We simultaneously fit the above parameters using a Bayesian approach (Section 3.2) over our study region with a spatial resolution of 2° (latitude) × 2.5° (longitude) to collection 5 of the LAI data from the MODIS satellite instrument, which was spatially averaged to this resolution (section 2.2.1).

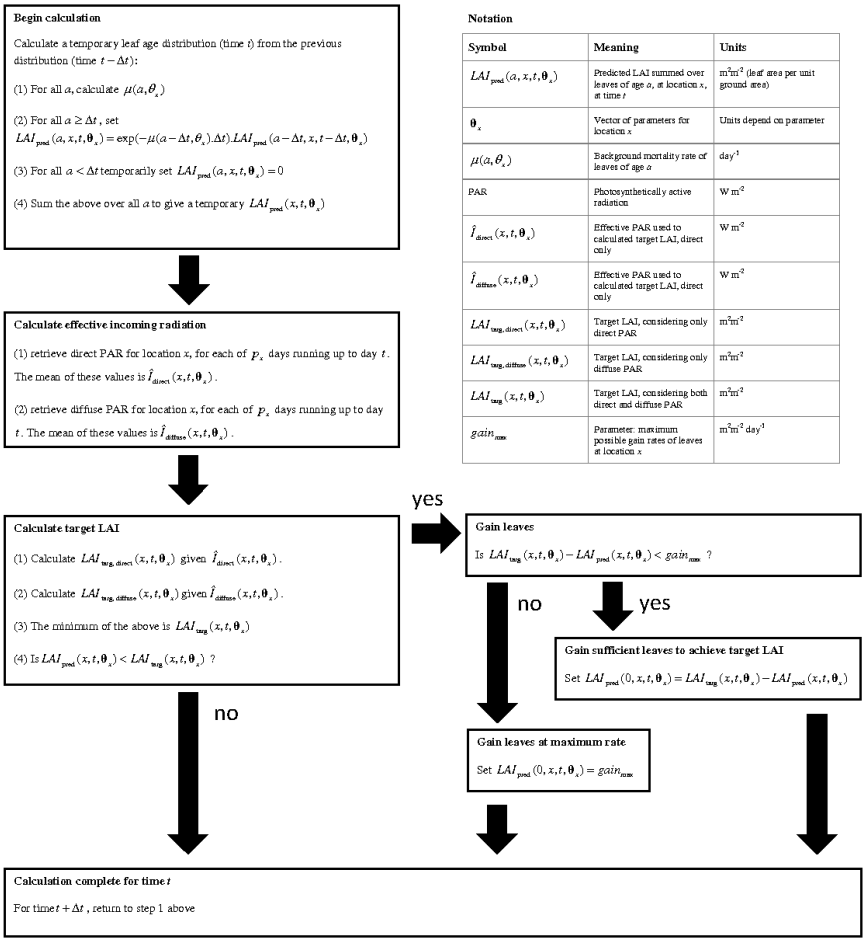

Figure 2.2: How to calculate the predicted leaf age distribution and predicted total LAI for a model driven only by light. Note that the calculation begins with the leaf age distribution from a previous time $t - \delta t$ at the same location, which is updated to account for background leaf mortality, and the addition of new (age=0) leaves as driven by the LAI target, producing a predicted leaf age distribution for time t.

2.4 Results

Figure 2.3 shows that the model reproduces the spatial distribution of mean LAI (Pearson correlation coefficient r^2=0.9), capturing the high values (up to 4.8±0.1 m^2m^{-2}) over the central and southern Amazon basin and lower values (4.0±0.2 m^2m^{-2}) over the Eastern regions. More importantly, the model

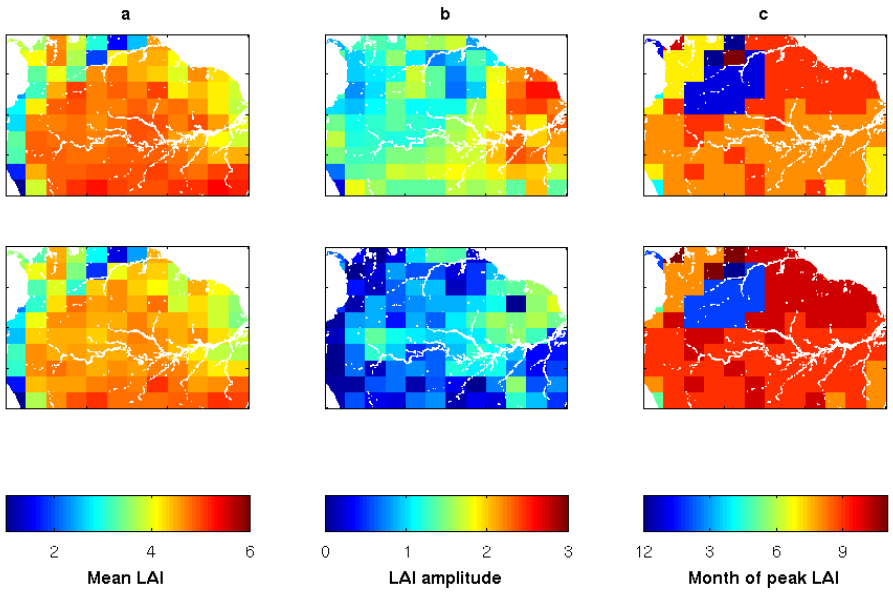

Figure 2.3: MODIS (top) and model (bottom) leaf area index (LAI) over the Amazon (10°N–10°S, 80°W–50°W), 2001–2005 averaged over a 1×1 km grid. (a) mean LAI (m^2m^{-2}), (b) mean annual amplitude of LAI (m^2m^{-2}), and (c) mean timing of peak LAI (day of year).

reproduces the broad spatial distribution of LAI amplitude, defined as the difference between the maximum and minimum monthly LAI, with a statistically significant correlation coefficient of r^2=0.46. This result supports our model structure because, unlike the mean LAI, the LAI amplitude is highly constrained by model assumptions; the maximum LAI amplitude is determined by the amplitude of incoming PAR.

Figure 2.4 shows that the model generally has a negative bias with respect to amplitude, which we attribute at least in part to measurement noise, with mean MODIS (model) LAI amplitude of 1.5±0.4 (0.7±0.4) m^2m^{-2}, but the MODIS value falls within the confidence intervals of the model (Figure 2.5). Similarly, the model reproduces the seasonal timing of LAI variation (Figure 2.4), which is also highly constrained by the model structure, as the greatest target LAI occurs at the time of peak incoming PAR. We find that our model generally describes

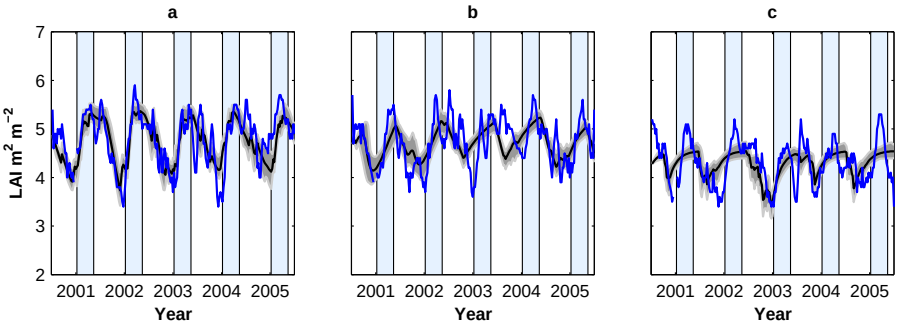

Figure 2.4: LAI time series in (a) the eastern Amazon (8^o N 62.5^o W), (b) the semi-deciduous Amazon (0^o N 72.5^o W), and (c) the evergreen central Amazon basin (4^o N 67.5^o W), as predicted by the model (black line) and MODIS LAI data (blue line). Gray shaded area represents 95% confidence intervals. Blue bands represent approximate dry seasons.

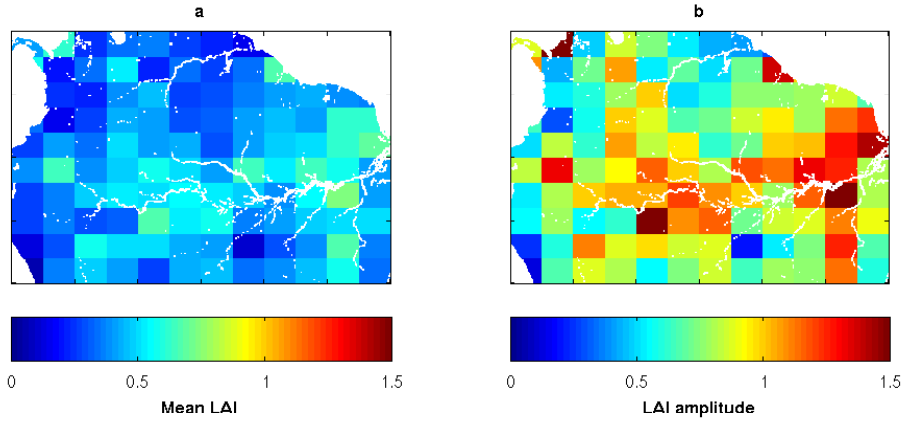

Figure 2.5: Model uncertainty for mean LAI and annual amplitude (the difference between the maximum and minimum monthly LAI). We used samples drawn from the posterior distribution to calculate model LAI values and then obtain posterior means and confidence intervals. Here, the uncertainty is represented as the difference between the upper and lower bounds of the 95% confidence intervals using parameter posterior distributions.

between 20–80% (median of 31%) of the observed temporal variability of LAI at any one 2°×2.5° grid cell.

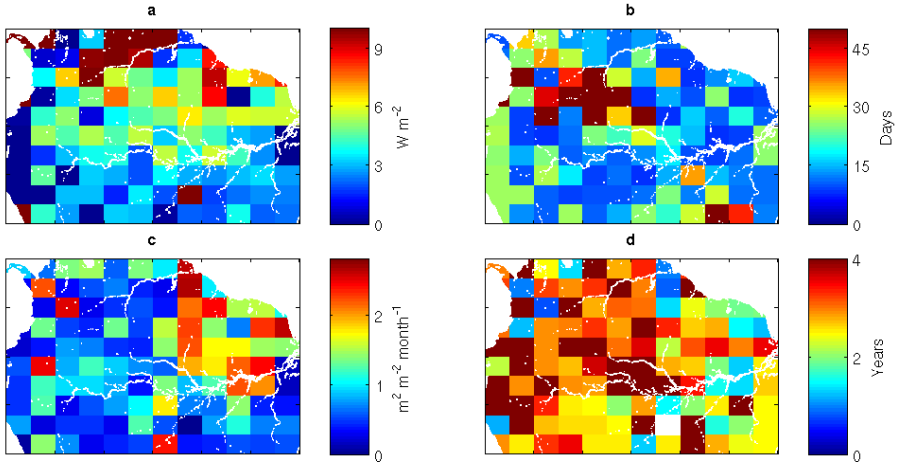

Figure 2.6: Mean posterior parameters that describe leaf gain and loss: (a) direct PAR compensation point, C_{direct} (W/m^2); (b) delay in vegetation response to changes in PAR, p (days); (c) maximum number of leaves that can be added over a month, $gain_{max}$ (m^{2}m^{-2}month^{-1}); and (d) mean cohort leaf lifetime τ_{95} defined as the time at which 95% of the leaves from a cohort have dropped (years).

Figure 2.6 shows posterior model parameters, which provide further insight into the underlying processes that determine observed variations in LAI. The spatial variations of the parameters are a reflection of not only the seasonality but also of species composition, soil type or nutrient availability. The two compensation points, C_{direct} and $C_{diffuse}$, can be interpreted as a measure of the shade adaptation in trees, with a lower compensation point indicating leaves that are adapted for lower light conditions. We estimate that C_{direct} is lower in the south of the Amazon, with values of 1.5 compared to 5 Wm^{-2} elsewhere. In contrast, $C_{diffuse}$, which effectively limits the overall compensation point during the dry season resulting in a lower LAI amplitude, is more homogeneous across the basin with mean values of 0.23 Wm^{-2}. Our values for the compensation points are broadly consistent with ground-based measurements (Riddoch *et al.*, 1991), providing further support for our methodology.

The delay p represents the time required for the vegetation to respond to changes

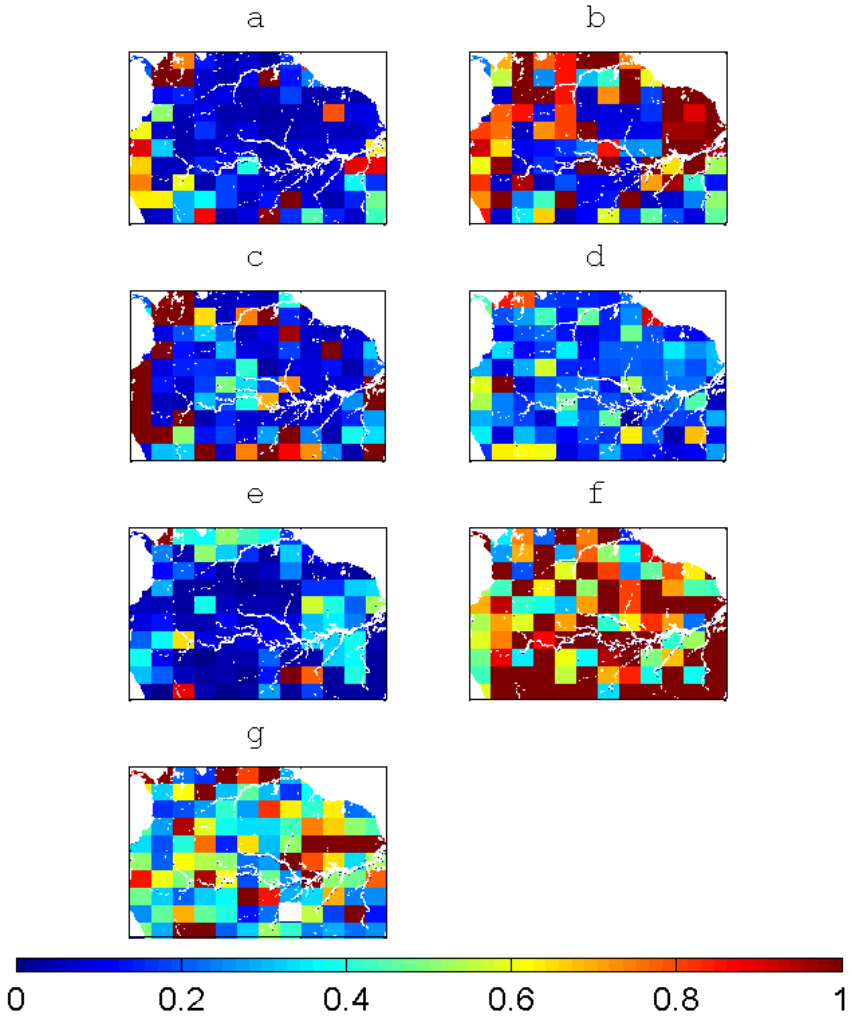

Figure 2.7: Parameter uncertainty derived from the posterior distribution, expressed as 95 % confidence intervals relative to posterior means for (a) direct PAR compensation point, C_{direct}; (b) diffuse PAR compensation point, $C_{diffuse}$; (c) delay in vegetation response to changes in PAR, p; (d) maximum number of leaves that can be added over a month, $gain_{max}$; (e) age after which age related decay starts, age_{crit}; (f) background decay constant, μ_0 and (g) age-related decay constant, μ_1.

in PAR. We find that p is generally 14 days for most of the basin. The exception is over the northwestern region, where p >1 month, suggesting that vegetation over this region is slower to respond to changes in PAR. The maximum gain of

LAI is typically around 1 $m^2m^{-2}month^{-1}$, with the highest values (up to 2.2 $m^2m^{-2}month^{-1}$) over the eastern, drier regions corresponding to an area with a higher LAI amplitude and a more pronounced seasonal cycle.

To help interpret our estimated leaf loss parameters, determined by the amplitude of the observed LAI seasonal cycle, we calculate a leaf lifespan τ_{95} as the time at which 95 % of the leaves from a cohort have dropped, based on the exponential decay rates μ_0 and μ_1 (Eq. 2.2):

$$\tau_{95} = -\frac{\ln 0.05}{\mu_1} - \frac{\mu_0}{\mu_1} a_{crit} + a_{crit}, \tag{2.4}$$

with variables as defined in Table 2.1. Figure 2.6 shows that τ_{95} is longest in the middle of the Amazon basin, with values of around 2.1±0.2 years, and lower in the Southern and Eastern regions (1.5±0.7 years), where the vegetation has a larger deciduous component. These lifetimes are consistent with sparse ground-based studies over the same region, which report values between 2 months and 6.4 years (Reich *et al.*, 2004) and in other tropical forests (up to 26 months (Sharpe, 1997; Osada *et al.*, 2001)).

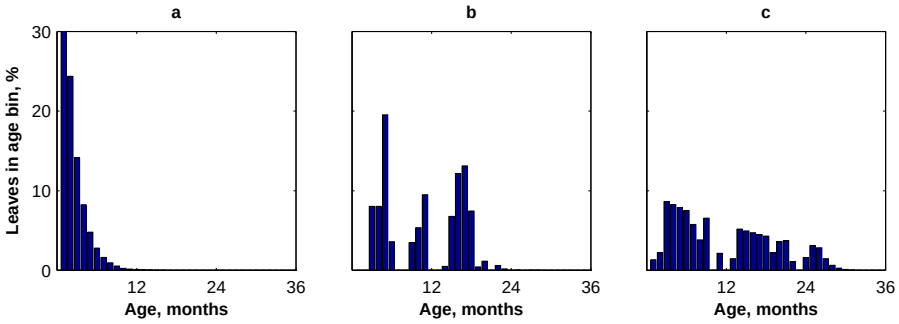

Figure 2.8: Estimated frequency distribution of leaf ages (months) over (a) the eastern Amazon, where leaves are typically short-lived, (b) over the semi-deciduous Amazon, and (c) over the evergreen central Amazon basin. All locations are the same as for Fig. 2.4.

To obtain an estimate of parameter uncertainty, we use the posterior distribution

resulting from the fitting algorithm to calculate 95% confidence intervals (Fig. 2.7). Most parameters are well constrained, with confidence intervals of 0.1 ($\pm$ 0.07) of the posterior mean for most parameters. The exceptions are two of the leaf mortality parameters (Fig. 2.7 (f) and (g)), with confidence intervals of 0.8 ($\pm$ 0.2) for the base mortality rates, μ_0 and 0.5 ($\pm$ 0.1) for the age related rate, μ_1. This can indicate a trade-off between the two parameters as they both contribute to determining the overall leaf lifespan. Also, the diffuse compensation point $C_{diffuse}$ (Fig. 2.7 (b)) is less well constrained in the north-eastern regions.

Our model also allows us to estimate the leaf age distribution at any point over the basin, something that would be extremely difficult to do using traditional means. Figure 2.8 shows that leaves in regions with a high leaf turnover rate are generally younger than one year, with a high proportion of very young leaves (less than 6 months) with an approximately exponential leaf age distribution which shows pronounced seasonality between wet and dry seasons. In contrast, over the evergreen areas of the central Amazon basin we estimate a higher proportion of leaves older than 1 year and a leaf age distribution with a less pronounced seasonality. In the more deciduous regions in the southern basin, we find distinct leaf cohorts originating from past growing seasons.

To provide an example of the potential impact of our new estimates of leaf age distribution on large-scale calculations of biogeochemistry, we incorporated this information into a simple model of carbon assimilation. We present three scenarios: (1) using a constant LAI and constant leaf age distribution throughout the year, (2) using the predicted LAI with a constant leaf age distribution and (3) using the predicted LAI and leaf age distribution. Figure 2.9 shows that the seasonality of the carbon flux is driven mainly by the incoming PAR and not by changes in LAI. When we include the predicted LAI, the overall photosynthesis is higher by only approximately 1 μmol $m^{-2}s^{-1}$ during the dry season. However, if we include a leaf age adjusting factor (Section 3.3), the assimilation rate is lower

by an average of 1.5 μmol $m^{-2}s^{-1}$ throughout the year. The largest difference (3.37 μmol $m^{-2}s^{-1}$) occurs in June, when the new leaves start appearing in response to increased sunlight. The assimilation also peaks later than when using a constant LAI, as new leaves reach peak photosynthetic rates only after a certain period of time. While some ground studies report a decrease in assimilation rate during dry periods (Malhi *et al.*, 1998; Miranda *et al.*, 2005) and during severe drought periods (Phillips *et al.*, 2009), the lower assimilation rate at the start of the dry season has been observed in ground studies (Hutyra *et al.*, 2007; Goulden *et al.*, 2004; Graham *et al.*, 2003; Bonal *et al.*, 2008; da Rocha *et al.*, 2004) but previous models were unable to predict this pattern. The hypothesis advanced by one of these studies (Hutyra *et al.*, 2007) was that the emergence of new leaves at the start of the dry season would create this pattern, which is quantitatively supported by the leaf demography predicted by our model.

2.5 Concluding remarks

We present a simple phenology model for the Amazon basin, which we fitted to 5 years of MODIS LAI data. We showed that our model reproduced the observed increase in LAI during the dry season as a response to an increase in direct solar radiation. Our model parameters provided further information about the vegetation in the Amazon basin. The model also provided leaf demography estimates, which can be used to improve predictions of the seasonal carbon cycle, which we demonstrated in principle using a simple carbon model. We showed that using our predicted leaf demography explains observed decrease in carbon assimilation at the start of the dry season. Carbon fixation is only one of many examples of leaf-age-dependent processes of which our current understanding is hampered by incomplete knowledge of leaf demography. Recent work has shown that including a better description of leaf phenology in Earth system models can

significantly revise estimates of land surface warming (Bounoua *et al.*, 2010). The demographic model presented here can be used to predict responses of Amazon leaf demography to future changes in climate and could be extended to include other tropical regions where leaf phenology is driven partially or wholly by soil moisture. We therefore anticipate that the insights afforded by our analysis will have far-reaching implications for improving current understanding of the natural carbon cycle in the Amazon and elsewhere.

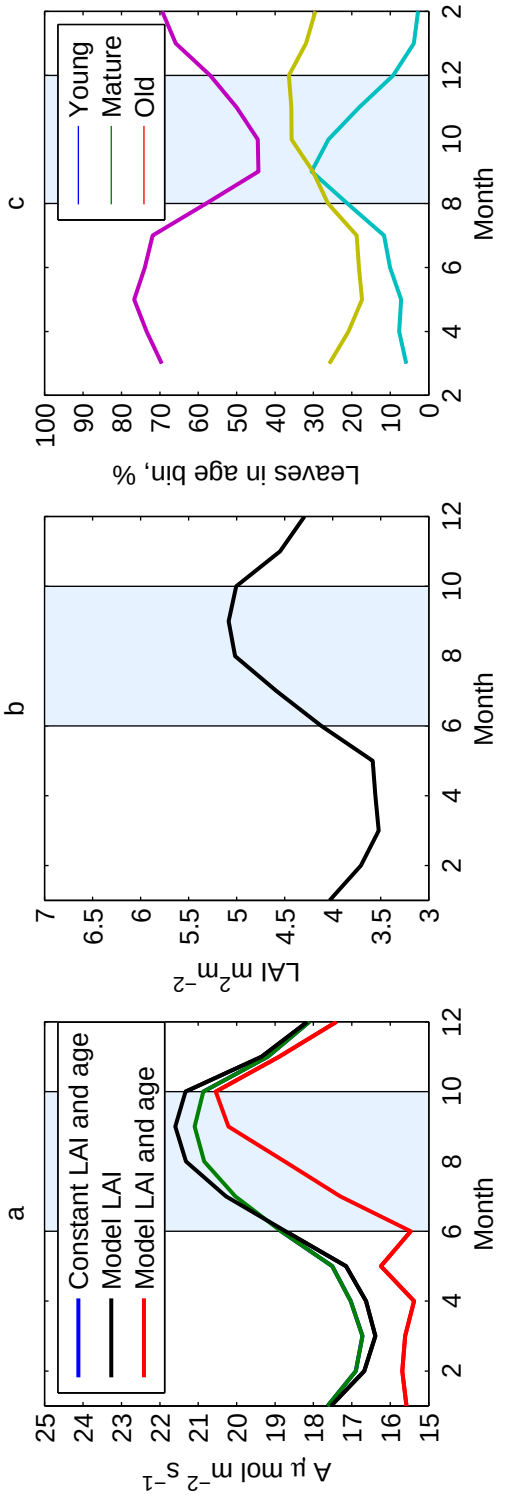

Figure 2.9: (a) Gross carbon assimilation calculated using a simple carbon model for a constant LAI, model LAI and model LAI including the temporal variations in leaf age, (b) seasonal variation in LAI and (c) variation in leaf age composition. All values presented are monthly means over a 5 year period at one location (8^o N 55^o W). The blue shaded area represents the dry season

Chapter 3

Inferring Amazon leaf demography from satellite observations of leaf area index. Supplementary information

3.1 Model structure

3.1.1 Attenuation Coefficient

To quantify the attenuation of photosynthetic active radiation (PAR) as it passes through a forest canopy, we used Beer's law:

$$I = I_0 e^{-\alpha L}, \tag{3.1}$$

where I_0 is the incoming PAR (Wm^{-2}) at the top of the canopy, I is the light level at layer L inside the canopy and α is the light attenuation coefficient. We assume a vertically homogeneous canopy with no leaf clumping. The light attenuation coefficient is a function of the solar inclination angle, ϕ. For a random distribution of leaf angles this is equal to $\alpha = \frac{0.5}{\sin\phi}$. We use a homogeneous canopy with no leaf clumping and a random leaf angle distribution as these assumptions are valid for canopies at a large scale. Because we are using daily time scales, we can, for simplicity, calculate the attenuation coefficient at its maximum value for a solar angle equal to 90°. For non-directional (diffuse) radiation the attenuation coefficient can be calculated as the median value over all possible radiation angles. The median is used here rather than the mean to avoid the excessive influence of very small or very large angles.

3.1.2 Soil Water Target

Soil water is widely recognised as a primary constraint in LAI, and the seasonality of LAI, in many different vegetation types around the world. For an individual tree, a greater leaf area implies a higher stomatal conductance and hence a greater potential rate of evapotranspiration. If this potential rate cannot readily be met with available soil moisture, the tree can either keep stomata open, risking excessive water loss, cavitation and hence drought death; or close the stomata, which greatly reduces water loss, but also shuts down photosynthesis and risks leaves overheating, causing permanent damage to the leaves; or the tree can reduce its total leaf area, thus allowing for individual leaves to maintain evapotranspiration and photosynthesis without excessive water use overall (McDowell *et al.*, 2008). The first two options are short term responses to unpredictable drought, whereas losing leaves is the more sensible response to the seasonal variation in soil moisture that drives leaf phenology. Therefore, we assume that where the current LAI

exceeds the water-limited LAI LAI_{targ}^{water}, trees would drop leaves in order to reach LAI_{targ}^{water}, starting with the oldest leaves, to produce a leaf demography that is sustainable in the long term (see Chapter 2).

Based on these assumptions, we specify a relationship between soil moisture and LAI_{targ}^{water} as:

$$LAI_{targ}^{water} = \beta_1 + \beta_2 W_s, \tag{3.2}$$

where W_s is the percentage soil moisture, and β_1 and β_2 are empirical coefficients. If the current LAI is above this target, trees will drop leaves until they reach LAI_{targ}^{water}.

We assume trees actively drop leaves when LAI exceeds LAI_{targ}^{water}, but do not do so when LAI exceeds LAI_{targ}^{light}. Where LAI exceeds LAI_{targ}^{light}, the leaves receiving the least light will be below their compensation point and so be a net sink, rather than source, of carbon. However, the magnitude of this sink will be relatively small, when compared with the magnitude of the source from the leaves receiving more light. Also, trees can store substantial amounts of labile carbon, which can be used to offset short term deficits in carbon fixation. Therefore, where LAI exceeds LAI_{targ}^{light}, the excess leaves are unlikely to be a cause of whole plant stress or death. In contrast, as outlined above, where LAI exceeds LAI_{targ}^{water}, the lack of water affects the entire tree, and so could cause damage to all leaves, or to the whole plant through cavitation. In addition, very few trees store an amount of water that is significant in comparison to daily water use. Therefore, when LAI exceeds LAI_{targ}^{water}, the excess leaves are an immediate source of danger to the whole tree.

We fit the model using the method as described in section 3.2 below, using NCEP/NCAR reanalysis derived soil moisture data (Kalnay *et al.*, 1996). The values obtained for the β_1 and β_2 parameters result in a water limited target LAI_{targ}^{water} that is higher than the light limited target LAI_{targ}^{light} at all locations

throughout the year, This implies that vegetation is never water limited. As a result we set $LAI_{targ} = LAI_{targ}^{water}$, which results in the model structure described in Figure 2.2.

3.2 Parameter estimation

The model has 7 free parameters (Table 2.1), which we fit independently for each location, resulting in 840 parameters.

Our aim was to estimate model parameters for location $\mathbf{x}$, which we denote as the vector $\theta_{\mathbf{x}}$, given the MODIS data for location $\mathbf{x}$, which we denote $Z_{\mathbf{x}}$. To do this we used a Bayesian approach, seeking to estimate the posterior probability distribution of $\theta_{\mathbf{x}}$, given $Z_{\mathbf{x}}$, which we denote $p(\theta_{\mathbf{x}}|Z_{\mathbf{x}})$. The posterior $p(\theta_{\mathbf{x}}|Z_{\mathbf{x}})$ is proportional to the product of the likelihood $L(Z_{\mathbf{x}}|\theta_{\mathbf{x}})$, and the prior $p(\theta_{\mathbf{x}})$ such that $p(\theta_{\mathbf{x}}|Z_{\mathbf{x}}) \propto L(Z_{\mathbf{x}}|\theta_{\mathbf{x}})p(\theta_{\mathbf{x}})$. Often, $p(\theta_{\mathbf{x}}|Z_{\mathbf{x}})$ covers too large a region of parameter space to be evaluated completely. In this case we instead use sampling methods, which provide a set of random samples of $\theta_{\mathbf{x}}$ drawn from $p(\theta_{\mathbf{x}}|Z_{\mathbf{x}})$. We used a Metropolis-Hastings Markov Chain Monte Carlo (MCMC) sampling routine (Gilks, 1996.).

We define the likelihood as

$$l(Z_{\mathbf{x}}|\theta_{\mathbf{x}}) = \sum_{t(\mathbf{x})} \ln[n(LAI_{obs}(\mathbf{x},t), LAI_{pred}(\mathbf{x},t,\theta_{\mathbf{x}}), \sigma_{\mathbf{x}})] \tag{3.3}$$

where $l(Z_{\mathbf{x}}|\theta_{\mathbf{x}})$ is the log-likelihood; $LAI_{pred}(\mathbf{x},t,\theta_{\mathbf{x}})$ is the predicted LAI at location $\mathbf{x}$ at time t (this depends on the model parameters $\theta_{\mathbf{x}}$); $LAI_{obs}(\mathbf{x},t)$ is the observed MODIS LAI at location $\mathbf{x}$ at time t; and $n(LAI_{obs}(\mathbf{x},t), LAI_{pred}(\mathbf{x},t,\theta_{\mathbf{x}}), \sigma_{\mathbf{x}})$ denotes the probability density for observing $LAI_{obs}(\mathbf{x},t)$ given a normal distribution with mean $LAI_{pred}(\mathbf{x},t,\theta_{\mathbf{x}})$ and standard

deviation $\sigma_{\mathbf{x}}$ where $\sigma_{\mathbf{x}}$ is a parameter that specifies the magnitude of unexplained variation in LAI. Eq. 3.3 represents a loop over all times t for which observed LAI were available for location $\mathbf{x}$ (this set of times is denoted $t(\mathbf{x})$ in Eq. 3.3).

We initially used non-informative, uniform priors for all parameters. We assumed that, *a priori*, all parameter combinations were equally likely. However, we found that, with non-informative priors on all parameters, we could not properly constrain all parameters for all locations. Therefore, we assigned an informative prior on one of the parameters affecting the rate of gain and loss of leaves. We did this for one parameter only to keep the overall influence of priors to a minimum. We base our prior on an extensive study (Reich *et al.*, 2004) of leaf lifespan (time after which all leaves are dead) in the northern Amazon. To define the prior we use the mean (2.35 years) and standard deviation (0.18 years) of these measurements. In our model, we define leaf lifespan $\tau_{95,\mathbf{x}}$ as the leaf age at which only 5% of leaves remain alive. This is a function of three model parameters: $\mu_{0,\mathbf{x}}$, $\mu_{1,\mathbf{x}}$ and $a_{crit,\mathbf{x}}$. Using this prior, the posterior in the MCMC sampling becomes:

$$\ln(p(\theta_{\mathbf{x}}|Z_{\mathbf{x}})) = l(Z_{\mathbf{x}}|\theta_{\mathbf{x}}) + \ln(n(\tau_{95,\mathbf{x}}, \hat{\tau}, \sigma_{\tau})), \tag{3.4}$$

where $n(\tau_{95,\mathbf{x}}, \hat{\tau}, \sigma_{\tau})$ is the probability density for $\theta_{95,\mathbf{x}}$ assuming that it is drawn from a normal distribution with mean $\hat{\tau}$ and standard deviation σ_{τ}. This measure is only proportional to the posterior because it does not take into account an integration constant. However, when using MCMC sampling this is unimportant because the constant cancels out when calculating the probability for acceptance and rejection. With this simple leaf lifespan constraint in place, we found that all parameters converged for all locations and that leaf lifespan varies substantially across the region, showing that the parameter estimates were not overly influenced by the prior (otherwise all leaf lifespans would have converged on $\hat{\tau}$). Also, parameters not directly affecting $\tau_{95,\mathbf{x}}$ were estimated to have reasonable values,

implying that the model structure, MODIS data, the prior on leaf lifespan, and previous knowledge on other parameters, were all consistent with each other.

We used Metropolis-Hastings MCMC sampling (hereafter MH-MCMC) to provide a set of 600 random samples from $p(\theta_{\mathbf{x}}|Z_{\mathbf{x}})$. MH-MCMC is a widely recognised and simple, albeit computational heavy, method to provide samples from the posterior parameter distribution. MH-MCMC samples this distribution simply by proposing new parameter sets and accepting or rejecting these on the basis of their posteriors, according to a standard Metropolis criterion. Given a sufficient number of steps, the random walk reaches a quasi-equilibrium, after which the average properties of the walk (e.g. the mean and standard deviation as measured against any one parameter) no longer change. After this quasi-equilibrium has been reached, the current position of the algorithm at any one time constitutes a random sample from the posterior (Gelman, 2004). However, there is a great deal of freedom in exactly how to carry out MH-MCMC for a particular case, especially in how new parameter sets are proposed. For our analysis we used Filzbach , a previously tested and robust algorithm.

We allowed 60,000 iterations for the burn-in (the period to quasi-equilibrium), then sampled every 100 iterations from a further 60,000 total iterations, thus providing our 600 samples from $p(\theta_{\mathbf{x}}|Z_{\mathbf{x}})$. From these samples we calculated, for each parameter, the posterior mean, and 95 confidence intervals. All values reported in the paper are posterior means. We have used parameter sets drawn from this distribution to obtain LAI values (Figure 2.2) and then calculate average LAI values and upper and lower 95% confidence bounds for all values.

Filzbach, a software library for carrying out Metropolis-Hastings Markov chain Monte Carlo parameter estimation in C++ or C#. Filzbach is under development in the Computational Science lab at Microsoft Research Cambridge and is available for download, complete with a suite of example uses, via `http://research.microsoft.com/en-us/groups/ecology/ecotechandtools.aspx`

3.2.1 Generating predicted LAI values

In order to both parameterize, and run simulations of, our model, it was necessary to generate predicted LAI values for each location $\mathbf{x}$ and time t, (e.g. see the likelihood defined above). Importantly, as a demographic model, our model as defined in Chapter 2 produces rates of change of the LAI held within different leaf age classes. Therefore, to produce $LAI(\mathbf{x}, t, \theta_{\mathbf{x}})$ it is necessary to first, set an initial leaf age distribution, and second, simulate the model forward in time from this initial state, until we reach time t. The schematic for this is given in Figure 2.2. To make our predictions for a given parameter set $\theta_{\mathbf{x}}$, we set the initial leaf age distribution as $LAI(a, \mathbf{x}, t, \theta_{\mathbf{x}}) = 0$ for all a (corresponding to no leaves) then simulated the year 2000 10 times over, each time beginning the simulated year, using as the initial state the leaf age distribution from the end of the previous simulated year. This acted to spin up the model to produce a reasonable initial leaf age distribution consistent with current parameters. After the spin-up, we then simulated the model forward in time in steps of 8 days, keeping note of $LAI(\mathbf{x}, t, \theta_{\mathbf{x}})$ for all t where we had observations of LAI with which to compare the predictions. Note that, although for the parameter estimation we only used the total LAI, $LAI(x, t, \theta_{\mathbf{x}})$, the model can only be simulated by keeping track of the LAI within each age class, $LAI(a, \mathbf{x}, t, \theta_{\mathbf{x}})$. Thus predicted leaf age distributions emerge as a natural outcome of applying our model.

3.3 Carbon Assimilation Model

To illustrate the impact that our model results have on the carbon cycle in the Amazon, we use a simple canopy model to describe leaf photosynthesis rates. We assume that the only limitation to photosynthesis is light availability, so that

carbon assimilation rates are a linear function of incoming PAR:

$$A(I) = \begin{cases} \phi I - q & , I < I_{max} \\ A_{max} & , I > I_{max} \end{cases} \tag{3.5}$$

where A_{max} is the maximum assimilation rate that occurs after photosynthesis reaches saturation with light for PAR levels above I_{max}. We use literature values (Kubiske and Pregitzer, 1996; Riddoch *et al.*, 1991; Langenheim *et al.*, 1984; Miranda *et al.*, 2005; Hutyra *et al.*, 2007; Kitajima *et al.*, 1997) to obtain an A_{max} of 6.12 μmol $m^{-2}s^{-1}$ and I_{max} equal to 150 μmol $m^{-2}s^{-1}$ (Hutyra *et al.*, 2007). The values cited above have been measured for various locations, species and light environments which we have averaged to obtain a canopy scale value. We then use these values to calculate ϕ and q, by assuming that assimilation is zero at a light level equal to the compensation point C_{direct}.

We use our posterior age distributions to correct photosynthetic rates for the effects of leaf ageing. Studies have shown (Kitajima *et al.*, 1997; Doughty and Goulden, 2008) that in tropical systems photosynthesis rates peak a few weeks after budburst and that measured rates decline with age, reaching half the peak value for leaves older than 1 year. Of course, these figures do not reflect the large variation in leaf lifespan in the Amazon. It has been observed that longer lived leaves show a slower decline in assimilation rates with age and are also slower to reach peak rates (Kitajima *et al.*, 1997).

To account for these changes we use an age correction factor. Assuming that the values defined above are correct for mature leaves, then a population composed entirely of mature foliage will have an age factor of 1, while populations with a combination of young, mature and old leaves will have a factor less than 1. We define this factor as

$$\gamma_{age} = f_{new}A_{new} + f_{mat}A_{mat} + f_{old}A_{old}, \tag{3.6}$$

where f_{new}, f_{mat} and f_{old} are the fractions of young (age$<0.07\tau_{95}$), mature and old (age$> age_{min}$) leaves respectively. The corresponding adjusting factors are equal to 0.05 for young leaves, 1 for mature and 0.5 for old. We assume that the A_{max} and I_{max} values used above are valid for fully mature leaves.

3.4 Predicted leaf litterfall

We compare model predictions against ground-based measurements of leaf litterfall (Table 3.1. This provides an evaluation of the model parameters that is independent of the LAI data used to parameterise the model. All litterfall measurements have been converted from mass units ($gm^{-2}month^{-1}$) to area units ($m^2m^{-2}month^{-1}$) using either the leaf mass per unit area value given by (Fyllas *et al.*, 2009) (94.85 gm^{-2}) or the specific value for that site if any is given in the study (mentioned in brackets).

Table 3.1: Comparison of leaf litterfall as predicted by the model and ground-based measurements across the Amazon basin.

Location	Measured litterfall	Predicted leaf loss	Reference
2°51'S 54°58'W	0.25 - 0.81(8.16)	0.47-0.62	Malhado *et al.* (2009), Doughty and Goulden (2008)
0°25'-1°30'S, 72º30'-70°40'W	0.24-0.55	0.03-0.11	Lips and Duivenvoorden (1996)
11°24'S 55°19'W	0.11-1.42	0.002-0.14	Sanches *et al.* (2008)
4°45'-05°30'N 60°30'-61°22'W	0.17 - 0.72	0.52-0.56	Dezzeo and Chacon (2006)

Chapter 4

A global phenology model based on a carbon benefit approach

4.1 Introduction

Leaf phenology refers to seasonal variations in leaf area, a direct constraint on carbon assimilation (White *et al.*, 1999) and evapotranspiration (Wilson and Baldocchi, 2000), making it essential to understanding global and regional biogeochemical cycles. Phenological cycles are highly dependent on climate and the timing and spatial patterns of phenological dates may change significantly in response to changes in climate (Korner and Basler, 2010). As such, leaf phenology needs to be incorporated in global carbon and climate models, ideally in the form of simple equations based on biological processes, with predictive capabilities. Recent work has shown that existing phenology components of ecosystem models cannot correctly capture seasonal cycles as observed in flux tower measurements and that a better understanding of phenology could improve current predictions of terrestrial systems (Richardson *et al.*, 2012). Here we present a global, process

based phenology model that aims to explain seasonal cycles as a function of environmental variables, allowing us to both understand and predict phenology.

The current understanding of spring phenology is that leaf budburst occurs after a given number of days with a temperature above a certain threshold (Kramer, 1994). Other factors include the photoperiod (day length requirement) and a chilling requirement necessary to prevent budburst after a warm period in winter (Chuine, 2000). Leaf senescence has been less intensely studied, but is believed to depend on either low temperatures or photoperiod (Hänninen *et al.*, 1990; White *et al.*, 1997), while some studies show that this is only dependent on day length and has a fixed date (Keskitalo *et al.*, 2005). The effects of warming on leaf phenology are mostly considered to result in an early spring (e.g. Menzel *et al.* (2006), Thompson and Clark (2008)), but the magnitude of this change varies widely between studies (Korner and Basler, 2010). Also, the combination of chilling effect and warming requirement can, in some species, lead to a late spring (Hanninen, 1990). Some studies have argued that, because of photoperiod constraints in temperate species , this earlier budburst date cannot be proportional to spring warming as a very early date, even if warm, would not have the required daylength (Korner and Basler, 2010). Furthermore, an earlier budburst date is not necessarily directly related to an increase in net ecosystem productivity productivity, as the seasonal response can be varied and associated changes in ecosystem respiration can lead to no net change, as shown by both measurement and modelling studies (Richardson *et al.*, 2010; Parmentier *et al.*, 2011).

The simplest method for describing the phenology component in climate and carbon models is to use prescribed budburst and senescence days (Sellers *et al.*, 1986; Schaefer *et al.*, 2008; Jain and Yang, 2005). Another method is to use satellite-derived vegetation data, which is well suited for large scale phenological studies because of its spatial and temporal coverage. Previous studies have used

satellite vegetation indices, such as NDVI (normalised difference vegetation index) and EVI (enhanced vegetation index) to determine budburst dates (Ju *et al.*, 2006; Medvigy *et al.*, 2009). Most of these studies use time-series techniques to determine onset and offset dates (Ludeke *et al.*, 1996; Zhang *et al.*, 2003). Whilst simple, these approaches lack the capability to predict phenology under a changing climate. The most common approach to describing phenology is to use a temperature dependency, often in the form of a growing degree day model, which uses the sum of days with temperatures above a given threshold, which is often fixed (White *et al.*, 1997; Sitch *et al.*, 2003; Krinner *et al.*, 2005; Knorr *et al.*, 2010). Some models use a carbon efficiency approach to determine phenological cycles and patterns (Arora and Boer, 2005).These model parametrisations often refer only to temperate deciduous forests, ignoring the large areas of dry and moist tropical forests that are often considered to lack a seasonal cycle (Cramer *et al.*, 2001). Dry tropical forests and shrublands are generally thought to lose leaves during dry periods to prevent excessive water loss by plants, but leafing is often asynchronous between species and can occur during the dry season (Borchert, 1994; Reich and Borchert, 1982). In the case of moist tropical forests, studies have shown that these do have a seasonal cycle, with a higher peak in the dry season (Myneni *et al.*, 2007) due to an increase in solar radiation, especially in areas with deep-rooted trees and sufficient water (Nepstad *et al.*, 1994). Caldararu *et al.* (2012) developed a mechanistic model of tropical leaf phenology for the Amazon basin and showed that these seasonal changes can be described as a response to variation in direct and diffuse radiation.

In this paper we present a global process based phenological model, building on the tropical model of Caldararu *et al.* (2012), based on the hypothesis that phenology is a strategy for achieving an optimal carbon gain. We fit this 14 parameter model globally at a resolution of 2° latitude by 2.5° longitude using leaf area index (LAI) data from the MODIS (Moderate Resolution Imaging Spectroradiometer)

instrument (Section 4.2). This can be applied without any prior information about leaf habit (i.e. deciduous or evergreen) or biome and is able to explain and predict phenology in both temperate and tropical regions (Section 4.3). We then present the predicted LAI spatial and temporal patterns (Section 4.4) and use the fitted model to predict growing season metrics (Section 4.4.1) and the spatial distribution of factors which impact phenology across the globe (Section 4.4.2).

4.2 Data

4.2.1 MODIS LAI

We use leaf area index (LAI) data collection 5 from the MODIS (Moderate Resolution Imaging Spectroradiometer) Terra platform. The LAI/fPAR (fraction of absorbed photosynthetically active radiation) product is available at a 1 km spatial resolution (MOD15A) for the period 2000-present and at a temporal resolution of 8 days. The data is split into 1200 km by 1200 km tiles (10° latitude by 10° longitude at the equator). We use tiles for the entire globe for the chosen study (2001-2005) and evaluation (2006) periods (available at `https://lpdaac.usgs.gov/`), corresponding to available GEOS 4 meteorological data.

The MODIS LAI retrievals are based on a reflectance algorithm (known as the main algorithm) which uses red and near infrared surface reflectance, illumination geometry and an eight biome landcover map used to obtain information on vegetation structure and optical properties and soil optical properties (Knyazikhin *et al.*, 1999). In cases where the main algorithm fails LAI values are calculated using an empirical relationship between NDVI and LAI (the back-up algorithm).

The quality flags associated with the LAI product provide information on the algorithm used, atmospheric conditions (cloud and aerosol presence) and snow cover. The data quality is affected mainly by cloud cover in tropical regions and snow at higher latitudes. Preliminary data analysis and ground validation studies (Cohen *et al.*, 2006) have shown that values obtained using the back-up algorithm underestimate LAI, especially in high LAI regions such as the Amazon basin. Snow contaminated pixels also have low quality data. As such, we have eliminated all pixels that were derived using the back-up algorithm or were snow contaminated. We reproject all LAI data from its native sinusoidal projection to an orthogonal grid and spatially average to the GEOS 4 PAR data resolution (Section 4.2.3).

4.2.2 Landcover type

The MODIS landcover product (MOD12Q1) provides 16 landcover classes under the IGBP classification. We have retained forest pixels classified as evergreen (broadleaf and needleleaf), deciduous (broadleaf and needleleaf) and mixed and also open and closed shrublands and woody savannahs. All cultivated pixels have been removed. Tropical forests are classed as >90% evergreen, while mid-latitude forests are classed mostly as mixed, with no clear differences between temperate and boreal forests. We would expect a different leaf seasonality for boreal evergreen forests, with a lower seasonal amplitude, which is not reflected in the MODIS LAI data. This issue can be caused by poor snow detection in areas that are only partly snow covered (Klein *et al.*, 1998; Beck *et al.*, 2006). As such we aggregate all forest types into a mixed forest class. Since we do not have any previous information about the phenology of the different shrub landcover types, we also aggregate all three types into a mixed shrubland class. We need to differentiate between forest and shrubs within a phenology model as the two

broad vegetation types generally have different rooting depth (Nepstad *et al.*, 1994), which is important for describing soil water stress. Our model does not require any further information the type of forest and its phenology type.

4.2.3 Environmental variables

The phenology model described in section 2.3 requires as inputs solar radiation, surface temperature and soil moisture. We use photosynthetically active radiation (PAR) data and surface temperature from assimilated meteorological data products of the Goddard Earth Observing System (GEOS-4) (Bey *et al.*, 2001). The data is provided at a spatial resolution of 2° latitude × 2.5° longitude and a temporal resolution of 3 hours, which we average to a one day resolution. To describe plant water availability within our model, we use volumetric soil moisture from the NCAR/NCEP reanalysis daily average surface flux data set (`http://www.esrl.noaa.gov/psd/data/gridded/data.ncep.reanalysis.surfaceflux.html`) (Kalnay *et al.*, 1996). Prior to model fitting we reproject all data onto the GEOS 4 orthogonal projection grid.

4.3 Phenology model

We present a model of phenology based on the hypothesis that trees adjust their number of leaves in order to achieve the maximum net carbon gain, that is, to achieve carbon optimality. The mechanism for leaf gain and loss account for the overall carbon balance and individual leaf construction costs and decreases in leaf photosynthetic capacity due to ageing. We outline leaf gain and loss processes as a function of temperature, available light, soil moisture and leaf ageing (Fig. 4.1).

4.3.1 Leaf gain

We base the leaf gain mechanism on the tropical phenology model described in Caldararu *et al.* (2012). We assume that trees add leaves in order to achieve the optimal leaf area for light absorption, in response to available PAR so that in the absence of other constraints, such as low temperatures or water stress, maximum LAI will occur at the time of peak solar radiation.

We define the target LAI, LAI_{targ}, as the optimal number of leaves that a tree will seek to achieve given a certain light level at the top of the canopy I_0 (Caldararu *et al.*, 2012). This is calculated as:

$$LAI_{targ} = -\frac{1}{\alpha}\ln(\frac{C}{I_0}), \tag{4.1}$$

where α is the attenuation coefficient and C is a parameter representing the light compensation point, beyond which leaves are no longer able to photosynthesise. To calculate I_0 and the attenuation coefficient throughout the year, we account for variations in solar declination angles and extinction coefficients with both latitude and day of year, according to Brock (1981). We calculate I_0 as the mean radiation over the previous p days. Given this target value, trees will add new leaves if their LAI is lower than LAI_{targ} at a given time t. The leaf production P at location $\mathbf{x}$ and time t is then calculated as:

$$P(\mathbf{x},t) = \begin{cases} gain_{max}, & LAI_{targ}(\mathbf{x},t) - LAI(\mathbf{x},t-1) > gain_{max} \\ LAI_{targ}(\mathbf{x},t) - LAI(\mathbf{x},t-1), & 0 < LAI_{targ}(\mathbf{x},t) - LAI(\mathbf{x},t-1) < gain_{max} \\ 0, & LAI_{targ}(\mathbf{x},t) - LAI(\mathbf{x},t-1) < 0 \end{cases} \tag{4.2}$$

Here the parameter $gain_{max}$ refers to the maximum leaf gain in a given time period and was introduced because trees have a limited leaf production rate.

To describe the role of temperature on phenology, important at higher latitudes,

we include a temperature threshold of 0 °C so that the conditions for leaf gain described above are only active if the average temperature over a number of p days is above this limit. Trial model fitting runs have shown that setting the temperature threshold as a free parameter does not result in an improvement in fit, so this has been set to 0 ° for easier fitting.

4.3.2 Leaf loss

We assume that leaves are lost once the leaf becomes inefficient, that is, once the leaf assimilation rate is lower than its respiration rate and carbon maintenance cost. Depending on biome, the reason for a decrease in assimilation rate can either be a decrease in incoming solar radiation in winter (temperate regions), a decrease in water availability (seasonally dry regions) or, lacking any external constraints, simply leaf ageing (tropical regions).

In its simplest form we can describe carbon assimilation of a mature, unstressed leaf as a linear function of total absorbed PAR, I_{tot}:

$$A_{light} = \phi I_{tot} - q, \tag{4.3}$$

where ϕ and q are parameters representing photosynthetic efficiency and overall canopy compensation point (the light level at which there is no photosynthesis anywhere in the canopy) respectively. At leaf level, carbon uptake saturates with incoming radiation and reaches a maximum value, A_{max}. However, it has been shown (Haxeltine and Prentice, 1996b) that at the canopy level for time periods of one day or longer the relationship is linear due to both the distribution of nitrogen within the canopy and the differences in A_{max} and compensation points for leaves at different depths. As we are looking at large spatial scales over a sufficiently long time period (Section 4.2.1), we use the linear form. We calculate absorbed

PAR, I_{tot} as a function of direct and diffuse PAR at the top of the canopy (I_0, see Section 4.3.1) and LAI, following the sun-shade model of dePury and Farquhar (1997).

As we do not use any prior information for the magnitude of carbon assimilation or the photosynthetic rate we choose to normalise all assimilation values by setting the maximum assimilation rate A_{max} to one (unitless). For any values of I_{tot} that result in a rate greater than one, we set the assimilation to A_{max}.

4.3.3 Water limitation

We know that, as soil water decreases, leaves are forced to partially or fully close their stomata, in order to avoid excessive water loss through transpiration, which leads to a lower carbon uptake. We define a water adjustment factor as:

$$f_w = \frac{S - W_{min}}{W_{max} - W_{min}}, \tag{4.4}$$

where S is the water supply to the trees described as a function of soil moisture W_S (see below), W_{max} is the water level above which soil moisture has no impact on photosynthesis and $f_W = 1$ and W_{min} is the water level at which complete stomatal closure occurs and photosynthesis shuts down ($f_w = 0$). For any water supply S greater than W_{max}, f_w is set to 1, while for S values lower than W_{min}, f_w is set to 0. Both W_{min} and W_{max} are dependent on the existing number of leaves, as shown below.

We express the water demand of a plant as the sum of the water used by the plant and the water lost through evapotranspiration and we assume that, under water stress conditions, trees adjust the number of leaves so that the water demand is equal to the soil water supply. The water available to the tree increases with soil

moisture (Prentice *et al.*, 1993), so that the supply, S is:

$$S = s_1(W_s)^{s_2}, \tag{4.5}$$

given the two water extraction factors, s_1 and s_2.

We can express W_{min} and W_{max} (Eq. 4.4) in terms of water demand. W_{min}, by definition, is the soil water level at which all stomata must be closed, so that there is no evapotranspiration and the water demand is equal to the water use, expressed as a function of the minimum water requirement per unit leaf area, u:

$$W_{min} = uLAI \tag{4.6}$$

W_{max} is the soil water from which there is no water stress, so that no stomatal control is required and water demand is equal to water use plus the maximum evapotranspiration rate per unit leaf area, ϵ:

$$W_{max} = uLAI + \epsilon LAI \tag{4.7}$$

Substituting these into Eq. 4.4, we calculate the water adjustment factor as a function of current LAI and soil moisture:

$$f_w = \frac{s_1(W_s)^{s_2}}{\epsilon LAI} - \frac{u}{\epsilon} \tag{4.8}$$

Here both ϵ and u are fitted parameters and do not vary in time with changes in environmental input, but account for local differences in plant evapotranspiration processes.

4.3.4 Leaf age effects

For each leaf age group we adjust the assimilation rate, as A decreases with age. Following the leaf loss model for tropical regions (Caldararu *et al.*, 2012), the age factor is for each cohort of age a:

$$f_a = min(1, \exp^{\mu(a_{crit}-a)}), \tag{4.9}$$

where μ is the rate of decrease with age after a limit age a_{crit}.

The total carbon assimilation, corrected for water and age effects is then

$$A_{tot} = A_{light} f_w f_a \tag{4.10}$$

Once this value reaches a minimum value A_{min}, making assimilation equal to respiration costs, the specific leaf cohort is lost. We then calculate leaf loss for each age cohort $LAI(\mathbf{x}, t, a)$ as:

$$L(\mathbf{x}, t, a) = \begin{cases} LAI(\mathbf{x}, t, a), & A_{tot}(t, a) < A_{min} \\ 0, & A_{tot}(t, a) \geq A_{min} \end{cases} \tag{4.11}$$

The overall change in LAI at each time step t and location $\mathbf{x}$ is then:

$$\frac{dLAI(\mathbf{x}, t)}{dt} = P(I_0(\mathbf{x}, t), LAI(\mathbf{x}, t-1)) - \sum_{a=0}^{a_{max}} L(\mathbf{x}, t, a), \tag{4.12}$$

where the production and loss processes are defined as in Eq 4.2 and 4.11. We fit the resulting 14 parameter model (Table 4.1 and 4.2) to 5 years of MODIS LAI data (2001-2005) using Filzbach, a Bayesian fitting algorithm (Caldararu *et al.*, 2012).

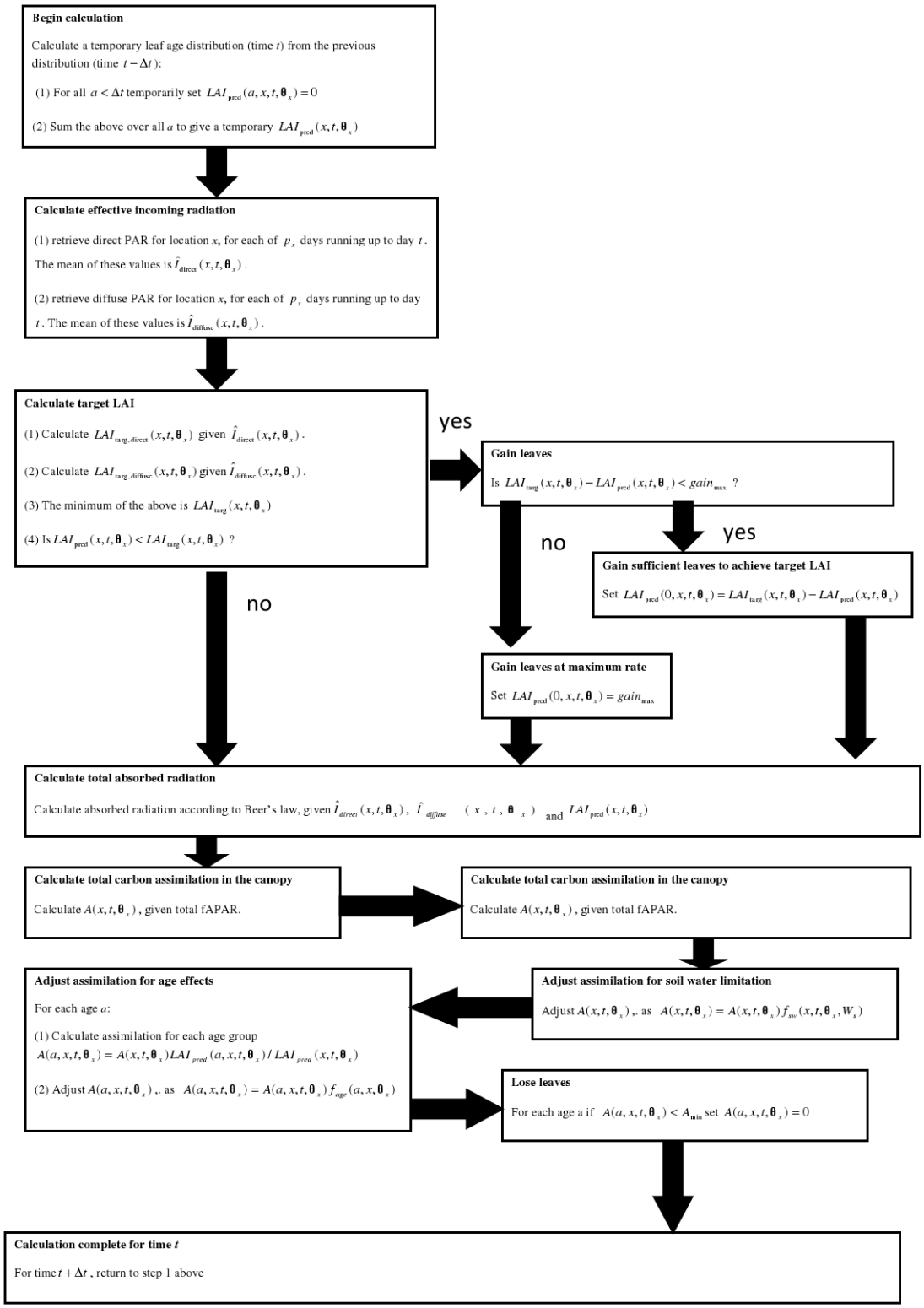

Figure 4.1: Model schematic

Table 4.1: Model parameters for leaf gain processes.

Symbol	Units	Description
C_{direct}	Wm^{-2}	Leaf level light compensation point for direct PAR
$C_{diffuse}$	Wm^{-2}	Leaf level light compensation point for diffuse PAR
p	days	Lag in response to incoming light
$gain_{max}$	m^2m^{-2}	Maximum gain

Table 4.2: Model parameters for leaf loss processes.

Symbol	Units	Description
ϕ	μmol s^{-1} W^{-1}	Photosynthetic efficiency
q	μmol m^{-2} s^{-1}	Canopy level compensation point
s_1	-	Plant water uptake parameter
s_2	-	Plant water uptake parameter
ϵ	mm	Evapotranspiration per unit leaf area
u	mm	Plant water use per unit leaf area
a_{crit}	years	Age after which leaves start ageing
μ	$years^{-1}$	Decay constant of photosynthesis with age
A_{min}	μmol m^{-2} s^{-1}	Assimilation rate equal to leaf maintenance costs

4.4 Results

Figure 4.2 shows that the model LAI generally agrees with the MODIS data, predicting the highest values of mean LAI in the tropical regions (3.4 $\pm$ 0.6 m^2m^{-2}) with values of up to 5.4 m^2m^{-2} in the central Amazon and Central Africa. Temperate regions have a lower mean LAI (1.2 $\pm$ 0.3 m^2m^{-2}) with higher values in the deciduous Eastern US and Europe. The temperate regions exhibit a higher seasonal amplitude of 1.9 m^2m^{-2} ($\pm$ 0.4 m^2m^{-2}), equivalent to 90% of

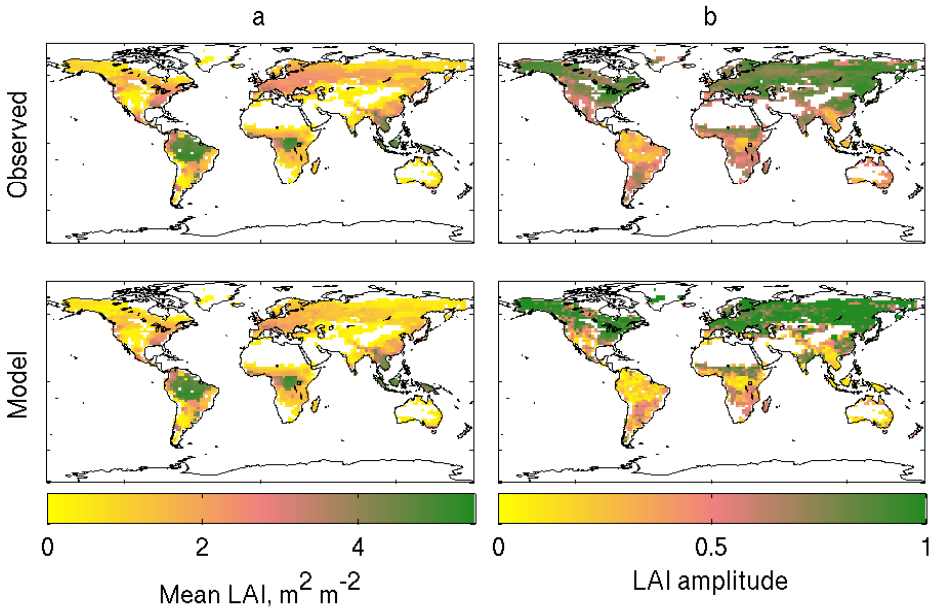

Figure 4.2: (a) Mean observed MODIS (top) and predicted (bottom) LAI and (b) relative annual amplitude expressed as the seasonal amplitude normalised by the maximum LAI value.

the maximum LAI while tropical forests have a much lower amplitude of 0.9 $\pm$ 0.3 m^2m^{-2}, representing only 30% of the maximum, as expected for evergreen tropical regions.

Figures 4.3 - 4.6 show posterior parameter means and Figure 4.5 shows 95% confidence intervals for all model parameters, which allows a further interpretation of the model results. The compensation point parameters (C_{direct} and $C_{diffuse}$), together with the magnitude of incoming PAR at the top of the canopy effectively limit the maximum possible LAI, a lower compensation point being an indication of higher maximum LAI. The direct compensation point, C_{direct} is higher in temperate forests (Fig. 4.3), reflecting the higher light availability in the tropics.

The diffuse compensation point is much more spatially heterogeneous and better constrained in tropical forests where the combined seasonal cycles of the direct and diffuse PAR drive changes in LAI (Caldararu *et al.*, 2012). The $gain_{max}$ parameter is a measure of how fast the forest is able to respond (by adding leaves) to favourable conditions. We show that places with shorter growing seasons have a higher $gain_{max}$ relative to the mean LAI to allow a quick response at the start of the favourable season.

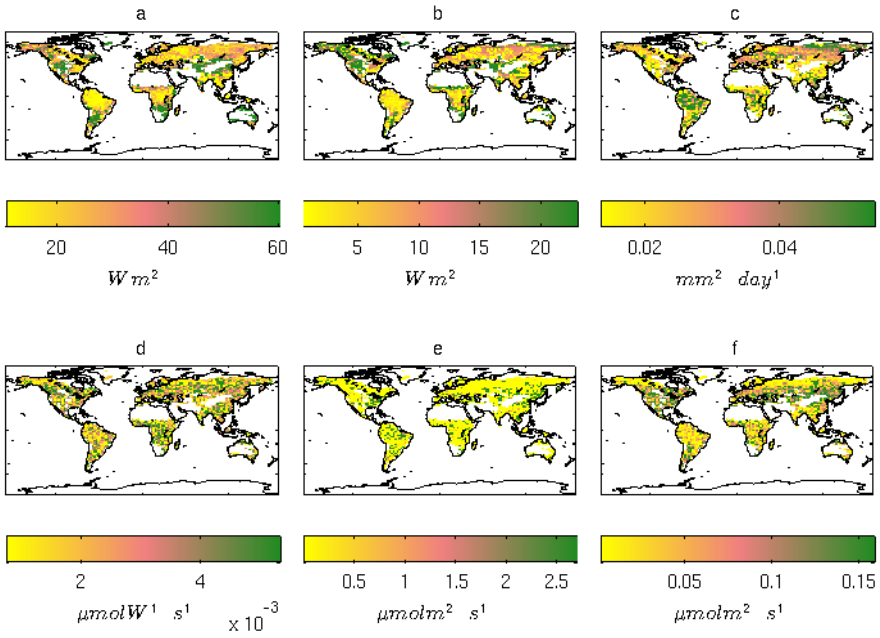

Figure 4.3: Posterior parameter values describing leaf gain and carbon assimilation: (a) direct compensation point, C_{direct}, (b) diffuse compensation point $C_{diffuse}$, (c) maximum gain $gain_{max}$, (d) photosynthetic efficiency ϕ, (e) canopy compensation point q and (f) assimilation limit A_{min}.

The two photosynthetic parameters, ϕ and q, represent the efficiency with which the forest can use available PAR. We acknowledge that these values are part of a phenological model and might not necessarily reflect leaf level measurements of equivalent characteristics. Figure 4.3f shows that the minimum assimilation

level that can still sustain leaves, A_{min}, is higher in temperate regions, indicating that these regions have higher sensitivity to unfavourable conditions such as low temperatures or low light levels.

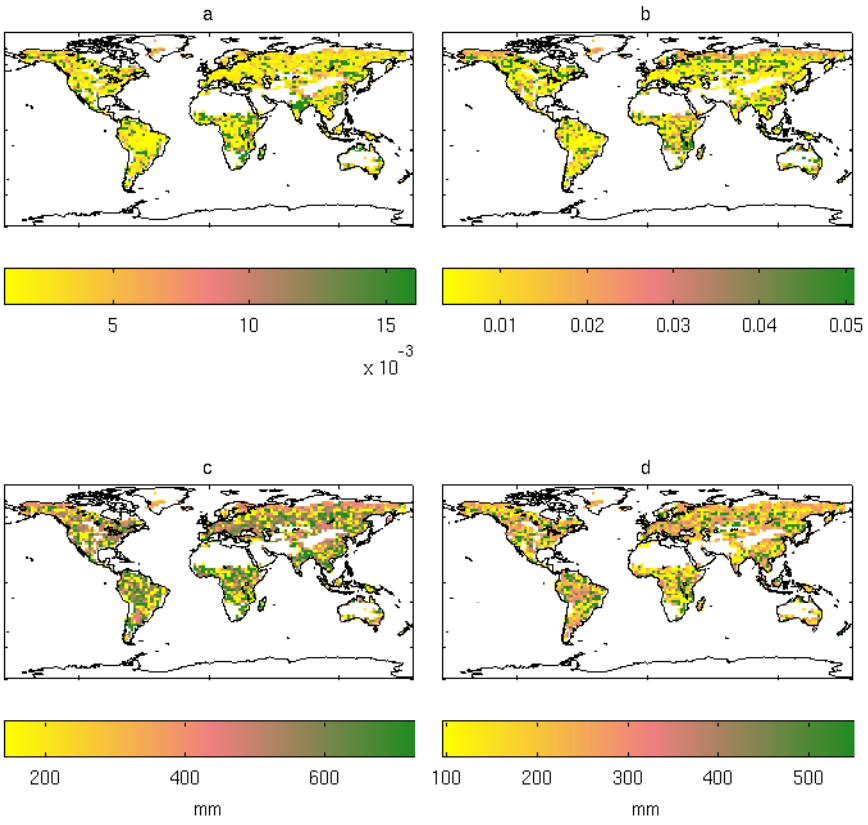

Figure 4.4: Posterior parameter values describing soil water effects: (a) and (b) soil water extraction parameters s_1 and s_2, (c) water use u and (d) evapotranspiration rate ϵ

The two parameters used to calculate plant water extraction, s_1 and s_2, are a measure of how much soil water is available for use by plants and reflect both the soil structure and root depth (Fig 4.4). The water demand and evapotranspiration parameters determine the extent to which carbon assimilation is affected by water availability. High water use implies a high sensitivity to available soil water,

but plants in water limited areas (e.g. the African savannah) are generally well adapted to low water conditions and exhibit a water limited seasonal cycle not because of their high water sensitivity but because of the very low soil moisture during the dry season. These four parameters are generally less well constrained over regions that are not impacted by water stress (Fig. 4.5).

Figure 4.6b shows the average age of the oldest leaf at any one point in time. As expected, leaves in tropical areas have longer leaf lifespans, while leaves in temperate regions never have leaves older than 1 year and mostly younger than 6 months (approximately equal to the growing season). We find that the leaf lifespan is not identical to the limit age parameter age_{crit}, particularly in temperate forests where the average age_{crit} is 1.4 years (Fig. 4.6a) but leaves always drop at the end of the favourable season, making the effective leaf age equal to the growing season. The two age related parameters are less well constrained within these regions (Fig. 4.5) as their effects are not observed.

4.4.1 Growing season

The length of the growing season is a valuable indicator of changes in phenology in response to climate. The definition of the growing season varies with the type of data used. For direct observations of budburst, the start of the growing season is defined as the date of first budburst and refers to single leaves. When using satellite data, the start of the growing season, at landscape scale has previously been defined using a threshold for vegetation indices or as the inflection point based on a fitted curve (White *et al.*, 1997). In studies which use flux tower data, the growing season is defined as the period in which GPP is higher than respiration rates, once again at landscape level (Richardson *et al.*, 2010), which is especially useful for evergreen boreal forests, which maintain leaf cover all year round.

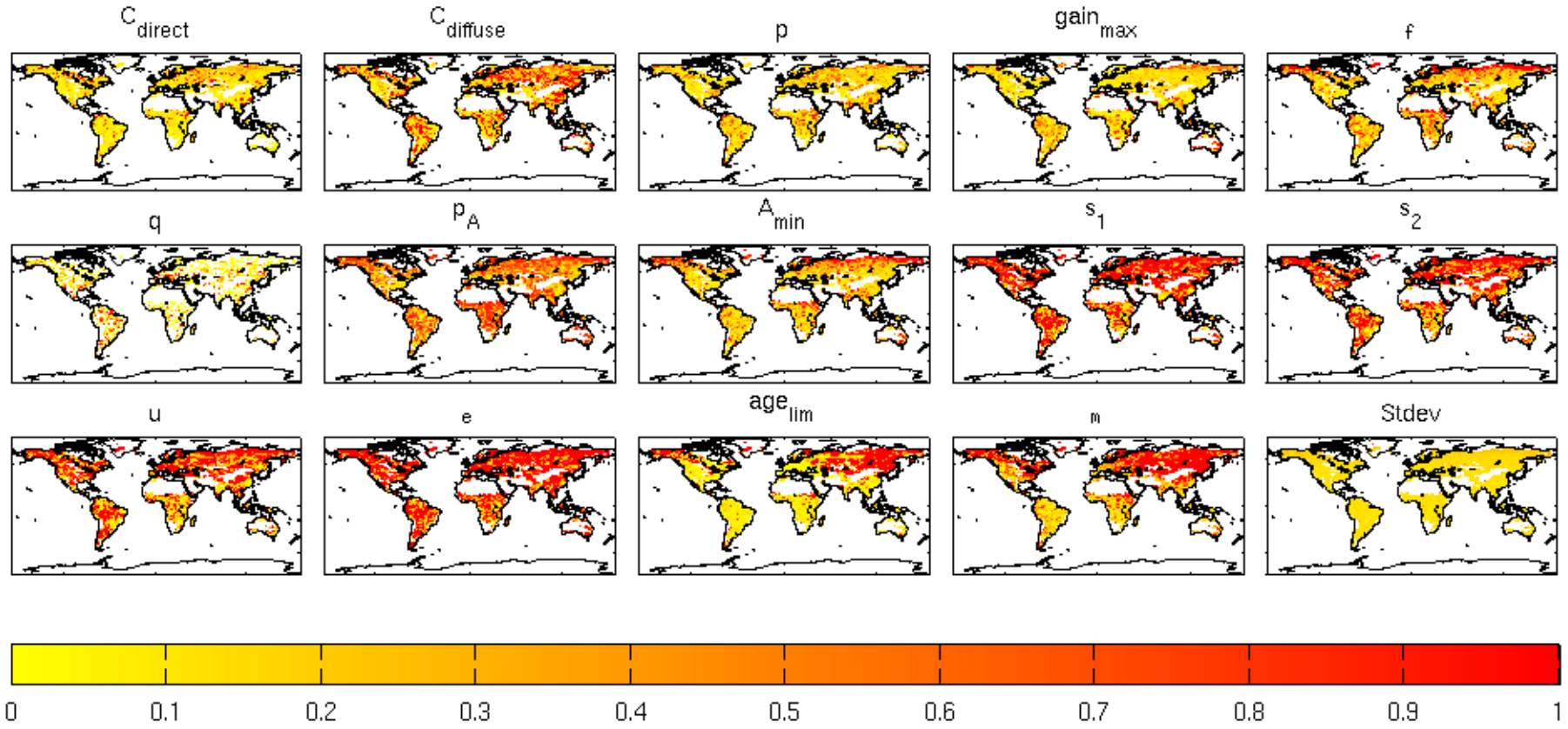

Figure 4.5: Relative 95% confidence intervals for all parameters derived from the posterior distribution. For parameter descriptions see Table 4.1 and 4.2 and Section 2.3.

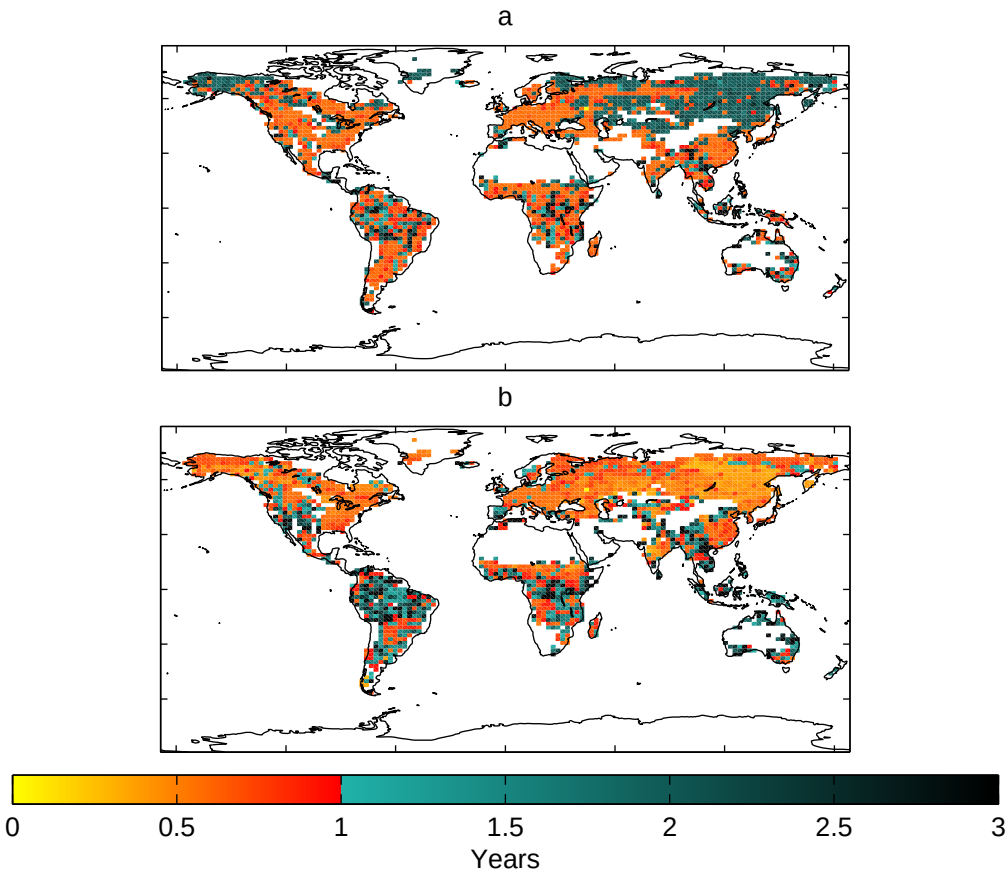

Figure 4.6: (a) Posterior parameter value for leaf ageing limit a_{crit} and (b) realised age of oldest leaves

For the purpose of comparing our results with other ground based studies (e.g. Richardson *et al.* (2012)), we define the growing season as the period over which the LAI value exceeds 0.2 of the maximum observed LAI in an average year, following Richardson *et al.* (2012). Figure 4.7 shows the average length of the growing season for the 5 years of the study period. We show that in tropical areas the length of the season covers the whole year, indicating that the trees are active throughout the year, whilst at higher latitudes the growing season is on average 225 days, decreasing with latitude (Fig. 4.8b). Figure 4.8a shows the variation in start and end date of the growing season for both forests and shrubs.

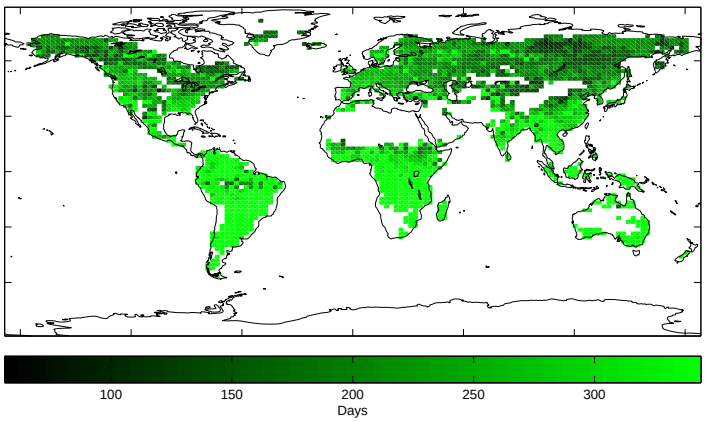

Figure 4.7: Length of growing season. All values are calculated for an average LAI for the 2000–2005 study period.

The start date for forest pixels varies from day 68 at 30° N to day 120 at 66° N. The shrubs follow the same trend with generally later start days. The end day of the growing season varies from day 285 to day 341.

The model predicts that high latitude, boreal areas have a short growing season and drop all or most of their leaves during winter, which contradicts observations of evergreen boreal forests. This behaviour is also observed in the MODIS LAI and has been explained by the difference between species and landscape-level phenology (Rautiainen *et al.*, 2012). The MODIS LAI captures the vegetation changes at the landscape level, often including forest gaps and the deciduous understory, which would lead to a stronger seasonal cycle (Rautiainen *et al.*, 2012). Also, pixels that are only partially snow covered at the start and end of winter may not be flagged as snow contaminated and hence not eliminated in the filtering process. This can lead to unrealistic lower LAI values.

Table 4.3: Comparison of model growing season dates with ground based budburst and senescence dates (day of year). Model dates are expressed as 20% and 50% canopy development in spring and canopy remaining in autumn. Ground based data was obtained from the Fluxnet fair-use database.

Site	Coordinates	Model 20% developed	Model 50% developed	Flux site budburst	Model 50% remaining	Model 20% remaining	Flux site leaf fall
Barlett Experimental Forest	44.66° -71.29°	48	104	133	272	280	302
Lost Creek	46.08° -79.98°	112	136	123	240	288	272
Morgan Monroe State Forest	39.32° -86.41°	80	120	113	256	312	292
Tonzi Ranch	38.43° -120.97°	80	104	225	288	304	148
Univ. of Michigan Biological Station	45.56° -84.71°	72	120	131			
Willow Creek	45.81° -90.08°	112	136	123	240	288	272

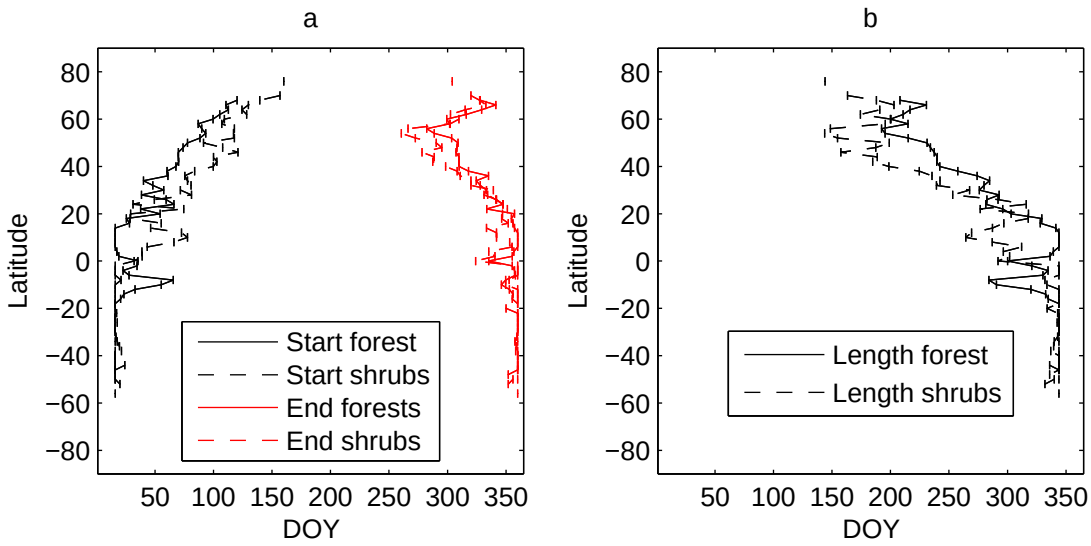

Figure 4.8: Variation in growing season (a) start date and end date and (b) length with latitude for forests and shrubs.

The model tends to predict the start of the growing season 16 days earlier than the observed MODIS LAI and the end of the growing season 24 days later on average. We must take into account that the temporal resolution of both the model and MODIS data is 8 days, making these differences only 2 and 3 time steps respectively. Table 4.3 shows ground based budburst and senescence dates respectively, measured at flux tower sites with available phenology data obtained from the FLUXNET network. The difference between observed and model start dates is on average 15 days, with the exception of the Tonzi Ranch site, which is a sub-tropical grassland and which includes both grass and oak leafing dates, variation which cannot be captured by our model due to the coarse spatial resolution. Our model generally predicts a later end date than site measurements by approximately 16 days. The fact that ground based budburst dates are closer to the date of 50% canopy development in our model suggests that the satellite data also captures leafing in the understory, which generally leafs out earlier.

4.4.2 Phenological limiting factors

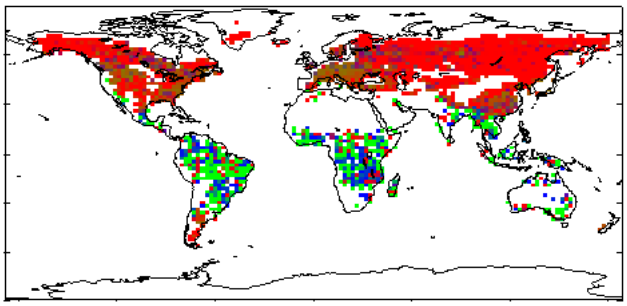

Figure 4.9: Regions where leaf loss is driven by temperature and light availability (red), water (blue) or age (green) as predicted by the model.

The fitted model parameters allow us to identify regions with a common limiting factor, i.e. light, soil moisture or leaf ageing using the three different triggers for leaf loss. Light and temperature limited regions are regions where the light response assimilation A_{light} is lower than the assimilation limit A_{min}, while in water limited areas $A_{light}f_w$is lower than the limit. Age limited areas are regions where only $A_{light}f_w f_{age}$ is lower than the threshold. In practice, some regions will show a combination of these three limitations, in particular regions on the edge of wet tropical forests. We calculate the relative importance of these three factors by comparing the number of days in a year when any of the three conditions described above are true. Figure 4.9 shows that the Amazon basin and parts of central Africa and South-East Asia are limited only by leaf ageing, indicating that the vegetation in these areas is wet tropical forests, while the drier sub-tropical areas around these forests are limited by water availability and/or leaf ageing. Vegetation at higher latitudes is limited by temperature and light availability but

the more deciduous forests in Europe and eastern US show some influences of leaf age, which agrees with field observations which show that autumn senescence has a fixed date (Keskitalo *et al.*, 2005).

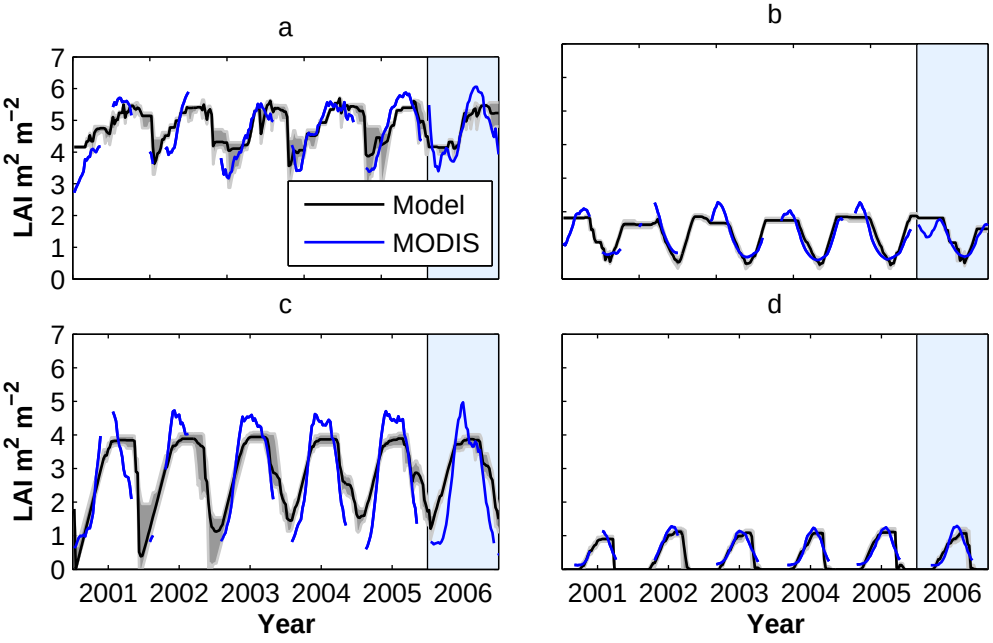

Figure 4.10: Predicted (black) and observed (blue) LAI for (a) tropical wet forests (6S 55W), (b) tropical dry forests (14S 20E), (c) temperate deciduous (46N 15E) and (d) temperate evergreen (54N 120E). Gray shaded area represents 95% confidence intervals calculated from the parameter posterior distribution. The blue shaded area (2006) represents the model evaluation period.

4.5 Model evaluation

We evaluate our results by running the model for 2006, year which has not been used in the model fitting, to asses the predictive capability of the model. Figure 4.10 shows LAI timeseries for both the fitting and validation period for four major

vegetation types. The model captures both the magnitude and seasonality of LAI at all four locations, with no major errors for the evaluation period.

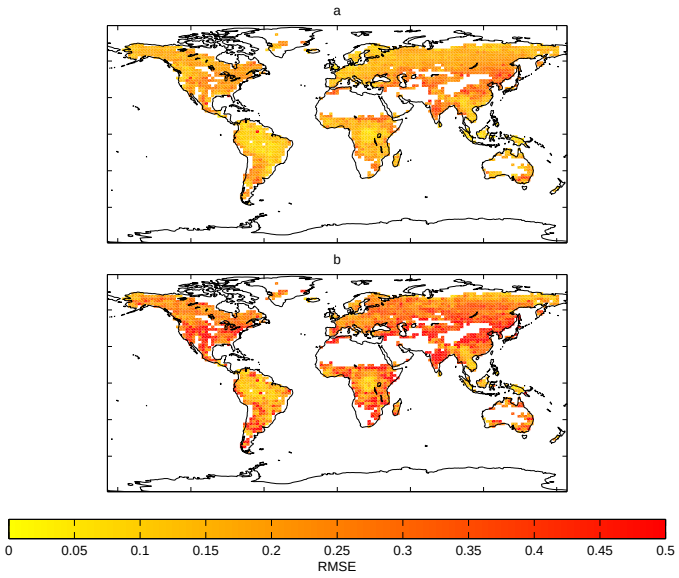

Figure 4.11: Root mean squared error (RMSE) of predicted LAI normalised by mean LAI for (a) the study period (2000–2005) and (b) the evaluation period (2006) .

Figure 4.11 shows the overall model error, expressed as root mean squared error (RMSE) relative to the mean LAI for both the fitting and evaluation periods. For the fitting period (Fig. 4.11a) the error is around 0.18, with higher values of up to 0.3 for shrubland regions. For the evaluation run, the RMSE is on average 0.25, slightly higher than that for the fitting period and follows the same spatial pattern, with higher values for shrublands. The model explains 99% of the spatial variation in mean LAI and 92% of the variation in amplitude for the model fitting period and 97% and 85% respectively for the mean and amplitude of the evaluation period. Figure 4.12 shows the relative difference between model and observed mean and amplitude. Our model underestimates the mean LAI value mostly at higher latitudes by 25 % (compared to only 2 % in the tropics). This bias increases with latitude, from 8.8 % at 30° N up to 37.5% at 54 ° N. The evaluation run shows similar differences. The model tends to underestimate

the seasonal amplitude in tropical regions by about 0.1 for both the fitting and evaluation period.

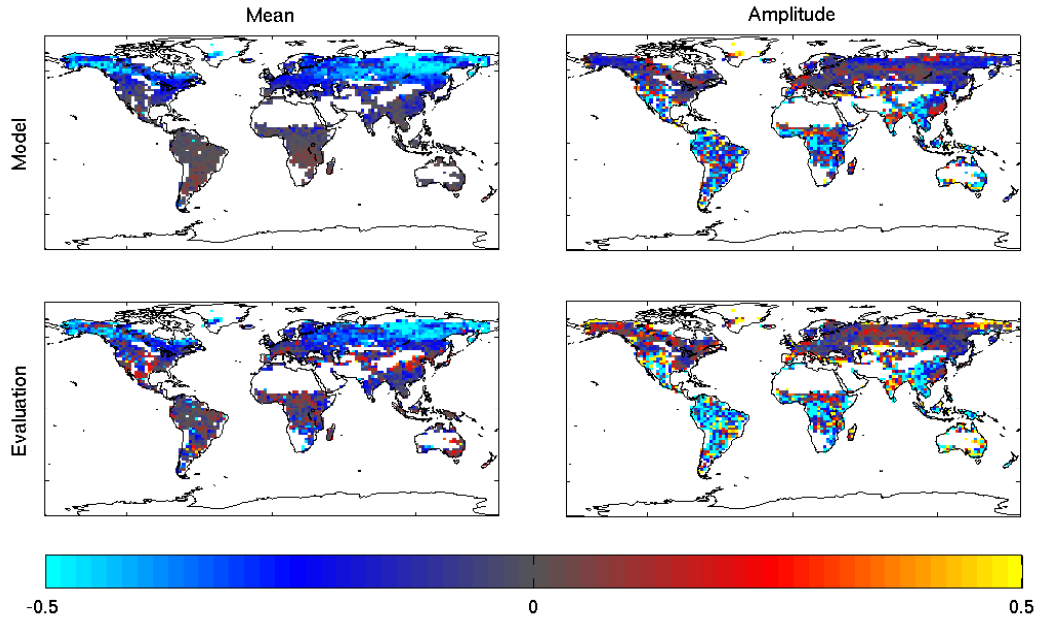

Figure 4.12: Relative model bias in mean LAI (left) and seasonal amplitude (right) for the model training period 2001-2005 (top) and evaluation period 2006 (bottom).

The evaluation shows that the model is able to predict phenology, but a longer time series would be necessary to fully explore the flexibility of our model, by including more extreme conditions, such as drought years. A longer evaluation period would also allow us to explore model error for a longer time span.

4.6 Conclusions

We present a mechanistic phenology model for the globe based on the assumption that trees adjust their leaf gain and loss to achieve optimal carbon assimilation

at the canopy level. We fit this model to 5 years of MODIS LAI data using a Bayesian fitting algorithm. We show that the model is able to capture the spatial and seasonal patterns of phenology for all biomes and can predict various phenology metrics such as growing season length. We believe that our model can improve current understanding of phenology and has the capacity to provide the necessary phenological information for earth system models. further model, such a mechanistic model has the flexibility necessary to predict phenology under future climate.

Chapter 5

Plant functional types vs. species traits: what is the best scale for phenology models?

5.1 Introduction

Leaf phenology, which refers to the timing of leaf seasonal events, is essential to understanding the earth system through impacts on the carbon and water cycles (White *et al.*, 1999; Wilson and Baldocchi, 2000) and climate (Hayden, 1998). Leaf seasonal cycles are most commonly described through a temperature dependency, so that leaf budburst starts in spring once the air temperature is higher than a certain threshold (e.g. Kramer (1994)), which implies that phenological patterns can change in future climates. Previous studies have shown that budburst is starting earlier in response to higher temperatures in spring (Menzel *et al.*, 2006; Thompson and Clark, 2008), but future impacts are still uncertain due to other factors influencing spring phenology such as daylength

(Korner and Basler, 2010) and low winter temperatures (Chuine, 2000). This stresses the fact that phenology is an essential component of earth system and ecosystem carbon models, but the best way to parametrise these processes is still unclear.

There are two main approaches to developing global scale models. Within the so-called bottom up models, model parameter values are obtained using field measurements at point locations. While this approach can give good results for small scale ecosystem models for which data is available (Braswell *et al.*, 2005; Keenan *et al.*, 2012), for global scale models those point measurements are scaled up to the globe based on plant functional types (PFTs) or biomes (Sellers *et al.*, 1996; Haxeltine and Prentice, 1996a; Kucharik *et al.*, 2000; Sitch *et al.*, 2003). Biomes are regions where vegetation has similar characteristics (Smith, 1997) and is found within certain bioclimatic regions (Prentice *et al.*, 1992; Haxeltine *et al.*, 1996). This is a technique often used in phenology models, as traditionally long term data on phenological cycles only exists in a few locations for individual species. Behind this approach lies the underlying assumption that all the vegetation in the same PFT has exactly the same behaviour and while this attribute lies at the base of the PFT definition it is unclear whether this hypothesis is true for every process and has not as yet been tested at large scales.

An alternative modelling approach is to fit the model using existing data through a data assimilation algorithm (Raupach *et al.*, 2005). This approach is frequently used for ecological models at local scales as the necessary data for model fitting is more readily available at such scales (Friend *et al.*, 2007; Fox *et al.*, 2009). The procedure can also be used at a larger scale, fitting the model on a given grid, often using satellite based data (e.g. Caldararu *et al.* (2012)). In such a situation, if we assume that the vegetation in each cell is completely independent from all other cells, the resulting number of parameters can be very large. Grouping the

cells based on similar vegetation behaviour before fitting would result in fewer parameters but again raises the question of plant traits within a PFT.

In a previous study (Caldararu *et al.*, 2013) a mechanistic phenology model was fitted on a global grid with parameters specific to every grid cell (Chapter 4). In this study we build on this to explore the extent to which vegetation within the same PFT exhibits similar phenological behaviour in response to environmental variables. To this purpose we use three different model setups (Section 5.2) to include a grid- and PFT-based fitting method. We fit the three different methods to five years of leaf area index (LAI) data from satellite observations (Section 5.3). We then compare the results of the different model setups in Section 5.4 and show that a PFT wide model cannot fully explain the spatial variation in phenology.

5.2 Model fitting

5.2.1 Model description

We use a global scale mechanistic phenology model (Caldararu *et al.*, 2012) which is based on a carbon benefit approach. Leaf gains and losses are adjusted to achieve the optimal carbon assimilation at the canopy level. The model has three different leaf loss components to account for the different drivers across the globe: light, soil water availability and leaf ageing (see Section 4.3). Table 4.1 and 4.2 show a summary of model parameters.

5.2.2 Model setup

The above model has previously been fitted at each location on the globe on a 2° latitude by 2.5° longitude grid, so that each location has its own set of 14 parameters. This approach implies that every location has a specific phenological behaviour. We will term this the 'location' model. Whilst this gives a good fit to the data, this approach involves a very large number of parameters (28574 parameters for all vegetated grid cells).

An alternative approach is to fit one parameter set (14 parameters) to a PFT, assuming that all vegetation within a PFT has the same phenological behaviour and the observed differences in the LAI seasonal cycle are due entirely to the differences in the environmental input. This results in a much simpler model, with only 182 parameters for the entire globe. We term this the 'PFT' model.

It can be considered unrealistic for plants to not have any location specific traits. As a combination between the location and PFT models we test a model setup in which one or more parameters are location specific while the rest have PFT wide values, with the underlying assumption that some characteristics of leaf phenology are dependent on location specific variables that are not included as input to the model, discussed below. We then term a parameter 'local' if it has a specific value at each grid cell. As there are a very large number of possible combinations of local parameters, we perform an initial analysis to determine which parameters would improve the model fit, if local. Assuming the parameter values obtained from the local model are correct within given confidence intervals, we perform principal component analysis (PCA) on these values to explore spatial variation in parameters. Results show that the main axis of variation correlates with the direct compensation point parameter C_{direct} (see Table 4.1 and 4.2 for parameter descriptions). We then fit 14 different model setups by having each parameter as a local parameter in turn. The model fit shows that the compensation point

is the only parameter that improves the fit significantly. Here we only discuss in detail one combination model, where the C_{direct} parameter is local. These initial model runs have also shown that the phenological characteristics of the different evergreen tropical regions (i.e. the Amazon basin, the Congo basin and South-East Asia and Borneo) are radically different. For the purpose of this analysis, the tropical evergreen PFT refers solely to the Amazon basin and future work will incorporate the other tropical regions.

We fit the three models using a custom Markov Chain Monte Carlo (MCMC) algorithm, known as the Filzbach algorithm, which has been described in detail in Caldararu *et al.* (2012) and Chapter 3. This is a search algorithm used to minimise the likelihood of the observed data Z given a model parameter set θ. For the local model setup this likelihood is minimised independently at each location $\mathbf{x}$ and is calculated as:

$$l(Z_{\mathbf{x}}|\theta_{\mathbf{x}}) = \sum_{t(\mathbf{x})} \ln[n(LAI_{obs}(\mathbf{x},t), LAI_{pred}(\mathbf{x},t,\theta_{\mathbf{x}}), \sigma_{\mathbf{x}})] \tag{5.1}$$

where $LAI_{pred}(\mathbf{x},t,\theta_{\mathbf{x}})$ is the predicted LAI at location $\mathbf{x}$ at time t (this depends on the model parameters $\theta_{\mathbf{x}}$); $LAI_{obs}(\mathbf{x},t)$ is the observed MODIS LAI at location $\mathbf{x}$ at time t; and $n(LAI_{obs}(\mathbf{x},t), LAI_{pred}(\mathbf{x},t,\theta_{\mathbf{x}}), \sigma_{\mathbf{x}})$ denotes the probability density for observing $LAI_{obs}(\mathbf{x},t)$ given a normal distribution with mean $LAI_{pred}(\mathbf{x},t,\theta_{\mathbf{x}})$ and standard deviation $\sigma_{\mathbf{x}}$ which expresses the magnitude of unexplained variation in LAI. The likelihood is calculated as a sum over all time steps at location $\mathbf{x}$, expressed as $t(\mathbf{x})$.

For the PFT model, the minimisation procedure is carried out at the PFT level, the likelihood being calculated as the sum at all locations $\mathbf{x}$ within a PFT $\mathbf{B}$, $\mathbf{x}(\mathbf{B})$:

$$l(Z_{\mathbf{B}}|\theta_{\mathbf{B}}) = \sum_{\mathbf{x}(\mathbf{B})} \sum_{t(\mathbf{x})} \ln[n(LAI_{obs}(\mathbf{x},t), LAI_{pred}(\mathbf{x},t,\theta_{\mathbf{B}}), \sigma_{\mathbf{B}})] \tag{5.2}$$

Here $Z_{\mathbf{B}}$ and $\theta_{\mathbf{B}}$ denote observed LAI and model parameters for a given PFT **B**. Within the combination model, the likelihood is again minimised for a whole PFT but in addition to the PFT level parameters $\theta_{\mathbf{B}}$ the predicted LAI is also a function of local parameters $\theta_{\mathbf{B},\mathbf{x}}$.

5.2.3 Goodness of fit metrics

To compare the different types of models described above, we define several goodness of fit metrics. The best model should be able to capture both the timing and magnitude of the seasonal cycle at each location and the spatial variability in seasonal cycles across the globe. As an overall measure of fit we use the root mean squared error (RMSE) normalised by the mean LAI which is a measure of the fit at each particular location. The mean LAI and LAI amplitude describe the magnitude of the seasonal cycle and we use the percent of variation explained to capture the extent to which the model describes their spatial distribution. Similarly, we use the start and end of the growing season to describe the timing. We define the start of the growing season as the first date of the year when the LAI reaches 0.2 of the maximum LAI, while the end of the growing season is the equivalent last date. To capture the timing in tropical areas with a less pronounced seasonal cycle, we also use the timing of maximum LAI.

5.3 Datasets used

5.3.1 LAI data

In this study we use leaf area index data from the Moderate Resolution Imaging Spectroradiometer (MODIS) on board the Terra platform. We use the MODIS

collection 5 product MOD15A which is available at 1 km spatial resolution and an 8 day time step (`https://lpdaac.usgs.gov/`). The MODIS LAI is based on a reflectance algorithm which uses the red and near infrared bands and includes corrections for canopy structure and background soil reflectance (Knyazikhin *et al.*, 1999). In cases where this main algorithm fails, a back up algorithm is used, which is based on an empirical relationship between LAI and NDVI (normalised difference vegetation index). In the present study we use the quality assurance flags provided with this product to filter pixels that were derived using the back up algorithm or which are classified as snow covered, as described in Caldararu *et al.* (2013). We regrid the data to the GEOS-4 base resolution of 2° latitude by 2.5° longitude.

5.3.2 Environmental variables

We use temperature and photosynthetically active radiation (PAR) data from assimilated meteorological data products of the Goddard Earth Observing System (GEOS-4) (Bey *et al.*, 2001), which is available at a spatial resolution of 2° latitude by 2.5° longitude and a temporal resolution of 3 hours, which we average to a one day temporal resolution. The soil moisture data required in the model was obtained from the NCAR/NCEP reanalysis daily average surface flux data set (`http://www.esrl.noaa.gov/psd/data/gridded/data.ncep.reanalysis.surfaceflux.html`) (Kalnay *et al.*, 1996).

5.3.3 Biome map

Both the PFT and combination models (section 5.2) require information on vegetation type. We use a global PFT map which is used in the Integrated Biosphere simulation model (IBIS) (Kucharik *et al.*, 2000). This differentiates

between 13 different plant functional types based on general plant properties (trees vs. grasses), temperature tolerance (tropical vs. temperate) and leaf habit (deciduous vs. evergreen). The PFT data is provided at a 1 km spatial resolution, which we re-grid at the GEOS 4 native resolution.

5.4 Results

Figure 5.1 shows the overall model error for all the different model setups. The PFT model has a much greater error than the local one, with a higher spatial variability between PFTs. RMSE values are much higher for the PFT model than for the local model, 0.7 $\pm$0.5 compared to only 0.2 $\pm$ 0.02. The combination model has a slightly lower error of 0.6 $\pm$ 0.6. These errors are much lower for tropical forests, typically 0.1 for the local model, compared to 0.3 for the PFT and 0.2 for the combination models. Similar errors occur in temperate deciduous areas. The highest errors are observed in high latitude grasslands for all models and specifically for the PFT model (0.7). Figure 5.2 shows the relative difference between model and observed LAI mean and amplitude. Both the location and combination models underestimate the mean LAI across all PFTs by 15.6 % and 32.0% respectively. The PFT model exhibits a higher bias, with a mean value of 43.4%, with the highest difference in tropical and temperate deciduous regions (over 90%). The PFT model underestimates the seasonal amplitude in tropical and boreal regions by up to 50% and overestimate it by 200% in subtropical and boreal regions. The combination model shows a similar pattern but a lower bias, with differences of 30% in tropical forests and 10% in temperate areas, similar to those of the location model.

Figures 5.3 and 5.4 show a comparison of predicted and observed LAI mean and amplitude for forest and grass PFTs respectively. The PFT model captures the

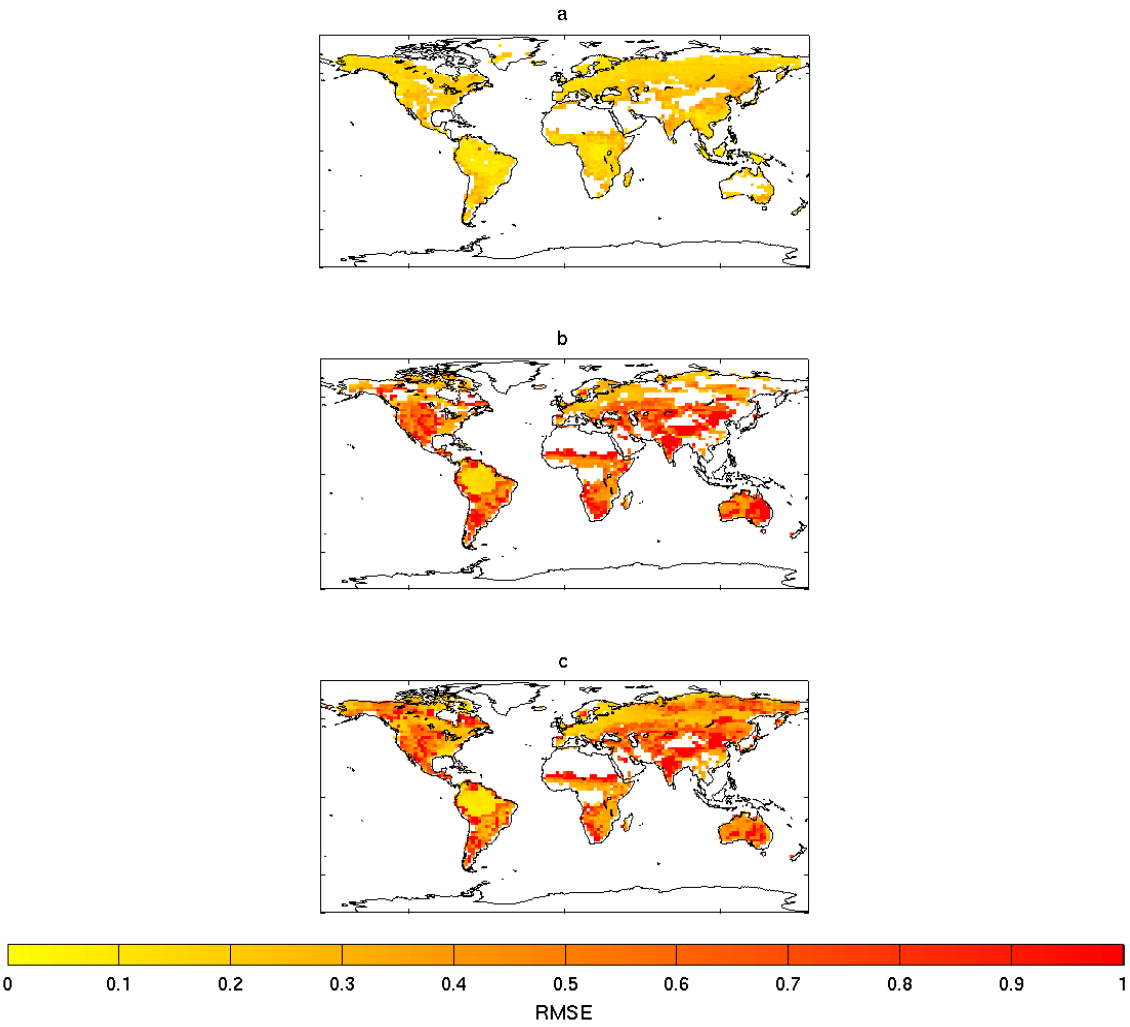

Figure 5.1: Root mean squared error (RMSE) for the (a) local, (b) PFT and (c) combined models. All values have been normalised to the mean observed LAI at all locations.

mean behaviour but is not able to predict the full range of values in either mean LAI or seasonal amplitude for any PFT, explaining on average only 20% and 10% respectively of the spatial variation in LAI mean and amplitude. The combination model shows an improvement in the mean LAI prediction, explaining on average 60% of the spatial variation but the amplitude is not as well predicted, only 30% across the globe, but with higher values in the temperate PFTs (50%).

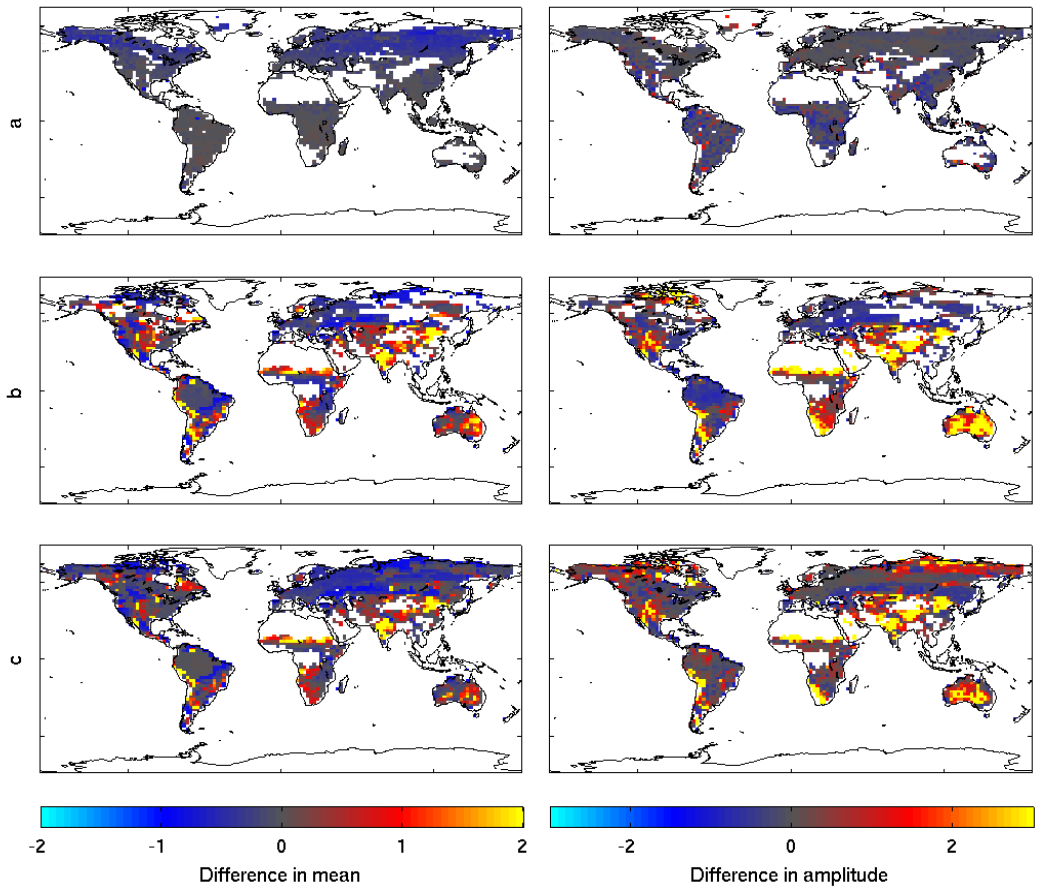

Figure 5.2: Difference between predicted and observed mean LAI (left) and seasonal amplitude (right) for the (a) local, (b) PFT and (c) combined models. All values have been normalised to the mean observed LAI at all locations

All models show a similar ability to predict the timing of the seasonal cycle, with an error of 16 days for the start of the growing season and differences of up to 30 days for the maximum and end of the growing season, with the exception of tropical evergreen forests where the time of maximum LAI is 2 months later compared to that shown by the MODIS data (Fig. 5.5).

Figure 5.6 shows LAI time series for four different PFTs. At the tropical evergreen

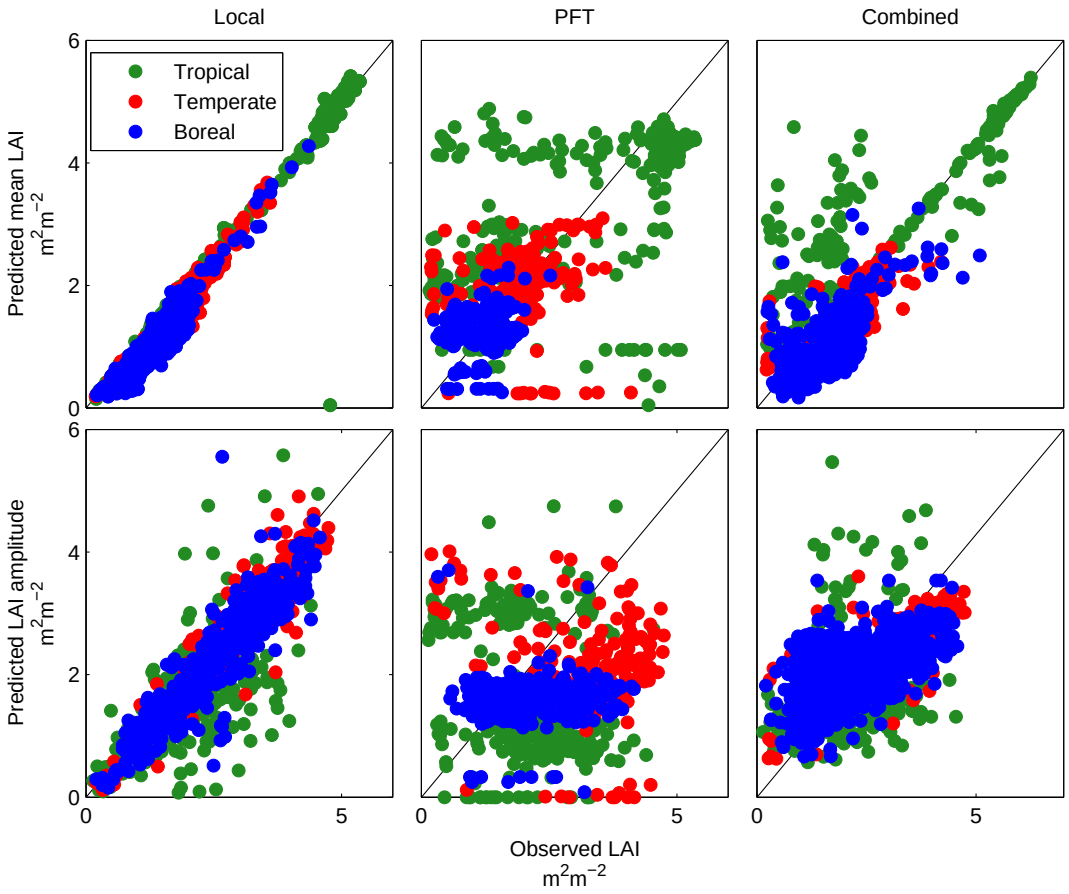

Figure 5.3: Comparison of predicted and observed mean LAI and seasonal amplitude for the (a) local, (b) PFT and (c) combined models for tropical (green), temperate (red) and boreal (blue) forest PFTs.

location (Fig. 5.6a) the local and combination model show a similar fit, whilst the PFT model cannot capture any seasonal cycle. At the dry tropical location (Fig. 5.6b), all models predict a higher seasonal amplitude and the PFT model has a much higher maximum LAI. For the temperate deciduous forest, all model capture the timing of the seasonal cycle, but the PFT model predicts a lower amplitude than that observed in the MODIS data. For the boreal grassland, both the PFT and combination model predict a higher LAI than that observed by MODIS.

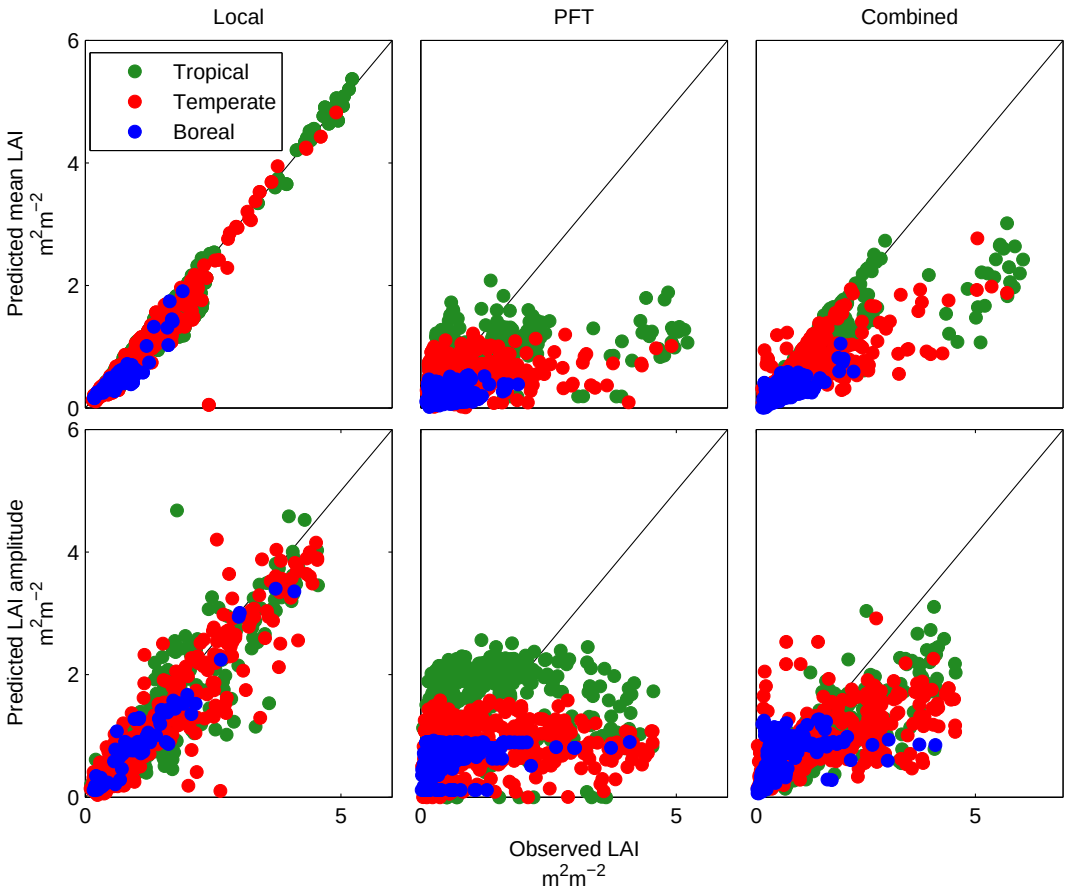

Figure 5.4: Comparison of predicted and observed mean LAI and seasonal amplitude for the (a) local, (b) PFT and (c) combined models for tropical (green), temperate (red) and boreal (blue) grass PFTs.

5.5 Discussion

We have shown that a model which describes the phenology within a PFT using one set of parameter gives an overall bad fit and is not able to describe the variation in LAI mean and amplitude across a PFT, but a model which combines local and PFT wide parameters is largely able to explain phenological patterns. This indicates that there are certain phenological characteristics specific to a particular location, even for a coarse spatial resolution as that used

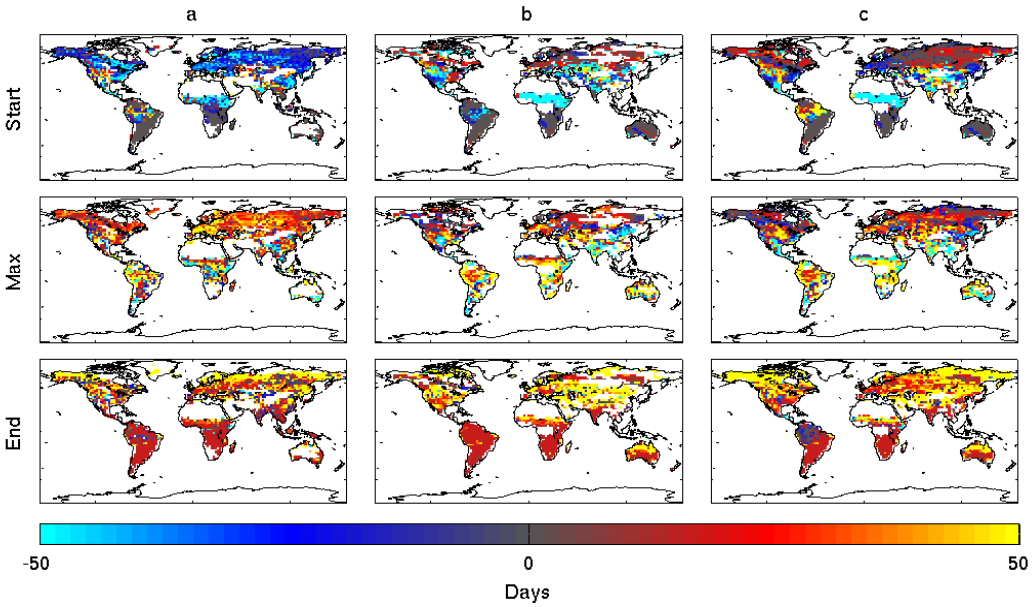

Figure 5.5: Difference between model and MODIS start and end date of the growing season and date of peak LAI for for the (a) local, (b) PFT and (c) combined models.

here. The question that arises is then what specific vegetation characteristics are determining this local behaviour. The parameter which gives the best fit within the combined model framework is the compensation point, C_{direct}. The compensation point represents the minimum light level for which leaves at the bottom of the canopy are still able to photosynthesise and represents a constraint on the maximum number of leaves (maximum LAI) for a given light level at the top of the canopy. If this parameter was a PFT level parameter, then the number of leaf layers that a forest can hold would only be limited by environmental conditions, i.e. PAR, soil moisture or temperature. If however the compensation point is local, this indicates that there are further factors limiting the maximum LAI. There are three main factors which can affect the compensation point:

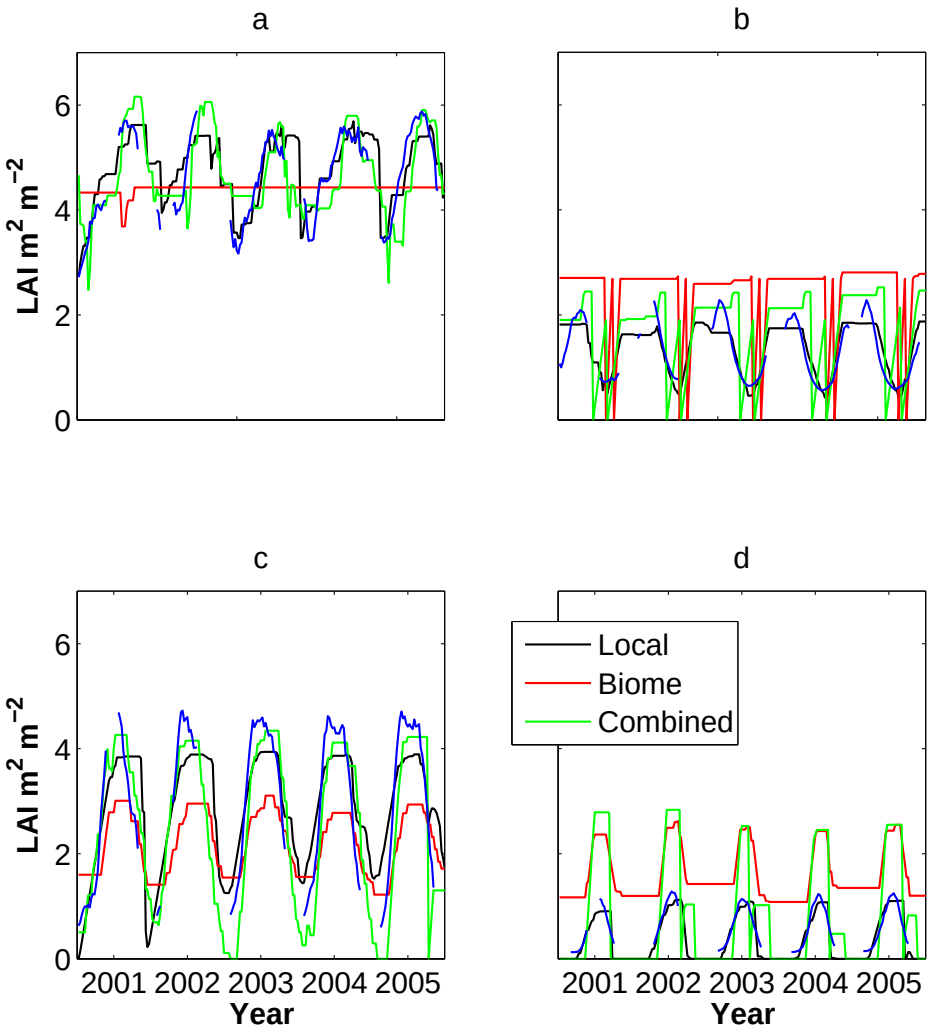

Figure 5.6: LAI timeseries for all models for tropical wet forests (6S 55W), tropical dry forests (14S 20E), temperate deciduous (46N 15E) and temperate evergreen (54N 120E). Gray shaded area represents 95% confidence intervals calculated from the parameter posterior distribution.

nutrient content, long term climate conditions and light environment through the canopy.

Nutrient availability. Leaf photosynthetic capacity is a function of leaf nitrogen content (Farquhar *et al.*, 1980; dePury and Farquhar, 1997; Hikosaka, 2003), a factor which has not been included in our model. According to current

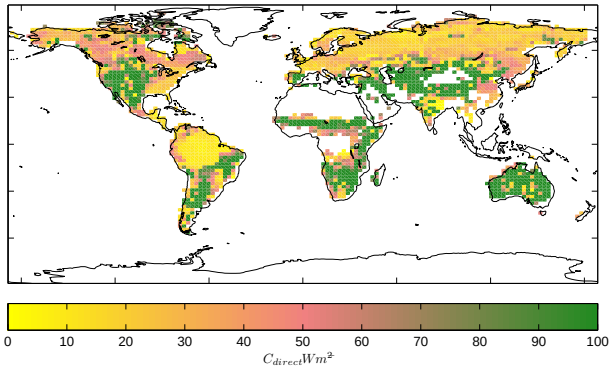

Figure 5.7: Posterior parameter means for the compensation point C_{direct} resulting from the combination model.

photosynthetic models (most commonly Farquhar *et al.* (1980)), a higher leaf nitrogen content would lead to a higher light limited photosynthetic rate and hence lower compensation point. Figure 5.7 shows the spatial distribution of the compensation point parameter as fitted in the combination model. The highest values are observed in grasslands, especially in the tropical region. In forest PFTs, the highest compensation point occurs over tropical forests, followed by temperate deciduous regions. This is supported by field studies, as higher latitude forests are generally more nitrogen limited while tropical and temperate grasslands are one of the most nutrient poor systems (Bustamante *et al.*, 2006; Elser *et al.*, 2007). To explore the intra-PFT distribution of nitrogen availability and fully explain the locality of our compensation point parameter we would need a global data set of nitrogen availability such as the nutrient limitation index derived as a function of evapotranspiration and ecosystem production (Fisher *et al.*, 2012) or the leaf nitrogen content derived from satellite measurements of surface albedo (Ryu *et al.*, 2011).

Adaptation to climate. Plants are adapted to their environment so that plant traits, such as the compensation point, can often be related to long term means of environmental variables. As the highest compensation point values are encountered in savannas and high latitude grasslands and the lowest values in very wet areas such as the Amazon basin, we can advance the hypothesis that water availability is a determining factor. We test this hypothesis by exploring correlations between the fitted compensation point and long term means of precipitation and soil moisture. We find that there is an inverse correlation between PFT level means, but not for values within a PFT. There was no significant correlation between compensation point values and mean annual precipitation or mean annual soil moisture between locations of the same PFT (correlation coefficient of -0.2, not significant at the 95% confidence level), with the exception of the savanna PFT where there is a weak correlation ($R = 0.5$, $p<0.05$). This indicates that there is a further factor affecting the distribution of compensation points within the same vegetation type in addition to water availability. Studies have shown that there is a covariation in water and nitrogen limitation because for low water availability there is a lower demand for nitrogen, which decreases the nitrogen limitation. This phenomenon would make it difficult to distinguish between the two factors without further information on nitrogen distribution (Hooper and Johnson, 1999).

Light availability. Canopy structure determines the light environment in the canopy and controls the actual amount of light that reaches the leaves. This means it can be an important value in determining the compensation point, both through model structure and long term impact on plant behaviour. Within the model used in this study, we assume a homogeneous canopy, with a random distribution of leaf angles and no clumping, assumptions which are valid at very large scales. It has been shown (Chen *et al.*, 2012) that including leaf clumping in a carbon assimilation model has a major impact on resulting global gross

primary productivity values. A leaf clumping factor would be used to adjust the attenuation coefficient α (Eq. 2.1) to improve the description of light transmission through the canopy. It is possible that the compensation point parameter C_{direct} artificially accounts for this variation in canopy structure, which explains its observed spatial variability. Further information such as the leaf clumping index map developed by Chen *et al.* (2005) would be needed to distinguish between the actual compensation point and canopy structure. This relationship is further complicated by the fact that plants adapt to their light environment, so that leaves in closed canopies will be better adapted to shaded conditions and will have lower compensation points. This can explain the fact that tropical forests, which are highly stratified, have a much lower compensation point than other systems. The question is further complicated by the fact that canopy structure itself can be an adaptation to the available resources such as light, water or nitrogen making it difficult to distinguish between all possible factors in the absence of further data.

5.6 Conclusion

In this paper we explored the extent to which plants within the same PFT exhibit the same phenological characteristics using a process-based global phenology model. We showed that a model with PFT wide parameters cannot explain the observed spatial variation in seasonal cycles, but that an intermediate model with one location specific parameter improves the overall fit. The spatial patterns of this local parameter, the light compensation point, might be explained by species adaptation to the local climate or nutrient and water availability and further data is needed to fully understand the observed distribution. The modelling approach used to determine the validity of PFT level models can provide further insight for global vegetation models which use plant functional types as a basis for upscaling

measured or fitted parameter values and can hence improve global simulations of ecosystem processes.

Chapter 6

Discussion

Over the last few chapters I have described a new global model of leaf phenology based on the hypothesis that phenology is a strategy for optimal carbon gain and shown that it is able to both explain and predict current phenology for all vegetation types. Here I outline the limitations and uncertainties of this model, as well as its possible uses for predicting the current and future global carbon cycle and climate. Section 6.1 discusses the problem of spatial resolution within global models and how this relates to phenology processes at different scales. Chapter 4 shows that our phenology model has the highest errors in boreal regions and how this relates to the issue of scale, a problem which is discussed in section 6.2. Section 6.3 discusses the choice of data assimilation algorithm and possible future improvements. This is followed by a discussion of the use of satellite based data for understanding phenology (Section 6.5) and the choice of environmental data and the further improvements which could be made by including other data streams (Section 6.6). Section 6.7 describes the possible uses of our model and some possible directions for future work.

6.1 Landscape phenology

Global scale models have, by necessity, a lower spatial resolution than regional and ecosystem level models, as the datasets required for input and model fitting are rarely both available across the globe and at a good spatial resolution because of measurement constraints. Also, if such global scale complex models were to have a high spatial resolution this would require a large amount of computer power. This low resolution means that the phenology observed by satellites and predicted by global models such as that presented here would necessarily differ from phenological observations on the ground. Previous studies have introduced the concept of landscape phenology (Morisette *et al.*, 2008) or green wave phenology (Schwartz, 1998). The measured satellite LAI (or vegetation index) represents the vegetation behaviour for the entire grid cell, including all species both in the understory and overstory, often averaging across multiple vegetation types within the same biome.

The general phenological behaviour at landscape scales is that species in the understory either leaf out early or keep leaves later in the autumn as an adaptation to their low light environment, as this maximises the amount of absorbed solar radiation, in the absence of leaves in the overstory (Richardson and OḰeefe, 2009). This would lead us to expect that the start date of the growing season predicted by our model is on average earlier than that observed in budburst dates for single species. We believe this is the main reason for the earlier start date, along with other early leafing species (Section 4.4.1).

The differences between landscape and single species phenology is even more pronounced in areas that include both deciduous and evergreen species, such as the high latitude boreal forests. Ground measurements in evergreen forests in the area show a higher LAI and less pronounced seasonal cycle than that observed in the MODIS LAI. This is the behaviour most commonly associated with coniferous

evergreen species. However, the satellite observations also include the deciduous component, resulting in a seasonal cycle more similar to that of temperate forests. A similar problem is encountered in areas that include a mosaic of grasses and forests which result in a lower LAI than expected if the pixel is classified as forest, or a higher LAI if it is classified as grassland.

These observed differences are due to measurements at a different spatial scale. Furthermore, carbon cycle models are often on large spatial scales which would make observations, and predictions of landscape phenology a suitable input.

6.2 The boreal regions

Vegetation in the boreal regions is formed of a mix of evergreen and deciduous species, varying from birch forests which lose their leaves during winter to evergreen forests with a deciduous understory, which makes phenological patterns complex and often scale dependent. Our model does capture the observed MODIS seasonal cycle, but the bias in the model increase with latitude (Section 4.4), indicating that either the model or the data lacks enough information about the seasonal cycle in this region. While there are some uncertainties in LAI data for boreal regions (as discussed in Chapter 4), the model itself does not hold any specific mechanism for high latitude evergreen species. Although such forests could exhibit a leaf age driven phenology similar to that encountered in tropical evergreen regions, the predicted model parameters do not support this hypothesis and parameters in boreal regions are similar to those obtained for temperate systems (Fig. 4.3).

Kikuzawa (1995) proposes a phenology model also based on a carbon benefit approach, which predicts leaf lifespan in evergreen forests based on the lifetime carbon gain of a leaf. In this model, trees at high latitudes do not shed their leaves

in winter because the short growing season does not allow the overall carbon gain to offset the initial carbon cost in building the leaf. Another possible model for describing boreal phenology would include both an understory and overstory component with different phenology. Another possible trigger for budburst in boreal regions and in montane forest is the timing of snow melt (Van Wijk *et al.*, 2003) as this provides the necessary soil moisture. Future work can include some of these model structures to improve phenology representation for the high latitudes.

6.3 Data assimilation

Data assimilation techniques offer the possibility of combining process knowledge with existing data, but the choice of data assimilation method, model and data can of course impact the uncertainties of the results.

In terms of choosing a minimisation algorithm such as the MCMC, the user can adjust various aspects of the algorithm, such as the jump rules and acceptance criteria, which can improve either or both algorithm efficiency and speed. One of the major problems to be solved when using such algorithms is the issue of convergence to a local minimum, particularly important for complex problems with more than a few parameters as is the case with our model. Ways to avoid this include relaxing the acceptance criteria and convergence checks that multiple chains (Gelman and Rubin, 1992), all of which were used in the present study. The problem of overall convergence was also tested during trial runs to determine the optimal chain length.

One of the advantages of using a Bayesian method for model fitting is that it allows the user to include any existing prior information on model parameters and state variables. In the current study we have only used uniform (flat) prior distributions for all parameters, with broad intervals, to allow the model maximum freedom.

However, there is a lot of information on phenological processes from both field and modelling studies, which can be used to improve parameter estimates. For example, measurements of photosynthetic capacity could be used to constrain parameters in the carbon assimilation component (ϕ, q, A_{lim}), eliminating the need for normalising parameters. This would make the model easier to compare and use with other ecosystem carbon models. Additional information on plant water extraction capabilities, which depend on plant species and soil type (McDowell *et al.*, 2008) would also improve the model predictions as both these factors are poorly represented by the soil moisture data used to fit the model.

In boreal regions, where the quality of the satellite LAI data is poor, the model predictions can be further improved by the addition of other data sources of LAI, such as field measurements (Chen *et al.*, 1997) or aircraft remote sensing campaigns (Pisek *et al.*, 2010). While these would only provide point measurements or measurements over relatively small areas compared to the satellite data, they would offer a further constraint on seasonal cycles and data quality.

6.4 Model parametrisation

As discussed in Chapter 5, the number of parameters that a model has is a constraint on its possible future uses, so that the local phenology model presented at length in Chapter 4 would need further improvements before it can be coupled with other more complex models. The combination parametrisation is a step towards this better model, but the overall model fit is not as good as that observed when using the local parametrisation. There are two paths towards improving this model. First, the model could include environmental variables not used in the current model, such as nutrient availability so that certain parameters in the

model would be a function of nutrient content, referring mostly to the direct compensation point and the other carbon assimilation parameters. The second approach would be to make current parameters a function of climate to reflect the plants' adaptation to the local long-term conditions.

6.5 Satellite data and phenology errors

Space based remote sensing of vegetation is particularly useful for global scale phenology studies because of its spatial coverage and continuous measurements. In this study we have used the MODIS LAI product to parametrise a mechanistic phenology model. When data is used in this way we have to assign a certain confidence in the data, as it is considered as the truth which we base our model parameters on. The Bayesian method we have chosen allows us to assign an uncertainty to the data in the form of an extra free parameter, providing us with information on how noisy the data is at a specific location.

Nevertheless, when discussing our results, we must take into account the caveats associated with such satellite data. Firstly, when measuring vegetation using optical methods there is the issue of saturation, in that the vegetation indices used become less sensitive over a certain LAI threshold, which is particularly important in evergreen tropical forests. Ground validation studies (e.g. Cohen *et al.* (2006)) have shown that the current version of the MODIS LAI product, collection 5, shows an improvement with regard to saturation problems. In addition most field studies report LAI values below the maximum LAI observed by MODIS, issue which has been discussed in more detail in Section 2.2.1.

Other sources of uncertainty include cloud cover, aerosol loading and the presence of snow. Methods used to account for this are temporal compositing and filtering using quality assurance flags, but these techniques often result in poor temporal

resolution and gaps in the time series, both of which would impact its usefulness for phenology. In this study we average the 1 km base resolution MODIS data to the model resolution (2° latitude by 2.5° longitude), which functions as both a smoothing and gap-filling procedure.

6.6 Choice of environmental variables

Within a data assimilation framework such as that used here, the data sets used as input have potential impacts on model results. Throughout this study we have used two environmental data sets, the GEOS 4 data for solar radiation and temperature and the NCAR/NCEP reanalysis for soil moisture. Here we discuss the overall accuracy of these datasets compared to alternative sources of data.

The GEOS family of products, of which the most recent is GEOS 5, is a result of data assimilation into a weather and atmospheric circulation model, producing spatially and temporally continuous fields of the required input variables. There are several sources of solar radiation data, including satellite measurements (e.g. Wielicki *et al.* (1996)) and ground based timeseries (e.g. Rich *et al.* (1993)). Ground based measurements are not suitable as the only data source for fitting global scale models because of their poor spatial cover. Satellite data provide continuous information but cannot partition the incoming short wave radiation into direct and diffuse streams, which are necessary for describing photosynthesis in the canopy (dePury and Farquhar, 1997).

We choose to describe the water available to plants using a soil moisture data set obtained through the reanalysis of point field based measurements (Kalnay *et al.*, 1996). This data is derived using a land surface model and is corrected using global precipitation data (Kanamitsu *et al.*, 2003). Soil moisture is one the most difficult variables to measure at large scales, together with most other soil

variables, as it is determined by a combination of environmental, above ground and below ground factors. This makes the reanalysis product difficult to validate at global scales and the few existing validation studies have proved inconclusive (Cheng-Hsuan *et al.*, 2005).

Recently, Piles *et al.* (2011) have developed a soil moisture product, using data from the Soil Moisture and Ocean Salinity (SMOS) space borne instrument, which would give the necessary spatial and temporal coverage. A much easier to obtain measure of water availability is precipitation, either at ground stations or from space borne instruments (Michaelides *et al.*, 2009). However, precipitation does not simply correlate with plant available water, and we would require an additional model component to obtain soil moisture, which would increase the number of parameters in our phenology model. Alternatively, our model can be coupled with a pre-existing hydrology model to provide the necessary input.

6.7 Applications of the model

Large scale, long term observations of LAI needed to inform both global earth system models and regional ecosystem models are lacking. Data on leaf age distributions and their seasonal changes is even more sparse, especially in tropical forest, with only one long term data set available (Reich *et al.*, 2004). This underlines the need for models which are able to combine existing knowledge on phenology and data to provide the necessary continuous data sets of LAI and leaf demography. Our model, based on a novel carbon efficiency approach is well suited for this purpose, as it can relate directly to the carbon cycle processes. The phenology schemes included in such models often have different parametrisations for different leaf habits (i.e. deciduous or evergreen), thus increasing the number of parameters (Haxeltine and Prentice, 1996a; Kucharik *et al.*, 2000; Sitch

et al., 2003), while our proposed model includes one global mechanism for leaf seasonality, making it particularly useful for large scale modelling studies.

Ecosystem scale carbon models usually cover smaller areas within a flux tower footprint, when all the input data is flux tower based (Fox *et al.*, 2009). Within the current study we have parametrised the phenology model at a much larger scale, as we were limited by the spatial resolution of the global data sets for environmental variables. It is possible that while the model accurately represents large scale seasonal patterns, the plant behaviour at smaller scales can be radically different. This is particularly true in regions where there is a mix of evergreen and deciduous forests and the particular site chosen for the modelling study is dominantly one leaf habit. Depending on the previous knowledge of the phenology in the area, it is possible to use the existing model parametrisation without any resulting large errors. Another option is to re-fit the model to the particular study area, using environmental data often available at permanent plots to obtain a more accurate description of phenology. Further studies would test the application of our model at different scales and the uncertainties associated with these fits.

One of the great advantages of the proposed model is that it predicts leaf age distributions, which are hard to measure accurately in the field and are not a direct output of most other phenology models. However, the way of including this information in existing models is still unclear. For certain processes, such as biogenic emissions of volatile organic compounds (BVOC), the relationship between leaf age and emission rate is relatively well established (Monson *et al.*, 1995; Guenther *et al.*, 1995). Studies have shown that photosynthetic capacity decreases with age (Kitajima *et al.*, 1997) but most existing carbon cycle models do not include this process. This is however essential especially if the model involves upscaling leaf processes to the canopy level, as the canopy can include different leaf age classes with different capacities, especially in evergreen forests.

It can be argued that such ecosystem or earth system models can simply use as input the MODIS LAI data used in this study to inform the phenology model, but such an approach does not offer any predictive capabilities for future conditions. Given sufficient environmental input data, the phenology model in the present study can be run forward for different future scenarios (IPCC, 2001a). Future climate conditions, including temperature, solar radiation and precipitation can be obtained from various sources, such as the WorldClim database. However, this data is often not at the required temporal resolution so we would lose some of the model accuracy. One of our model inputs is soil moisture which is not directly available for future conditions, but this can be replaced with precipitation, as discussed above (Section 6.6).

One factor limiting the predictive capabilities of our model is the fact that we do not include CO_2 fertilisation effects (Schimel *et al.*, 2001) which would impact both the compensation point and carbon assimilation parameters (Eq. 4.3). We anticipate that including such effects would lead to both an earlier spring through a lower light compensation point C and a later autumn, through a higher overall assimilation. Currently it cannot be anticipated whether these changes can overcome the limitation of daylength and this problem would be similar to that discussed previously of growing season lengthening related to higher temperatures. A further study of future vegetation behaviour would be necessary to answer these questions. Other effects of increased atmospheric CO_2 include impacts on the water use parameters, as the water stress on photosynthesis reduces with increased CO_2 concentrations. this would imply that certain regions which are currently water limited might change their phenology pattern.

For vegetation predictions, we must also consider changes in vegetation distribution. First, how representative are the model values of the underlying vegetation behaviour and to what extent do these values reflect the observed data that they were fitted to? Weng and Luo (2011) show that the information content provided

by assimilated data declines in time for model predictions, especially for long term processes, such as the formation of woody biomass. Phenological processes are controlled on seasonal scales, which would indicate that the current fitted parameters can be used for future predictions, but a sensitivity analysis would be able to answer this question more clearly.

For very long scales vegetation can adapt its behaviour in response to climate, so that using existing models for predicting phenology at these time scales is unrealistic. How fast will the vegetation in a given location change over time? Using the existing model parameters for future climates has the underlying assumption that the current species composition and vegetation behaviour will remain constant. However, studies show that species distribution is likely to change in response to changes in climate (Sala *et al.*, 2000; Guisan and Thuiller, 2005). Such species distribution changes can be predicted with the use of dynamic global vegetation models (DGVMs) (e.g. Kucharik *et al.* (2000) Sitch *et al.* (2003), which bases its prediction on PFT vegetation classifications, making the PFT model described in chapter 5 more suitable for prediction purposes than the simple location model.

We believe that the stand alone phenology model presented here has the potential to predict future phenology in the near term, but it requires extra information on vegetation changes, such as those provided by a DGVM to predicted phenology at longer time scales. To incorporate such information on changes in vegetation we need to link the fitted parameters to either species distribution (biome type) or to climatic conditions, to allow us to track changes in the spatial distribution of parameters. The biome and combination parametrisations presented in Chapter 5 are a first step towards such a model, but future work should include a more robust relationship between parameter values and nutrient limitation or climate conditions.

Appendix A

Biogeosciences, 9, 1389–1405, 2012
www.biogeosciences.net/9/1389/2012/
doi:10.5194/bg-9-1389-2012

Biogeosciences

Inferring Amazon leaf demography from satellite observations of leaf area index

S. Caldararu[1], **P. I. Palmer**[1], **and D. W. Purves**[2]

[1]School of GeoSciences, University of Edinburgh, Edinburgh, UK
[2]Microsoft Research, Cambridge, UK

Correspondence to: S. Caldararu (s.caldararu@sms.ed.ac.uk)

Received: 25 September 2011 – Published in Biogeosciences Discuss.: 25 October 2011
Revised: 20 March 2012 – Accepted: 27 March 2012 – Published: 16 April 2012

Abstract. Seasonal and year-to-year variations in leaf cover imprint significant spatial and temporal variability on biogeochemical cycles, and affect land-surface properties related to climate. We develop a demographic model of leaf phenology based on the hypothesis that trees seek an optimal leaf area index (LAI) as a function of available light and soil water, and fit it to spaceborne observations of LAI over the Amazon basin, 2001–2005. We find the model reproduces the spatial and temporal LAI distribution whilst also predicting geographic variation in leaf age from the basin centre (2.1 ± 0.2 years), through to the lowest values over the deciduous eastern and southern Amazon (6 ± 2 months). The model explains the observed increase in LAI during the dry season as a net addition of leaves in response to increased solar radiation. We anticipate our work to be a starting point from which to develop better descriptions of leaf phenology to incorporate into more sophisticated earth system models.

1 Introduction

Seasonal and year-to-year variations in leaf area imprint significant spatial and temporal variability on biogeochemical cycles and affect land-surface properties related to climate (Hayden, 1998). For example, the transfer of water from the soil to the atmosphere is mostly via leaves through evapotranspiration, subsequently affecting humidity, air temperature and rainfall (Wilson and Baldocchi, 2000). Similarly, carbon enters vegetated ecosystems through carbon fixation via photosynthesis (White et al., 1999).

Over temperate regions leaf phenology is known to be driven by changes in day length and temperature (Schwartz, 1999), although the relative importance of these determining factors and how they might change with climate is poorly understood (Korner and Basler, 2010).

However, the majority of the world's forests retain leaves year round: boreal forests which are dominated by evergreen needle-leaf trees and often mixed with deciduous broadleaf and needle-leaf species; and mesic tropical forests, dominated by evergreen broadleaf species, which are responsible for the majority of terrestrial carbon fixation (Malhi and Grace, 2000). Observed LAI over these evergreen forests, particularly over the tropics, still show seasonal and year-to-year variations (Myneni et al., 2007), but we lack knowledge about the magnitude, geography, timing, and the processes driving such variation, partly reflecting the difficulty of taking year-round measurements. Consequently many modelling studies assume that tropical leaf area is constant (Cramer et al., 2001; Arora and Boer, 2005).

Space-borne observations of LAI offer the best opportunity to develop a quantitative model of large-scale controls of leaf area by virtue of their frequency and global coverage. We focus our study on the Amazon basin (10° N–10° S, 80° W–50° W). The vegetation in the region is mainly semi-deciduous or evergreen tropical forest, but the species composition varies widely due to the differences in soil type and altitude across the basin (Sombroek et al., 2000).

The Amazon basin experiences wet and dry seasons, with the dry season generally running from June–September, with longer and drier periods in the south-eastern regions (Sombroek, 2001). Fig. 1 shows that the timing of low precipitation coincides with an increase in direct radiation mainly due to a decrease in cloud cover. Levels of diffuse radiation are comparatively constant throughout the year.

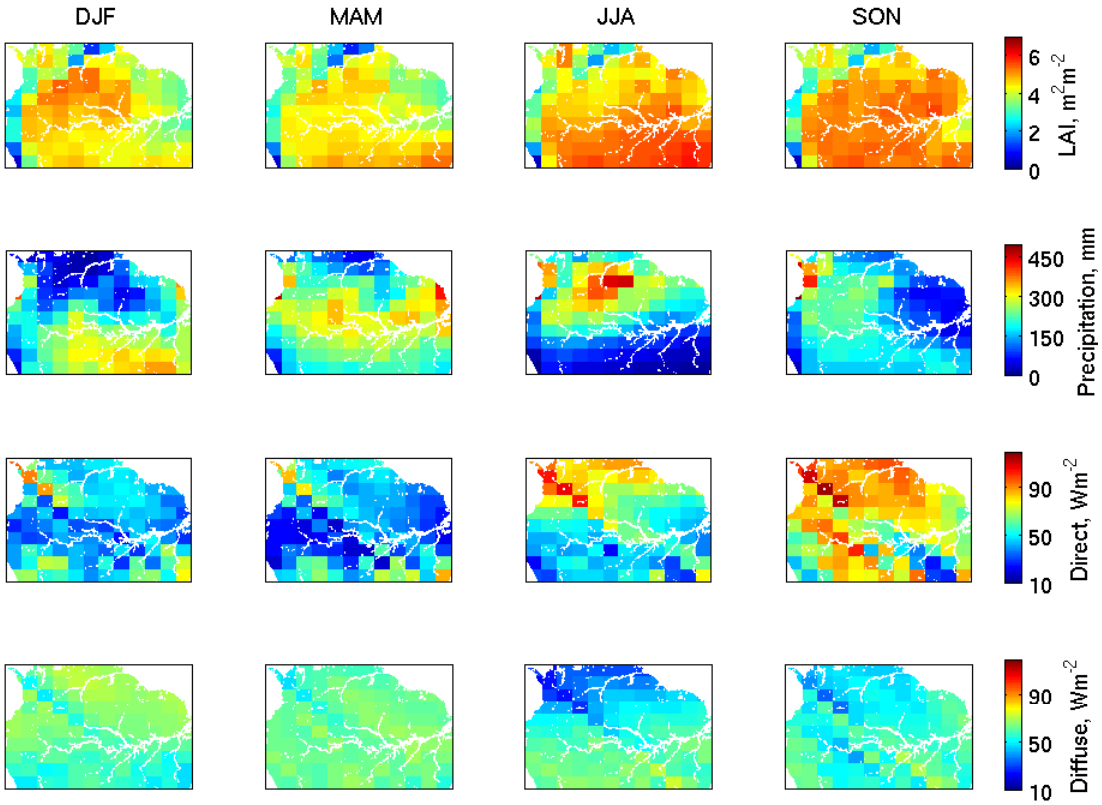

Fig. 1. From top to bottom: MODIS leaf area index ($m^2\ m^{-2}$), WorldClim precipitation (mm) (Hijmans et al., 2005), GEOS-4 direct and diffuse photosynthetically active radiation, PAR (Wm^{-2}) across the study region. The dry season, with precipitation levels of under 100 mm, runs generally from July–September, period which coincides with an increase in direct PAR due to a decrease in cloud cover. We can observe that the LAI also peaks during this period, reaching its lowest levels in the wet season.

Ground-based studies have reported an increase in leaf litterfall during the dry period (Malhado et al., 2009; Chave et al., 2010), but without simultaneous measurements of leaf gain we cannot determine whether the increased litterfall represents a net loss of leaves. Studies using space-borne vegetation data (Myneni et al., 2007; Huete et al., 2006) have reported an increase in greenness during the dry season over the Amazon, even during severe droughts (Saleska et al., 2007), but these drought observations have been disputed (Samanta et al., 2010; Doughty and Goulden, 2008). These observations are consistent with indirect evidence from the seasonal cycle of satellite-observed emission of biogenic trace gases (Barkley et al., 2009). The dry-season increase in leaf area could be explained by soil moisture dynamics: water is available all year round in the deeper soil layers (Harper et al., 2010), which can be readily accessed by the large rooting depths of Amazonian vegetation (Nepstad et al., 1994; Jipp et al., 1998). Under these circumstances, we expect that light availability is the primary controlling factor for determining changes in leaf area (Wright and Vanschaik, 1994). This implies that trees will carry more leaves in the dry season when direct radiation is greater. To test this idea and to enable predictive modelling of Amazon leaf phenology, we develop a simple leaf phenology model for the Amazon tropical forest. Sect. 3 describes this model, which we fit to MODIS LAI data (Sect. 2) to obtain parameter values for the Amazon basin. We discuss our results in Sect. 4 and demonstrate how, in principle, our predictions of leaf area and age distribution could impact carbon assimilation using a simple carbon model. We conclude our paper in Sect. 5.

2 Data sets used

2.1 MODIS LAI data

We use leaf area index (LAI) data obtained from the MODIS (Moderate Resolution Imaging Spectroradiometer) instrument aboard the NASA Terra platform. The LAI/fPAR (fraction of absorbed photosynthetically active radiation) product collection 5 (MOD15A2) is available globally at a spatial resolution of 1 km every 8 days for the period 2000–present and has been downloaded from https://lpdaac.usgs.gov/. The 8 day temporal resolution is a result of compositing, i.e. assigning the best value for the 8 day period based on maximum fPAR. The data set is split into tiles (10° latitude by 10° longitude at the equator), which cover northern South America and include the Amazon basin. We use tiles h10-12v08 and h10-12v09 for the years 2001 to 2005.

The LAI is calculated using a radiative transfer algorithm (the main algorithm), which uses the red (648 nm) and near-infrared (858 nm) bands. The algorithm uses biome-specific vegetation structure and height, leaf type and soil brightness to obtain LAI values (Yang et al., 2006; Knyazikhin et al., 1997, 1999). In conditions where the main algorithm cannot be applied, a back-up algorithm is used, in which case the LAI value is calculated using an empirical relationship between Normalised Difference Vegetation Index (NDVI) and LAI. The data quality is affected by the presence of cloud, atmospheric aerosol loading and snow cover. Snow cover is not an issue for our study region, but cloud cover can affect the quality of the data, especially during the wet season, while aerosols from biomass burning can interfere with measurements during the dry season. The quality flags provided along with the LAI data offer information on overall data quality, the algorithm used, cloud cover and aerosol presence. Ground validation studies (Cohen et al., 2006) have shown that the back-up algorithm is often unreliable and our analysis of the data over the Amazon region shows that values assigned by the backup algorithm are often unrealistically low, leading to large week-to-week swings in LAI. As a consequence, we remove any LAI values calculated using the back-up algorithm prior to spatial averaging.

LAI retrievals of vegetation often have saturation problems in that LAI becomes insensitive to changes in reflectance. Studies have shown that this was an issue for high-biomass areas for collections 3 and 4, but this has been considerably improved for collection 5 (Yang et al., 2006). Ground based values of LAI in the Amazon basin range from 3.5–6 $m^2\,m^{-2}$ (Malhado et al., 2009; Aragão et al., 2005; Roberts et al., 1996; Meir et al., 2000), with values of up to 10 $m^2\,m^{-2}$ registered by some studies (Doughty and Goulden, 2008), with differences arising from the different measurement methods. MODIS LAI values are in the range 2–6 $m^2\,m^{-2}$, which provides us with some confidence that there are no major saturation problems.

When relating leaf reflectance measurements to seasonal cycles we must take into account the fact that changes in observed reflectance can also be caused by changes in the number of young leaves, as these have different reflectance properties. This has been advanced as an explanation for the observed seasonal swings over the Amazon basin by several studies (Doughty and Goulden, 2008; Asner and Alencar, 2010; Aragão et al., 2009; Brando et al., 2010). However, the observed seasonal changes in LAI are too large to be attributed to a flush of new leaves only (Samanta et al., 2012).

The study region includes lowland tropical forests, alpine forests, savannas and grasslands. As our study is focused on forests, we use the MODIS landcover product MOD12Q1 to filter non-forested pixels. We use the provided IGBP classification scheme and have retained only pixels in classes 1–5, evergreen needleleaf forest, deciduous needleleaf forests, deciduous broadleaf forest, evergreen broadleaf forest and mixed forest. As there is no way to distinguish between lowland and alpine forests we include both in our analysis.

We reproject the LAI data to an orthogonal projection and average it to the resolution of the GEOS-4 PAR data (2° latitude and 2.5° longitude) and subsequently fit our model at this resolution.

2.2 Radiation data

We use photosynthetic active radiation (PAR) fields from assimilated meteorological data products of the Goddard Earth Observing System (GEOS-4) based at the NASA Global Modeling and Assimilation Office (GMAO) (Bey et al., 2001). The temporal resolution of this data is 1 day and the spatial resolution is $2^\circ \times 2.5^\circ$.

2.3 Soil moisture data

We use the volumetric soil moisture for 10–200 cm depth from the NCAR/NCEP reanalysis daily average surface flux data set (http://www.esrl.noaa.gov/psd/data/gridded/data.ncep.reanalysis.surfaceflux.html) (Kalnay et al., 1996). The data is available at global scales at daily timesteps for the period 1948 to present on a Gaussian grid. We reproject the data onto the orthogonal GEOS-4 grid for model fitting.

3 Leaf phenology model

The central assumption of our model is that trees adjust their gains and losses of leaves in order to try to achieve, at any given time, an optimal LAI, which we refer to as the target LAI, LAI_{targ}. The value of LAI_{targ} is determined as the minimum of a light-limited target, LAI^{light}_{targ}, and a water-limited target, LAI^{water}_{targ}. We define LAI^{light}_{targ} such that the bottom layer of leaves receives just enough light to return a positive carbon balance, i.e., receives light at the light compensation

Table 1. Model parameters

Symbol	Units	Description
C_{direct}	Wm^{-2}	Light compensation point for direct PAR (Eq. 1, main paper)
C_{diffuse}	Wm^{-2}	Light compensation point for diffuse PAR (Eq. 1, main paper)
p	days	Length of time window for average PAR
gain_{max}	$\text{m}^2\,\text{m}^{-2}$	Maximum gain rate for new leaves
a_{crit}	years	Age after which leaves start ageing
μ_0	years^{-1}	Background decay constant
μ_1	years^{-1}	Age-related decay constant

point C as derived from Beer's law:

$$\text{LAI}_{\text{targ}}^{\text{light}} = -\frac{1}{\alpha}\ln(\frac{C}{I_0}), \quad (1)$$

where I_0 is the incoming PAR at the top of the canopy and α is the light attenuation coefficient applying to Beer's Law, which we have fixed to 0.5 (Appendix A1). To recognise the potentially important difference between direct and diffuse light we apply Eq. 1 separately for both direct and diffuse PAR, to determine their respective compensation points (C_{direct} and C_{diffuse}), and then keep the minimum of the two values. For both diffuse and direct PAR we assume that, in order to avoid sub-optimal responses to very short-term variation in light, trees calculate the target $\text{LAI}_{\text{targ}}^{\text{light}}$ using an effective I_0, defined as the average over the previous p days. We drive Eq. 1 with GEOS-4 reanalysis estimates of incoming PAR (Sect. 2.2). We define the water-limited target as $\text{LAI}_{\text{targ}}^{\text{water}} = \beta_1 + \beta_2 W_{\text{s}}$, where W_{s} is soil moisture (from the NCAR/NCEP Reanalysis, Sect. 2.3) and β_1 and β_2 are empirical coefficients (Appendix A2) We assume leaf demography (the gain and loss of leaves of different ages) is determined by the factor limiting LAI_{targ}. If the current LAI is below LAI_{targ} trees add new leaves of age $a = 0$ at a maximum rate gain_{max} to reach LAI_{targ}. If LAI_{targ} is water limited and the current LAI is above LAI_{targ}, to avoid excessive water loss or overheating leaves, trees lose leaves, beginning with the oldest leaves, until they achieve LAI_{targ}. When LAI_{targ} is light limited and LAI is above LAI_{targ}, trees add no new leaves, but do not actively drop leaves. In all of the above cases, leaves are subject to continuous leaf loss according to a mortality rate μ due to leaf ageing that depends only on leaf age a. We define a minimum age, a_{crit} (years), below which we only consider the background loss, e.g. herbivory, branch loss, so that the mortality is $\mu = \exp^{-\mu_0}$. Leaves older than a_{crit} are lost at a faster rate $\mu = exp^{-\mu_1}$ which is caused by leaf ageing. In order to calculate the age-dependent mortality we introduce the concept of leaf cohorts, defined as a group of leaves of the same age. For each cohort $\text{LAI}(a, \mathbf{x}, t)$ we apply the mortality rate as:

$$\text{LAI}(a, \mathbf{x}, t) = \mu(a)\text{LAI}(a-1, \mathbf{x}, t-1), \quad (2)$$

with the mortality rate μ defined as above. The overall LAI at each time step, $\text{LAI}(\mathbf{x}, t)$ is the sum of all leaf cohorts.

Overall the rate of change of LAI at each location $\mathbf{x}$ and time t (Fig. 2) is:

$$\frac{d}{dt}(\text{LAI}(\mathbf{x}, t)) = P(I_0(\mathbf{x}, t), \text{LAI}(\mathbf{x}, t-1)) - \\ -L(\text{LAI}(\mathbf{x}, t), W_{\text{s}}(\mathbf{x}, t)), \quad (3)$$

where $P(I_0(\mathbf{x}, t), \text{LAI}(\mathbf{x}, t-1))$ denotes production processes and $L(\text{LAI}(\mathbf{x}, t)W_{\text{s}}(\mathbf{x}, t))$, refers to loss processes due to both the age-related mortality rate and active leaf dropping due to water stress. When integrated over time t, Eq. 3 provides, for each location $\mathbf{x}$ and time t, a predicted LAI (Appendix B1) given environmental drivers (direct and diffuse PAR, and available soil moisture), and given the value of 9 parameters specific to location $\mathbf{x}$: $C_{\text{direct}}, C_{\text{diffuse}}, p, \text{gain}_{\text{max}}, a_{\text{crit}}, \mu_0, \mu_1, \beta_1, \beta_2$ (Table 1). Initial parameter estimates (not shown) estimated that $\text{LAI}_{\text{targ}}^{\text{light}} < \text{LAI}_{\text{targ}}^{\text{water}}$ for nearly all locations at nearly all times, such that the fit to data was not statistically improved by considering water limitation of leaf area so that we can set $\text{LAI}_{\text{targ}} = \text{LAI}_{\text{targ}}^{\text{light}}$; consequently we do not discuss soil moisture further.

We simultaneously fit the above parameters using a Bayesian approach (Appendix B) over our study region with a spatial resolution of 2° (latitude) × 2.5° (longitude) to collection 5 of the LAI data from the MODIS satellite instrument, which was spatially averaged to this resolution (Sect. 2.1).

4 Results

Fig. 3 shows that the model reproduces the spatial distribution of mean LAI (Pearson correlation coefficient $r^2 = 0.9$), capturing the high values (up to $4.8 \pm 0.1\,\text{m}^2\,\text{m}^{-2}$) over the central and southern Amazon basin and lower values ($4.0 \pm 0.2\,\text{m}^2\,\text{m}^{-2}$) over the Eastern regions. More importantly, the model reproduces the broad spatial distribution of LAI amplitude, defined as the difference between the maximum and minimum monthly LAI, with a statistically significant correlation coefficient of $r^2 = 0.46$. This result supports

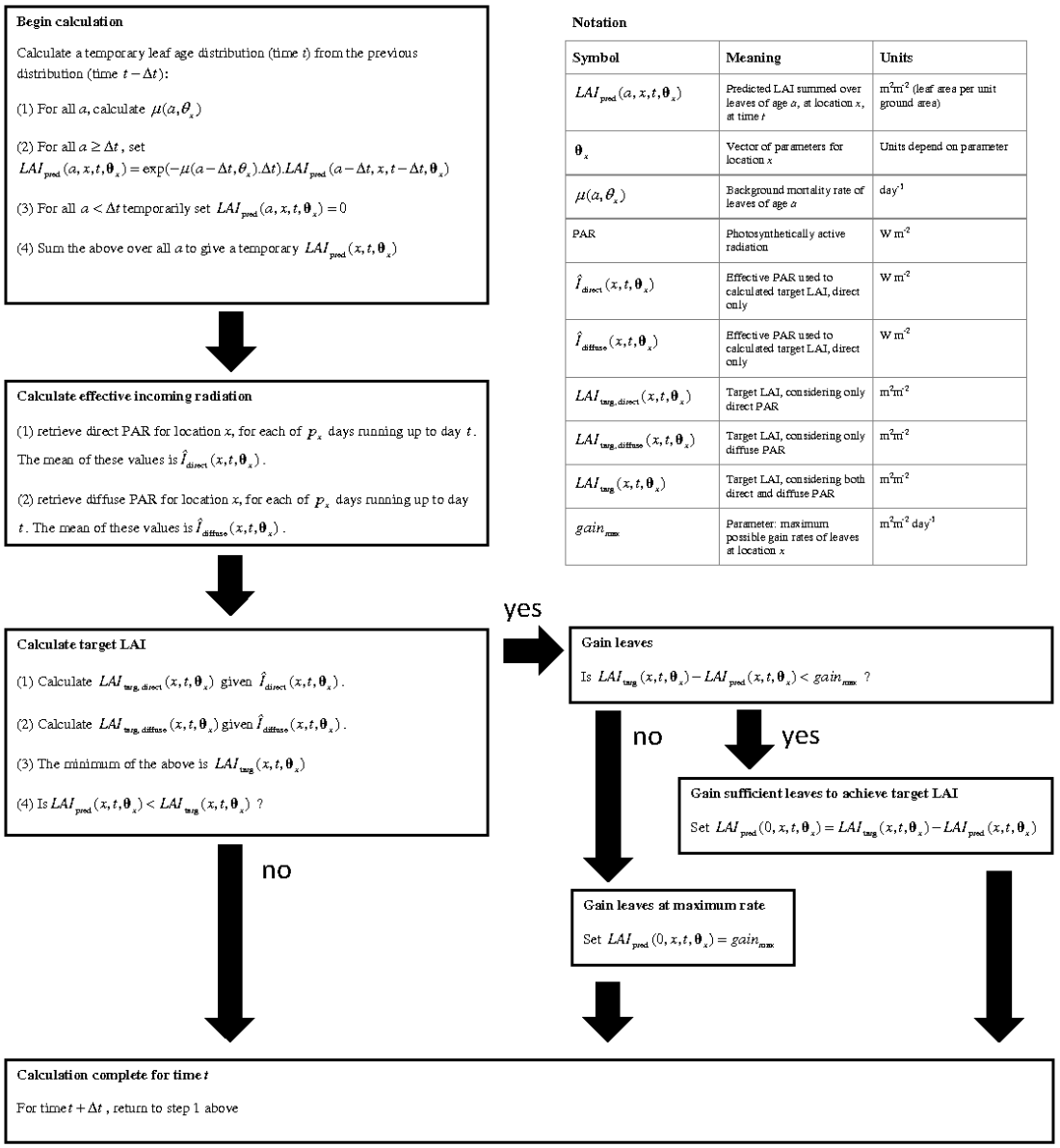

Notation

Symbol	Meaning	Units
$LAI_{pred}(a,x,t,\theta_x)$	Predicted LAI summed over leaves of age a, at location x, at time t	m^2m^{-2} (leaf area per unit ground area)
θ_x	Vector of parameters for location x	Units depend on parameter
$\mu(a,\theta_x)$	Background mortality rate of leaves of age a	day^{-1}
PAR	Photosynthetically active radiation	$W\,m^{-2}$
$\hat{I}_{direct}(x,t,\theta_x)$	Effective PAR used to calculated target LAI, direct only	$W\,m^{-2}$
$\hat{I}_{diffuse}(x,t,\theta_x)$	Effective PAR used to calculated target LAI, direct only	$W\,m^{-2}$
$LAI_{targ,direct}(x,t,\theta_x)$	Target LAI, considering only direct PAR	m^2m^{-2}
$LAI_{targ,diffuse}(x,t,\theta_x)$	Target LAI, considering only diffuse PAR	m^2m^{-2}
$LAI_{targ}(x,t,\theta_x)$	Target LAI, considering both direct and diffuse PAR	m^2m^{-2}
$gain_{max}$	Parameter: maximum possible gain rates of leaves at location x	$m^2m^{-2}\,day^{-1}$

Fig. 2. How to calculate the predicted leaf age distribution and predicted total LAI for a model driven only by light. Note that the calculation begins with the leaf age distribution from a previous time $t-\delta t$ at the same location, which is updated to account for background leaf mortality, and the addition of new (age = 0) leaves as driven by the LAI target, producing a predicted leaf age distribution for time t.

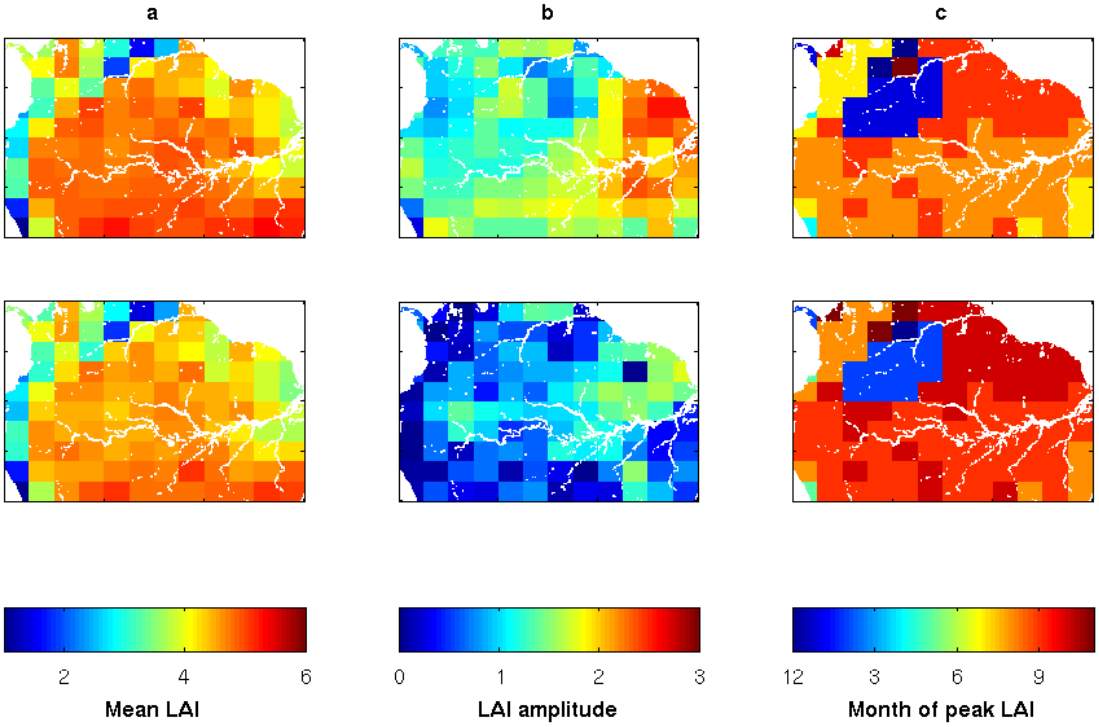

Fig. 3. MODIS (top) and model (bottom) leaf area index (LAI) over the Amazon (10°N–10°S, 80°W–50°W), 2001–2005 averaged over a 1×1 km grid. **(a)** mean LAI ($m^2\ m^{-2}$), **(b)** mean annual amplitude of LAI ($m^2\ m^{-2}$), and **(c)** mean timing of peak LAI (day of year).

our model structure because, unlike the mean LAI, the LAI amplitude is highly constrained by model assumptions; the maximum LAI amplitude is determined by the amplitude of incoming PAR.

Figure 4 shows that the model generally has a negative bias with respect to amplitude, which we attribute at least in part to measurement noise, with mean MODIS (model) LAI amplitude of 1.5 ± 0.4 (0.7 ± 0.4) $m^2\ m^{-2}$, but the MODIS value falls within the confidence intervals of the model (Fig. 5). Similarly, the model reproduces the seasonal timing of LAI variation (Fig. 4), which is also highly constrained by the model structure, as the greatest target LAI occurs at the time of peak incoming PAR. We find that our model generally describes between 20–80 % (median of 31 %) of the observed temporal variability of LAI at any one $2° \times 2.5°$ grid cell.

Fig. 6 shows posterior model parameters, which provide further insight into the underlying processes that determine observed variations in LAI. The spatial variations of the parameters are a reflection of not only the seasonality but also of species composition, soil type or nutrient availability. The two compensation points, C_{direct} and C_{diffuse}, can be interpreted as a measure of the shade adaptation in trees, with a lower compensation point indicating leaves that are adapted for lower light conditions. We estimate that C_{direct} is lower in the south of the Amazon, with values of 1.5 compared to $5\,Wm^{-2}$ elsewhere. In contrast, C_{diffuse}, which effectively limits the overall compensation point during the dry season resulting in a lower LAI amplitude, is more homogeneous across the basin with mean values of $0.23\,Wm^{-2}$. Our values for the compensation points are broadly consistent with ground-based measurements (Riddoch et al., 1991), providing further support for our methodology.

The delay p represents the time required for the vegetation to respond to changes in PAR. We find that p is generally 14 days for most of the basin. The exception is over the northwestern region, where $p > 1$ month, suggesting that vegetation over this region is slower to respond to changes in PAR. The maximum gain of LAI is typically around $1\,m^2\,m^{-2}\,month^{-1}$, with the highest values (up to $2.2\,m^2\,m^{-2}\,month^{-1}$) over the eastern, drier regions corresponding to an area with a higher LAI amplitude and a more pronounced seasonal cycle.

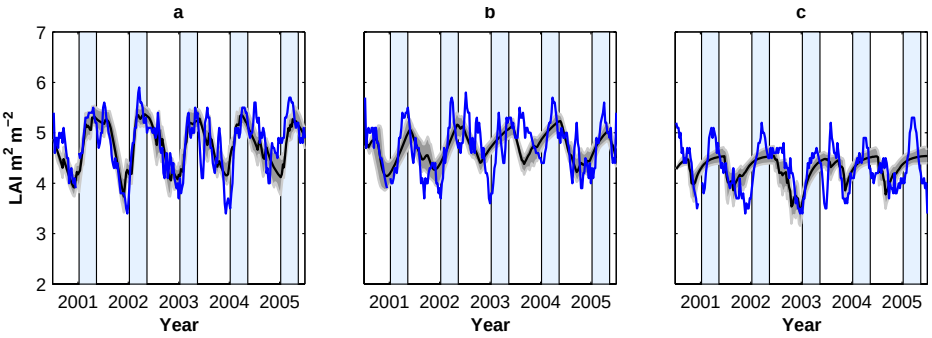

Fig. 4. LAI time series in **(a)** the eastern Amazon (8° N 62.5° W), **(b)** the semi-deciduous Amazon (0° N 72.5° W), and **(c)** the evergreen central Amazon basin (4° N 67.5° W), as predicted by the model (black line) and MODIS LAI data (blue line). Gray shaded area represents 95 % confidence intervals. Blue bands represent aproximate dry seasons.

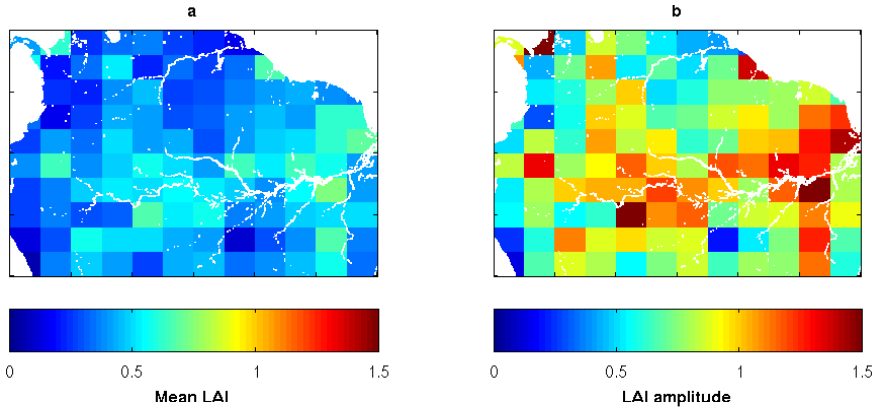

Fig. 5. Model uncertainty for mean LAI and annual amplitude (the difference between the maximum and minimum monthly LAI). We used samples drawn from the posterior distribution to calculate model LAI values and then obtain posterior means and confidence intervals. Here, the uncertainty is represented as the difference between the upper and lower bounds of the 95 % conidence intervals using parameter posterior distributions.

To help interpret our estimated leaf loss parameters, determined by the amplitude of the observed LAI seasonal cycle, we calculate a leaf lifespan τ_{95} as the time at which 95 % of the leaves from a cohort have dropped, based on the exponential decay rates μ_0 and μ_1 (Eq. 2):

$$\tau_{95} = -\frac{\ln 0.05}{\mu_1} - \frac{\mu_0}{\mu_1} a_{\text{crit}} + a_{\text{crit}}, \quad (4)$$

with variables as defined in Table 1. Figure 6 shows that τ_{95} is longest in the middle of the Amazon basin, with values of around 2.1 ± 0.2 years, and lower in the Southern and Eastern regions (1.5 ± 0.7 years), where the vegetation has a larger deciduous component.

These lifetimes are consistent with sparse ground-based studies over the same region, which report values between 2 months and 6.4 years (Reich et al., 2004) and in other tropical forests (up to 26 months (Sharpe, 1997; Osada et al., 2001)).

To obtain an estimate of parameter uncertainty, we use the posterior distribution resulting from the fitting algorithm to calculate 95% confidence intervals (Fig. 7). Most parameters are well constrained, with confidence intervals of 0.1 ($\pm$0.07) of the posterior mean for most parameters. The exceptions are two of the leaf mortality parameters (Fig. 7f and g), with confidence intervals of 0.8 ($\pm$0.2) for the base mortality rates, μ_0 and 0.5 ($\pm$0.1) for the age related rate, μ_1. This can indicate a trade-off between the two parameters as they both contribute to determining the overall leaf lifespan. Also, the diffuse compensation point C_{diffuse} (Fig. 7b) is less well constrained in the north-eastern regions.

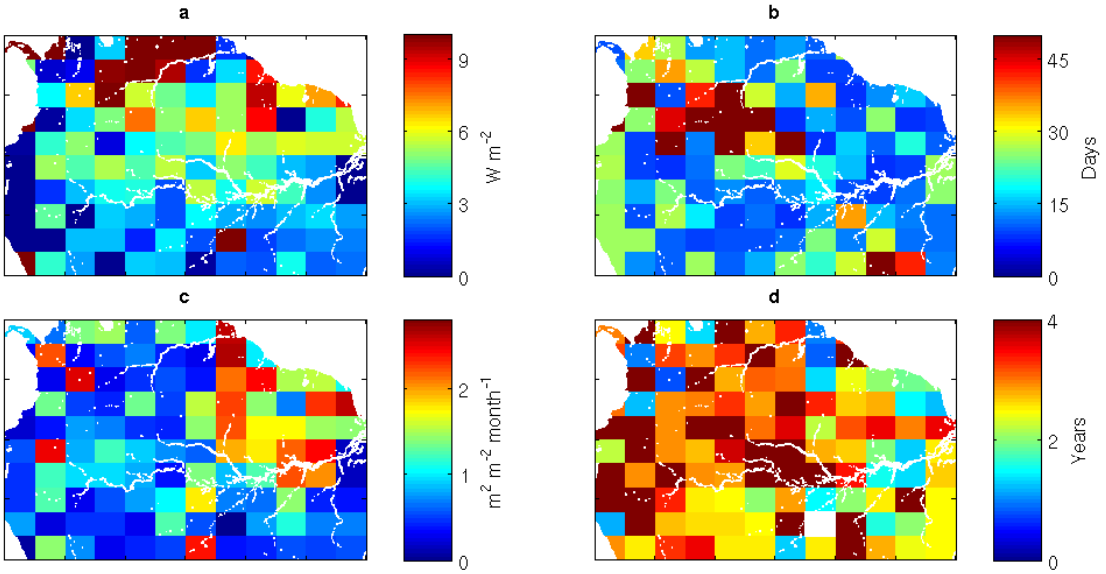

Fig. 6. Mean posterior parameters that describe leaf gain and loss: **(a)** direct PAR compensation point, C_{direct} (W m^{-2}); **(b)** delay in vegetation response to changes in PAR, p (days); **(c)** maximum number of leaves that can be added over a month, gain$_{\text{max}}$ (m^2 m^{-2} month^{-1}); and **(d)** mean cohort leaf lifetime τ_{95} defined as the time at which 95 % of the leaves from a cohort have dropped (years).

Our model also allows us to estimate the leaf age distribution at any point over the basin, something that would be extremely difficult to do using traditional means. Fig. 8 shows that leaves in regions with a high leaf turnover rate are generally younger than one year, with a high proportion of very young leaves (less than 6 months) with an approximately exponential leaf age distribution which shows pronounced seasonality between wet and dry seasons. In contrast, over the evergreen areas of the central Amazon basin we estimate a higher proportion of leaves older than 1 year and a leaf age distribution with a less pronounced seasonality. In the more deciduous regions in the southern basin, we find distinct leaf cohorts originating from past growing seasons.

To provide an example of the potential impact of our new estimates of leaf age distribution on large-scale calculations of biogeochemistry, we incorporated this information into a simple model of carbon assimilation. We present three scenarios: (1) using a constant LAI and constant leaf age distribution throughout the year, (2) using the predicted LAI with a constant leaf age distribution and (3) using the predicted LAI and leaf age distribution. Fig. 9 shows that the seasonality of the carbon flux is driven mainly by the incoming PAR and not by changes in LAI. When we include the predicted LAI, the overall photosynthesis is higher by only approximately 1 µmol m^{-2} s^{-1} during the dry season. However, if we include a leaf age adjusting factor (Appendix C), the assimilation rate is lower by an average of 1.5 µmol m^{-2} s^{-1} throughout the year. The largest difference (3.37 µmol m^{-2} s^{-1}) occurs in June, when the new leaves start appearing in response to increased sunlight. The assimilation also peaks later than when using a constant LAI, as new leaves reach peak photosynthetic rates only after a certain period of time. While some ground studies report a decrease in assimilation rate during dry periods (Malhi et al., 1998; Miranda et al., 2005) and during severe drought periods (Phillips et al., 2009), the lower assimilation rate at the start of the dry season has been observed in ground studies (Hutyra et al., 2007; Goulden et al., 2004; Graham et al., 2003; Bonal et al., 2008; da Rocha et al., 2004) but previous models were unable to predict this pattern. The hypothesis advanced by one of these studies (Hutyra et al., 2007) was that the emergence of new leaves at the start of the dry season would create this pattern, which is quantitatively supported by the leaf demography predicted by our model.

5 Concluding remarks

We present a simple phenology model for the Amazon basin, which we fitted to 5 years of MODIS LAI data. We showed that our model reproduced the observed increase in LAI during the dry season as a response to an increase in direct solar radiation. Our model parameters provided further information about the vegetation in the Amazon basin. The

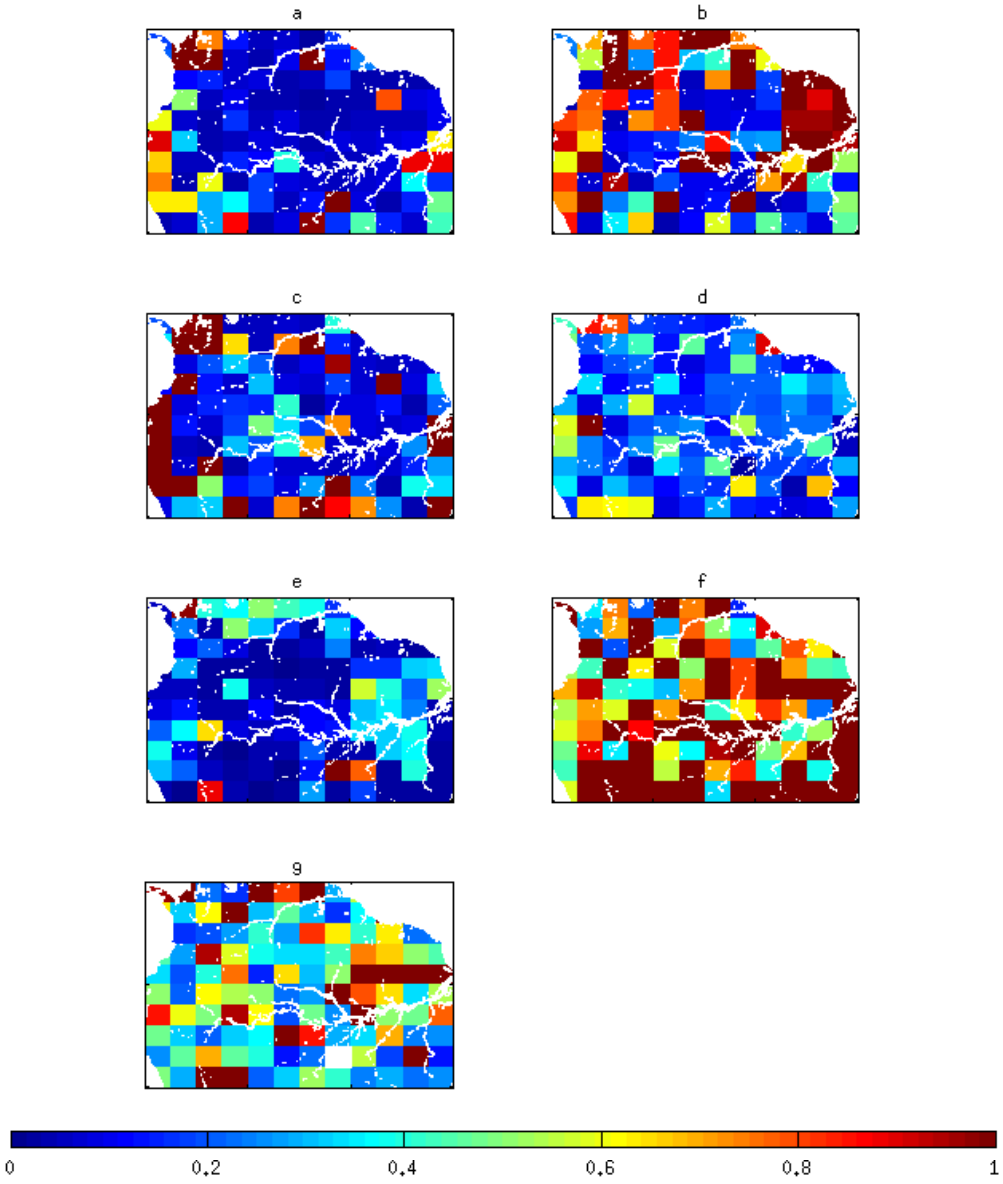

Fig. 7. Parameter uncertainty derived from the posterior distribution, expressed as 95 % confidence intervals relative to posterior means for **(a)** direct PAR compensation point, C_{direct}; **(b)** diffuse PAR compensation point, $C_{diffuse}$; **(c)** delay in vegetation response to changes in PAR, p; **(d)** maximum number of leaves that can be added over a month, $gain_{max}$; **(e)** age after which age related decay starts, age_{crit}; **(f)** background decay constant, μ_0 and **(g)** age-related decay constant, μ_1.

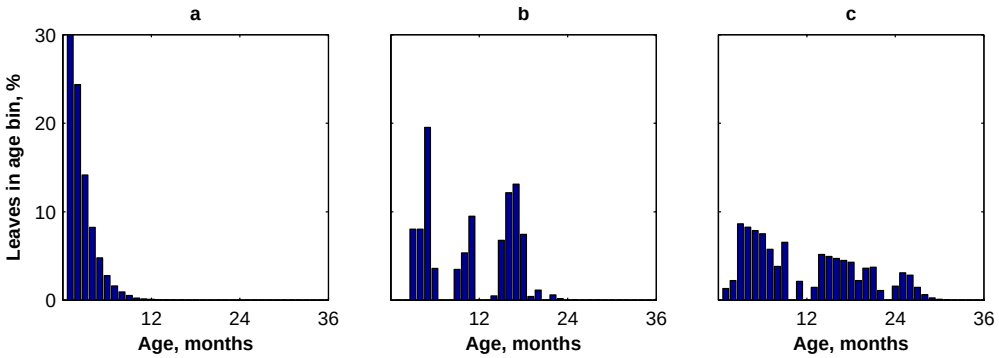

Fig. 8. Estimated frequency distribution of leaf ages (months) over **(a)** the eastern Amazon, where leaves are typically short-lived, **(b)** over the semi-deciduous Amazon, and **(c)** over the evergreen central Amazon basin. All locations are the same as for Fig. 4.

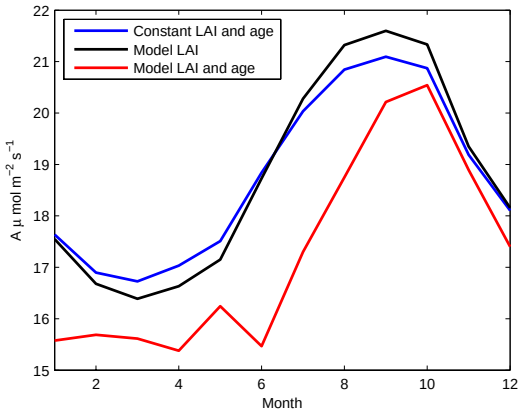

Fig. 9. Gross carbon assimilation calculated using a simple carbon model for a constant LAI, model LAI and model LAI including the temporal variations in leaf age. The values presented are monthly means over a 5 year period at one location (8° N 55° W). All values are $\mu\text{mol}\,\text{m}^{-1}\,\text{s}^{-1}$.

model also provided leaf demography estimates, which can be used to improve predictions of the seasonal carbon cycle, which we demonstrated in principle using a simple carbon model. We showed that using our predicted leaf demography explains observed decrease in carbon assimilation at the start of the dry season. Carbon fixation is only one of many examples of leaf-age-dependent processes of which our current understanding is hampered by incomplete knowledge of leaf demography. Recent work has shown that including a better description of leaf phenology in Earth system models can significantly revise estimates of land surface warming (Bounoua et al., 2010). The demographic model presented here can be used to predict responses of Amazon leaf demography to future changes in climate and could be extended to include other tropical regions where leaf phenology is driven partially or wholly by soil moisture. We therefore anticipate that the insights afforded by our analysis will have far-reaching implications for improving current understanding of the natural carbon cycle in the Amazon and elsewhere.

Appendix A

Model structure

A1 Attenuation Coefficient

To quantify the attenuation of photosynthetic active radiation (PAR) as it passes through a forest canopy, we used Beer's law:

$$I = I_0 e^{-\alpha L}, \tag{A1}$$

where I_0 is the incoming PAR (Wm^{-2}) at the top of the canopy, I is the light level at layer L inside the canopy and α is the light attenuation coefficient. We assume a vertically homogeneous canopy with no leaf clumping. The light attenuation coefficient is a function of the solar inclination angle, ϕ. For a random distribution of leaf angles this is equal to $\alpha = \frac{0.5}{\sin\phi}$. We use a homogeneous canopy with no leaf clumping and a random leaf angle distribution as these assumptions are valid for canopies at a large scale. Because we are using daily time scales, we can, for simplicity, calculate the attenuation coefficient at its maximum value for a solar angle equal to 90°. For non-directional (diffuse) radiation the attenuation coefficient can be calculated as the median value over all possible radiation angles. The median is used here rather than the mean to avoid the excessive influence of very small or very large angles.

Table A1. Comparison of leaf litterfall as predicted by the model and ground-based measurements across the Amazon basin.

Location	Measured litterfall	Predicted leaf loss	Reference
2°51′ S 54°58′ W	0.25–0.81(8.16)	0.47–0.62	Malhado et al. (2009), Doughty and Goulden (2008)
0°25′–1°30′ S, 72°30′–70°40′ W	0.24–0.55	0.03–0.11	Lips and Duivenvoorden (1996)
11°24'S 55°19′ W	0.11-1.42	0.002–0.14	Sanches et al. (2008)
4°45′–05°30′ N 60°30′–61°22′ W	0.17–0.72	0.52–0.56	Dezzeo and Chacon (2006)

A2 Soil Water Target

Soil water is widely recognised as a primary constraint in LAI, and the seasonality of LAI, in many different vegetation types around the world. For an individual tree, a greater leaf area implies a higher stomatal conductance and hence a greater potential rate of evapotranspiration. If this potential rate cannot readily be met with available soil moisture, the tree can either keep stomata open, risking excessive water loss, cavitation and hence drought death; or close the stomata, which greatly reduces water loss, but also shuts down photosynthesis and risks leaves overheating, causing permanent damage to the leaves; or the tree can reduce its total leaf area, thus allowing for individual leaves to maintain evapotranspiration and photosynthesis without excessive water use overall (McDowell et al., 2008). The first two options are short term responses to unpredictable drought, whereas losing leaves is the more sensible response to the seasonal variation in soil moisture that drives leaf phenology. Therefore, we assume that where the current LAI exceeds the water-limited LAI $\mathrm{LAI}_{\mathrm{targ}}^{\mathrm{water}}$, trees would drop leaves in order to reach $\mathrm{LAI}_{\mathrm{targ}}^{\mathrm{water}}$, starting with the oldest leaves, to produce a leaf demography that is sustainable in the long term (see main text).

Based on these assumptions, we specify a relationship between soil moisture and $\mathrm{LAI}_{\mathrm{targ}}^{\mathrm{water}}$ as:

$$\mathrm{LAI}_{\mathrm{targ}}^{\mathrm{water}} = \beta_1 + \beta_2 W_{\mathrm{s}}, \tag{A2}$$

where W_{s} is the percentage soil moisture, and β_1 and β_2 are empirical coefficients. If the current LAI is above this target, trees will drop leaves until they reach $\mathrm{LAI}_{\mathrm{targ}}^{\mathrm{water}}$.

We assume trees actively drop leaves when LAI exceeds $\mathrm{LAI}_{\mathrm{targ}}^{\mathrm{water}}$, but do not do so when LAI exceeds $\mathrm{LAI}_{\mathrm{targ}}^{\mathrm{light}}$. Where LAI exceeds $\mathrm{LAI}_{\mathrm{targ}}^{\mathrm{light}}$, the leaves receiving the least light will be below their compensation point and so be a net sink, rather than source, of carbon. However, the magnitude of this sink will be relatively small, when compared with the magnitude of the source from the leaves receiving more light. Also, trees can store substantial amounts of labile carbon, which can be used to offset short term deficits in carbon fixation. Therefore, where LAI exceeds $\mathrm{LAI}_{\mathrm{targ}}^{\mathrm{light}}$, the excess leaves are unlikely to be a cause of whole plant stress or death. In contrast, as outlined above, where LAI exceeds $\mathrm{LAI}_{\mathrm{targ}}^{\mathrm{water}}$, the lack of water affects the entire tree, and so could cause damage to all leaves, or to the whole plant through cavitation. In addition, very few trees store an amount of water that is significant in comparison to daily water use. Therefore, when LAI exceeds $\mathrm{LAI}_{\mathrm{targ}}^{\mathrm{water}}$, the excess leaves are an immediate source of danger to the whole tree.

We fit the model using the method as described in Sect. B below, using NCEP/NCAR reanalysis derived soil moisture data (Kalnay et al., 1996). The values obtained for the β_1 and β_2 parameters result in a water limited target $\mathrm{LAI}_{\mathrm{targ}}^{\mathrm{water}}$ that is higher than the light limited target $\mathrm{LAI}_{\mathrm{targ}}^{\mathrm{light}}$ at all locations throughout the year, This implies that vegetation is never water limited. As a result we set $\mathrm{LAI}_{\mathrm{targ}} = \mathrm{LAI}_{\mathrm{targ}}^{\mathrm{water}}$, which results in the model structure described in Fig. 2.

Appendix B

Parameter estimation

The model has 7 free parameters (Table 1), which we fit independently for each location, resulting in 840 parameters.

Our aim was to estimate model parameters for location $\mathbf{x}$, which we denote as the vector $\theta_{\mathbf{x}}$, given the MODIS data for location $\mathbf{x}$, which we denote $Z_{\mathbf{x}}$. To do this we used a Bayesian approach, seeking to estimate the posterior probability distribution of $\theta_{\mathbf{x}}$, given $Z_{\mathbf{x}}$, which we denote $p(\theta_{\mathbf{x}}|Z_{\mathbf{x}})$. The posterior $p(\theta_{\mathbf{x}}|Z_{\mathbf{x}})$ is proportional to the product of the likelihood $L(Z_{\mathbf{x}}|\theta_{\mathbf{x}})$, and the prior $p(\theta_{\mathbf{x}})$ such that $p(\theta_{\mathbf{x}}|Z_{\mathbf{x}}) \propto L(Z_{\mathbf{x}}|\theta_{\mathbf{x}})p(\theta_{\mathbf{x}})$. Often, $p(\theta_{\mathbf{x}}|Z_{\mathbf{x}})$ covers too large a region of parameter space to be evaluated completely. In this case we instead use sampling methods, which provide a set of random samples of $\theta_{\mathbf{x}}$ drawn from $p(\theta_{\mathbf{x}}|Z_{\mathbf{x}})$. We used a Metropolis-Hastings Markov Chain Monte Carlo (MCMC) sampling routine (Gilks, 1996.).

We define the likelihood as

$$l(Z_{\mathbf{x}}|\theta_{\mathbf{x}}) = \sum_{t(\mathbf{x})} \ln[n(\mathrm{LAI}_{\mathrm{obs}}(\mathbf{x},t), \mathrm{LAI}_{\mathrm{pred}}(\mathbf{x},t,\theta_{\mathbf{x}}), \sigma_{\mathbf{x}})] \tag{B1}$$

where $l(Z_{\mathbf{x}}|\theta_{\mathbf{x}})$ is the log-likelihood; $\mathrm{LAI}_{\mathrm{pred}}(\mathbf{x},t,\theta_{\mathbf{x}})$ is the predicted LAI at location $\mathbf{x}$ at time t (this depends on the model parameters $\theta_{\mathbf{x}}$); $\mathrm{LAI}_{\mathrm{obs}}(\mathbf{x},t)$ is the observed MODIS LAI at location $\mathbf{x}$ at time t; and $n(\mathrm{LAI}_{\mathrm{obs}}(\mathbf{x},t),$

$\mathrm{LAI}_{\mathrm{pred}}(\mathbf{x}, t, \theta_{\mathbf{x}}), \sigma_{\mathbf{x}})$ denotes the probability density for observing $\mathrm{LAI}_{\mathrm{obs}}(\mathbf{x}, t)$ given a normal distribution with mean $\mathrm{LAI}_{\mathrm{pred}}(\mathbf{x}, t, \theta_{\mathbf{x}})$ and standard deviation $\sigma_{\mathbf{x}}$ where $\sigma_{\mathbf{x}}$ is a parameter that specifies the magnitude of unexplained variation in LAI. Eq. B1 represents a loop over all times t for which observed LAI were available for location $\mathbf{x}$ (this set of times is denoted $t(\mathbf{x})$ in Eq. B1).

We initially used non-informative, uniform priors for all parameters. We assumed that, a priori, all parameter combinations were equally likely. However, we found that, with non-informative priors on all parameters, we could not properly constrain all parameters for all locations. Therefore, we assigned an informative prior on one of the parameters affecting the rate of gain and loss of leaves. We did this for one parameter only to keep the overall influence of priors to a minimum. We base our prior on an extensive study (Reich et al., 2004) of leaf lifespan (time after which all leaves are dead) in the northern Amazon. To define the prior we use the mean (2.35 years) and standard deviation (0.18 years) of these measurements. In our model, we define leaf lifespan $\tau_{95,\mathbf{x}}$ as the leaf age at which only 5 % of leaves remain alive. This is a function of three model parameters: $\mu_{0,\mathbf{x}}$, $\mu_{1,\mathbf{x}}$ and $a_{\mathrm{crit},\mathbf{x}}$. Using this prior, the posterior in the MCMC sampling becomes:

$$\ln(p(\theta_{\mathbf{x}}|Z_{\mathbf{x}})) = l(Z_{\mathbf{x}}|\theta_{\mathbf{x}}) + \ln(n(\tau_{95,\mathbf{x}}, \hat{\tau}, \sigma_{\tau})), \quad \text{(B2)}$$

where $n(\tau_{95,\mathbf{x}}, \hat{\tau}, \sigma_{\tau})$ is the probability density for $\theta_{95,\mathbf{x}}$ assuming that it is drawn from a normal distribution with mean $\hat{\tau}$ and standard deviation σ_{τ}. This measure is only proportional to the posterior because it does not take into account an integration constant. However, when using MCMC sampling this is unimportant because the constant cancels out when calculating the probability for acceptance and rejection. With this simple leaf lifespan constraint in place, we found that all parameters converged for all locations and that leaf lifespan varies substantially across the region, showing that the parameter estimates were not overly influenced by the prior (otherwise all leaf lifespans would have converged on $\hat{\tau}$). Also, parameters not directly affecting $\tau_{95,\mathbf{x}}$ were estimated to have reasonable values, implying that the model structure, MODIS data, the prior on leaf lifespan, and previous knowledge on other parameters, were all consistent with each other.

We used Metropolis-Hastings MCMC sampling (hereafter MH-MCMC) to provide a set of 600 random samples from $p(\theta_{\mathbf{x}}|Z_{\mathbf{x}})$. MH-MCMC is a widely recognised and simple, albeit computational heavy, method to provide samples from the posterior parameter distribution. MH-MCMC samples this distribution simply by proposing new parameter sets and accepting or rejecting these on the basis of their posteriors, according to a standard Metropolis criterion. Given a sufficient number of steps, the random walk reaches a quasi-equilibrium, after which the average properties of the walk (e.g. the mean and standard deviation as measured against any one parameter) no longer change. After this quasi-equilibrium has been reached, the current position of the algorithm at any one time constitutes a random sample from the posterior (Gelman, 2004). However, there is a great deal of freedom in exactly how to carry out MH-MCMC for a particular case, especially in how new parameter sets are proposed. For our analysis we used "Filzbach" [1], a previously tested and robust algorithm.

We allowed 60 000 iterations for the burn-in (the period to quasi-equilibrium), then sampled every 100 iterations from a further 60 000 total iterations, thus providing our 600 samples from $p(\theta_{\mathbf{x}}|Z_{\mathbf{x}})$. From these samples we calculated, for each parameter, the posterior mean, and 95 confidence intervals. All values reported in the paper are posterior means. We have used parameter sets drawn from this distribution to obtain LAI values (Fig. 2) and then calculate average LAI values and upper and lower 95 % confidence bounds for all values.

B1 Generating predicted LAI values

In order to both parameterize, and run simulations of, our model, it was necessary to generate predicted LAI values for each location $\mathbf{x}$ and time t, (e.g. see the likelihood defined above). Importantly, as a demographic model, our model as defined in the main text produces rates of change of the LAI held within different leaf age classes. Therefore, to produce $\mathrm{LAI}(\mathbf{x}, t, \theta_{\mathbf{x}})$ it is necessary to first, set an initial leaf age distribution, and second, simulate the model forward in time from this initial state, until we reach time t. The schematic for this is given in Fig. 2. To make our predictions for a given parameter set $\theta_{\mathbf{x}}$, we set the initial leaf age distribution as $\mathrm{LAI}(a, \mathbf{x}, t, \theta_{\mathbf{x}}) = 0$ for all a (corresponding to no leaves) then simulated the year 2000 10 times over, each time beginning the simulated year, using as the initial state the leaf age distribution from the end of the previous simulated year. This acted to spin up the model to produce a reasonable initial leaf age distribution consistent with current parameters. After the spin-up, we then simulated the model forward in time in steps of 8 days, keeping note of $\mathrm{LAI}(\mathbf{x}, t, \theta_{\mathbf{x}})$ for all t where we had observations of LAI with which to compare the predictions. Note that, although for the parameter estimation we only used the total LAI, $\mathrm{LAI}(x, t, \theta_{\mathbf{x}})$, the model can only be simulated by keeping track of the LAI within each age class, $\mathrm{LAI}(a, \mathbf{x}, t, \theta_{\mathbf{x}})$. Thus predicted leaf age distributions emerge as a natural outcome of applying our model.

[1] Filzbach, a software library for carrying out Metropolis-Hastings Markov chain Monte Carlo parameter estimation in C++ or C#. Filzbach is under development in the Computational Science lab at Microsoft Research Cambridge and is available for download, complete with a suite of example uses, via http://research.microsoft.com/en-us/groups/ecology/ecotechandtools.aspx

Appendix C

Carbon Assimilation Model

To illustrate the impact that our model results have on the carbon cycle in the Amazon, we use a simple canopy model to describe leaf photosynthesis rates. We assume that the only limitation to photosynthesis is light availability, so that carbon assimilation rates are a linear function of incoming PAR:

$$A(I) = \begin{cases} \phi I - q & , I < I_{\max} \\ A_{\max} & , I > I_{\max} \end{cases} \quad \text{(C1)}$$

where $A_{\max}$ is the maximum assimilation rate that occurs after photosynthesis reaches saturation with light for PAR levels above $I_{\max}$. We use literature values (Kubiske and Pregitzer, 1996; Riddoch et al., 1991; Langenheim et al., 1984; Miranda et al., 2005; Hutyra et al., 2007; Kitajima et al., 1997) to obtain an $A_{\max}$ of $6.12\,\mu\text{mol}\,\text{m}^{-2}\,\text{s}^{-1}$ and $I_{\max}$ equal to $150\,\mu\text{mol}\,\text{m}^{-2}\,\text{s}^{-1}$ (Hutyra et al., 2007). The values cited above have been measured for various locations, species and light environments which we have averaged to obtain a canopy scale value. We then use these values to calculate ϕ and q, by assuming that assimilation is zero at a light level equal to the compensation point C_{direct}.

We use our posterior age distributions to correct photosynthetic rates for the effects of leaf ageing. Studies have shown (Kitajima et al., 1997; Doughty and Goulden, 2008) that in tropical systems photosynthesis rates peak a few weeks after budburst and that measured rates decline with age, reaching half the peak value for leaves older than 1 year. Of course, these figures do not reflect the large variation in leaf lifespan in the Amazon. It has been observed that longer lived leaves show a slower decline in assimilation rates with age and are also slower to reach peak rates (Kitajima et al., 1997).

To account for these changes we use an age correction factor. Assuming that the values defined above are correct for mature leaves, then a population composed entirely of mature foliage will have an age factor of 1, while populations with a combination of young, mature and old leaves will have a factor less than 1. We define this factor as

$$\gamma_{\text{age}} = f_{\text{new}} A_{\text{new}} + f_{\text{mat}} A_{\text{mat}} + f_{\text{old}} A_{\text{old}}, \quad \text{(C2)}$$

where f_{new}, f_{mat} and f_{old} are the fractions of young (age$<0.07\tau_{95}$), mature and old (age$>$age$_{\min}$) leaves respectively. The corresponding adjusting factors are equal to 0.05 for young leaves, 1 for mature and 0.5 for old. We assume that the $A_{\max}$ and $I_{\max}$ values used above are valid for fully mature leaves.

Appendix D

Predicted leaf litterfall

We compare model predictions against ground-based measurements of leaf litterfall 9Table A1. This provides an evaluation of the model parameters that is independent of the LAI data used to parameterise the model. All litterfall measurements have been converted from mass units ($\text{gm}^{-2}\,\text{month}^{-1}$) to area units ($\text{m}^2\,\text{m}^{-2}\,\text{month}^{-1}$) using either the leaf mass per unit area value given by (Fyllas et al., 2009) ($94.85\,\text{gm}^{-2}$) or the specific value for that site if any is given in the study (mentioned in brackets).

Acknowledgements. This project was funded through a Microsoft Research studentship. We would like to thank the developers of the MODIS LAI product for providing the data that forms the basis for our work. We would also like to thank our colleague Prof. Roy Thompson for comments on the manuscript.

Edited by: X. Wang

References

Aragão, L., Shimabukuro, Y. E., Santo, F., and Williams, M.: Landscape pattern and spatial variability of leaf area index in Eastern Amazonia, Forest Ecol. Manag., 211, 240–256, 2005.

Aragão, L. E. O. C., Malhi, Y., Metcalfe, D. B., Silva-Espejo, J. E., Jiménez, E., Navarrete, D., Almeida, S., Costa, A. C. L., Salinas, N., Phillips, O. L., Anderson, L. O., Alvarez, E., Baker, T. R., Goncalvez, P. H., Huamán-Ovalle, J., Mamani-Solórzano, M., Meir, P., Monteagudo, A., Patiño, S., Peñuela, M. C., Prieto, A., Quesada, C. A., Rozas-Dávila, A., Rudas, A., Silva Jr., J. A., and Vásquez, R.: Above- and below-ground net primary productivity across ten Amazonian forests on contrasting soils, Biogeosciences, 6, 2759–2778, doi:10.5194/bg-6-2759-2009, 2009.

Arora, V. K. and Boer, G. J.: A parameterization of leaf phenology for the terrestrial ecosystem component of climate models, Glob. Change Biol., 11, 39–59, 2005.

Asner, G. P. and Alencar, A.: Drought impacts on the Amazon forest: the remote sensing perspective, New Phytol., 187, 569–578, doi:10.1111/j.1469-8137.2010.03310.x, http://dx.doi.org/10.1111/j.1469-8137.2010.03310.x, 2010.

Barkley, M. P., Palmer, P. I., De Smedt, I., Karl, T., Guenther, A., and Van Roozendael, M.: Regulated large-scale annual shutdown of Amazonian isoprene emissions?, Geophys. Res. Lett., 36, L04803, doi:10.1029/2008GL036843, 2009.

Bey, I., Jacob, D., Yantosca, R., Logan, J., Field, B., Fiore, A., Li, Q., Liu, H., Mickley, L., and Schultz, M.: Global modeling of tropospheric chemistry with assimilated meteorology: Model description and evaluation, J. Geophys. Res., 106, 23073–23095, 2001.

Bonal, D., Bosc, A., Ponton, S., Goret, J.-Y., Burban, B., Gross, P., Bonnefond, J.-M., Elbers, J., Longdoz, B., Epron, D., Guehl, J.-M., and Granier, A.: Impact of severe dry season on net ecosystem exchange in the Neotropical rainforest of French Guiana, Glob. Change Biol., 14, 1917–

1933, doi:10.1111/j.1365-2486.2008.01610.x, http://dx.doi.org/10.1111/j.1365-2486.2008.01610.x, 2008.

Bounoua, L., Hall, F. G., Sellers, P. J., Kumar, A., Collatz, G. J., Tucker, C. J., and Imhoff, M. L.: Quantifying the negative feedback of vegetation to greenhouse warming: A modeling approach, Geophys. Res. Lett., 37, L23701, http://dx.doi.org/10.1029/2010GL045338, 2010.

Brando, P. M., Goetz, S. J., Baccini, A., Nepstad, D. C., Beck, P. S. A., and Christman, M. C.: Seasonal and interannual variability of climate and vegetation indices across the Amazon, Proceedings of the National Academy of Sciences, 107, 14 685–14 690, doi:10.1073/pnas.0908741107, http://www.pnas.org/content/107/33/14685.abstract, 2010.

Chave, J., Navarrete, D., Almeida, S., Álvarez, E., Aragão, L. E. O. C., Bonal, D., Châtelet, P., Silva-Espejo, J. E., Goret, J.-Y., von Hildebrand, P., Jiménez, E., Patiño, S., Peñuela, M. C., Phillips, O. L., Stevenson, P., and Malhi, Y.: Regional and seasonal patterns of litterfall in tropical South America, Biogeosciences, 7, 43–55, doi:10.5194/bg-7-43-2010, 2010.

Cohen, W. B., Maiersperger, T. K., Turner, D. P., Ritts, W. D., Pflugmacher, D., Kennedy, R. E., Kirschbaum, A., Running, S. W., Costa, M., and Gower, S. T.: MODIS land cover and LAI collection 4 product quality across nine sites in the western hemisphere, IEEE T. Geosci. Remote., 44, 1843–1857, 2006.

Cramer, W., Bondeau, A., Woodward, F., Prentice, I., Betts, R., Brovkin, V., Cox, P., Fisher, V., Foley, J., Friend, A., Kucharik, C., Lomas, M., Ramankutty, N., Sitch, S., Smith, B., White, A., and Young-Molling, C.: Global response of terrestrial ecosystem structure and function to CO_2 and climate change: results from six dynamic global vegetation models, Glob. Change. Biol., 7, 357–373, 2001.

da Rocha, H. R., Goulden, M. L., Miller, S. D., Menton, M. C., Pinto, L., de Freitas, H. C., and Figueira, A.: Seasonality of water and heat fluxes over a tropical forest in eastern Amazonia, Ecol. Appl., 14, S22–S32, 2004.

Dezzeo, N. and Chacon, N.: Litterfall and nutrient input in undisturbed and adjacent fire disturbed forests of the Gran Sabana, Southern Venezuela, Interciencia, 31, 894–899, 2006.

Doughty, C. E. and Goulden, M. L.: Seasonal patterns of tropical forest leaf area index and CO_2 exchange, J. Geophys. Res., 113, doi:10.1029/2007JG000590, 2008.

Fyllas, N. M., Patiño, S., Baker, T. R., Bielefeld Nardoto, G., Martinelli, L. A., Quesada, C. A., Paiva, R., Schwarz, M., Horna, V., Mercado, L. M., Santos, A., Arroyo, L., Jiménez, E. M., Luizão, F. J., Neill, D. A., Silva, N., Prieto, A., Rudas, A., Silviera, M., Vieira, I. C. G., Lopez-Gonzalez, G., Malhi, Y., Phillips, O. L., and Lloyd, J.: Basin-wide variations in foliar properties of Amazonian forest: phylogeny, soils and climate, Biogeosciences, 6, 2677–2708, doi:10.5194/bg-6-2677-2009, 2009.

Gelman, A.: Bayesian data analysis, Texts in statistical science, Chapman & Hall, Boca Raton; London, 2 Edn., 2004.

Gilks, W. R.: Markov chain Monte Carlo in practice, edited by: Gilks, W. R., Richardson, S., and Spiegelhalter, D. J., 1996.

Goulden, M. L., Miller, S. D., da Rocha, H. R., Menton, M. C., de Freitas, H. C., Figueira, A., and de Sousa, C. A. D.: Diel and seasonal patterns of tropical forest CO_2 exchange, Ecol. Appl., 14, S42–S54, 2004.

Graham, E. A., Mulkey, S. S., Kitajima, K., Phillips, N. G., and Wright, S. J.: Cloud cover limits net CO_2 uptake and growth of a rainforest tree during tropical rainy seasons, Proc. Natl. Acad. Sci., 100, 572–576, doi:10.1073/pnas.0133045100, http://www.pnas.org/content/100/2/572.abstract, 2003.

Harper, A. B., Denning, A. S., Baker, I. T., Branson, M. D., Prihodko, L., and Randall, D. A.: Role of deep soil moisture in modulating climate in the Amazon rainforest, Geophys. Res. Lett., 37, L05802, 2010.

Hayden, B. P.: Ecosystem feedbacks on climate at the landscape scale, Philos. T. R. Soc. Lond., 353, 5–18, doi:10.1098/rstb.1998.0186, http://rstb.royalsocietypublishing.org/content/353/1365/5.abs%tract, 1998.

Hijmans, R., Cameron, S., Parra, J., Jones, P., and Jarvis, A.: Very high resolution interpolated climate surfaces for global land areas, Int. J. Climatol., 25, 1965–1978, 2005.

Huete, A. R., Didan, K., Shimabukuro, Y. E., Ratana, P., Saleska, S. R., Hutyra, L. R., Yang, W. Z., Nemani, R. R., and Myneni, R.: Amazon rainforests green-up with sunlight in dry season, Geophys. Res. Lett., 33, doi:10.1029/2005GL025583, 2006.

Hutyra, L. R., Munger, J. W., Saleska, S. R., Gottlieb, E., Daube, B. C., Dunn, A. L., Amaral, D. F., de Camargo, P. B., and Wofsy, S. C.: Seasonal controls on the exchange of carbon and water in an Amazonian rain forest, J. Geophys. Res.-Biogeo., 112, doi:10.1029/2006JG000365, 2007.

Jipp, P. H., Nepstad, D. C., Cassel, D. K., and Reis De Carvalho, C.: Deep Soil Moisture Storage and Transpiration in Forests and Pastures of Seasonally-Dry Amazonia, Climatic Change, 39, 395–412, http://dx.doi.org/10.1023/A:1005308930871, doi:10.1023/A:1005308930871, 1998.

Kalnay, E., Kanamitsu, M., Kistler, R., Collins, W., Deaven, D., Gandin, L., Iredell, M., Saha, S., White, G., Woollen, J., Zhu, Y., Chelliah, M., Ebisuzaki, W., Higgins, W., Janowiak, J., Mo, K., Ropelewski, C., Wang, J., Leetmaa, A., Reynolds, R., Jenne, R., and Joseph, D.: The NCEP/NCAR 40-year reanalysis project, Bull. Am. Meteorol. Soc., 77, 437–471, 1996.

Kitajima, K., Mulkey, S., and Wright, S.: Decline of photosynthetic capacity with leaf age in relation to leaf longevities for five tropical canopy tree species, Am. J. Botan., 84, 702–708, 1997.

Knyazikhin, Y., Miessen, G., Panfyorov, O., and Gravenhorst, G.: Small-scale study of three-dimensional distribution of photosynthetically active radiation in a forest, Agr. Forest Meteorol., 88, 215–239, 1997.

Knyazikhin, Y., J., G., Privette, J. L., Tian, Y., Lotsch, A., Zhang., Y., Wang, Y., Morisette, J. T., P.Votava, Myneni, R., Nemani, R. R., and Running, S. W.: MODIS Leaf Area Index (LAI) and Fraction of Photosynthetically Active Radiation Absorbed by Vegetation (FPAR) Product (MOD15) Algorithm Theoretical Basis Document, http://eospso.gsfc.nasa.gov/atbd/modistables, 1999.

Korner, C. and Basler, D.: Phenology Under Global Warming, Science, 327, 1461–1462, doi:10.1126/science.1186473, http://www.sciencemag.org, 2010.

Kubiske, M. and Pregitzer, K.: Effects of elevated CO_2 and light availability on the photosynthetic light response of trees of contrasting shade tolerance, Tree Physiol., 16, 351–358, 1996.

Langenheim, J., Osmond, C., Brooks, A., and Ferrar, P.: Photosynthetic responses to light in seedlings of selected Amazonian and Australian rainforest tree species, Oecologia, 63, 215–224, 1984.

Lips, J. M. and Duivenvoorden, J. F.: Fine litter input to terrestrial humus forms in Colombian amazonia, Oecologia, 108, 138–150,

1996.

Malhado, A. C. M., Costa, M. H., de Lima, F. Z., Portilho, K. C., and Figueiredo, D. N.: Seasonal leaf dynamics in an Amazonian tropical forest, Forest Ecol. Manag., 258, 1161–1165, 2009.

Malhi, Y. and Grace, J.: Tropical forests and atmospheric carbon dioxide, Trends Ecol Evol, 15, 332–337, doi:10.1016/S0169-5347(00)01906-6, http://www.sciencedirect.com/science/article/B6VJ1-40RSGFC-K/%2/4d3875b9b3882ec9d060a675b016ff41, 2000.

Malhi, Y., Nobre, A. D., Grace, J., Kruijt, B., Pereira, M. G. P., Culf, A., and Scott, S.: Carbon dioxide transfer over a Central Amazonian rain forest, J. Geophys. Res., 103, 31593–31612, http://dx.doi.org/10.1029/98JD02647, 1998.

McDowell, N., Pockman, W. T., Allen, C. D., Breshears, D. D., Cobb, N., Kolb, T., Plaut, J., Sperry, J., West, A., Williams, D. G., and Yepez, E. A.: Mechanisms of plant survival and mortality during drought: why do some plants survive while others succumb to drought?, New Phytol., 178, 719–739, doi:10.1111/j.1469-8137.2008.02436.x, http://dx.doi.org/10.1111/j.1469-8137.2008.02436.x, 2008.

Meir, P., Grace, J., and Miranda, A. C.: Photographic method to measure the vertical distribution of leaf area density in forests, Agricultural and Forest Meteorology, 102, 105–111, doi:10.1016/S0168-1923(00)00122-2, http://www.sciencedirect.com/science/article/B6V8W-4007P2P-3/%2/a926c21c4ceb866d3ee12536a4df4869, 2000.

Miranda, E., Vourlitis, G., Priante, N., Priante, P., Campelo, J., Suli, G., Fritzen, C., Lobo, F., and Shiraiwa, S.: Seasonal variation in the leaf gas exchange of tropical forest trees in the rain forest-savanna transition of the southern Amazon Basin, J. Trop. Ecol., 21, 451–460, doi:10.1017/S0266467405002427, 2005.

Myneni, R. B., Yang, W. Z., Nemani, R. R., Huete, A. R., Dickinson, R. E., Knyazikhin, Y., Didan, K., Fu, R., Juarez, R. I. N., Saatchi, S. S., Hashimoto, H., Ichii, K., Shabanov, N. V., Tan, B., Ratana, P., Privette, J. L., Morisette, J. T., Vermote, E. F., Roy, D. P., Wolfe, R. E., Friedl, M. A., Running, S. W., Votava, P., El-Saleous, N., Devadiga, S., Su, Y., and Salomonson, V. V.: Large seasonal swings in leaf area of Amazon rainforests, Proc. Natl. Acad. Sci. USA, 104, 4820–4823, 2007.

Nepstad, D. C., de Carvalho, C. R., Davidson, E. A., Jipp, P. H., Lefebvre, P. A., Negreiros, G. H., da Silva, E. D., Stone, T. A., Trumbore, S. E., and Vieira, S.: The role of deep roots in the hydrological and carbon cycles of Amazonian forests and pastures, Nature, 372, 666–669, http://dx.doi.org/10.1038/372666a0, 1994.

Osada, N., Takeda, H., Furukawa, A., and Awang, M.: Leaf Dynamics and Maintenance of Tree Crowns in a Malaysian Rain Forest Stand, J. Ecol., 89, 774–782, http://www.jstor.org/stable/3072151, 2001.

Phillips, O. L., Aragão, L. E. O. C., Lewis, S. L., Fisher, J. B., Lloyd, J., Lopez-Gonzalez, G., Malhi, Y., Monteagudo, A., Peacock, J., Quesada, C. A., van der Heijden, G., Almeida, S., Amaral, I., Arroyo, L., Aymard, G., Baker, T. R., Banki, O., Blanc, L., Bonal, D., Brando, P., Chave, J., de Oliveira, A. C. A., Cardozo, N. D., Czimczik, C. I., Feldpausch, T. R., Freitas, M. A., Gloor, E., Higuchi, N., Jimenez, E., Lloyd, G., Meir, P., Mendoza, C., Morel, A., Neill, D. A., Nepstad, D., Patino, S., Penuela, M. C., Prieto, A., Ramirez, F., Schwarz, M., Silva, J., Silveira, M., Thomas, A. S., Steege, H. t., Stropp, J., Vasquez, R., Zelazowski, P., Davila, E. A., Andelman, S., Andrade, A., Chao, K.-J., Erwin, T., Di Fiore, A., C, E. H., Keeling, H., Killeen, T. J., Laurance, W. F., Cruz, A. P., Pitman, N. C. A., Vargas, P. N., Ramirez-Angulo, H., Rudas, A., Salamao, R., Silva, N., Terborgh, J., and Torres-Lezama, A.: Drought Sensitivity of the Amazon Rainforest, Science, 323, 1344–1347, 2009.

Reich, P. B., Uhl, C., Walters, M. B., Prugh, L., and Ellsworth, D. S.: Leaf demography and phenology in Amazonian rain forest: A census of 40 000 leaves of 23 tree species, Ecol. Monogr., 74, 3–23, 2004.

Riddoch, I., Lehto, T., and Grace, J.: Photosynthesis of Tropical Tree Seedlings in Relation to Light and Nutrient Supply, New Phytol, 119, 137–147, http://www.jstor.org/stable/2557718, 1991.

Roberts, J., Cabral, O., Costa, J., da, P., McWilliam, A.-L., Sa', T., and de, A.: Amazonian Deforestation and Climate, chap. An overview of the leaf area index and physiological measurements during ABRACOS, 287–306, John Wiley & Sons, Chichester, 1996.

Saleska, S. R., Didan, K., Huete, A. R., and da Rocha, H. R.: Amazon forests green-up during 2005 drought, Science, 318, 612–612, 2007.

Samanta, A., Ganguly, S., Hashimoto, H., Devadiga, S., Vermote, E., Knyazikhin, Y., Nemani, R. R., and Myneni, R. B.: Amazon forests did not green-up during the 2005 drought, Geophys. Res. Lett., 37, L05401, doi:10.1029/2009GL042154, 2010.

Samanta, A., Knyazikhin, Y., Xu, L., Dickinson, R. E., Fu, R., Costa, M. H., Saatchi, S. S., Nemani, R. R., and Myneni, R. B.: Seasonal changes in leaf area of Amazon forests from leaf flushing and abscission, J. Geophys. Res., 117, G01015, http://dx.doi.org/10.1029/2011JG001818, 2012.

Sanches, L., Valentini, C. M. A., JÃºnior, O. B. P., Nogueira, J. d. S., Vourlitis, G. L., Biudes, M. S., da Silva, C. J., Bambi, P., and Lobo, F. d. A.: Seasonal and interannual litter dynamics of a tropical semideciduous forest of the southern Amazon Basin, Brazil, J. Geophys. Res., 113, doi:10.1029/2007JG000593, 2008.

Schwartz, M. D.: Advancing to full bloom: planning phenological research for the 21st century, Int. J. Biometeorol., 42, 113–118, 1999.

Sharpe, J.: Leaf growth and demography of the rheophytic fern Thelypteris angustifolia (Willdenow) Proctor in a Puerto Rican rainforest, Plant. Ecol., 130, 203–212, 1997.

Sombroek, W.: Spatial and temporal patterns of Amazon rainfall – Consequences for the planning of agricultural occupation and the protection of primary forests, Ambio, 30, 388–396, 2001.

Sombroek, W., Fearnside, P., and Cravo, M.: Geographic assessment of carbon stored in Amazonian terrestrial ecosystems and their soils in particular, in: Global Climate Change and Tropical Ecosystems, edited by Lal, R and Kimble, JM and Stewart, BA, 375–389, CRC PRESS-TAYLOR & FRANCIS GROUP, Boca Raton, 2000.

White, M. A., Running, S. W., and Thornton, P. E.: The impact of growing-season length variability on carbon assimilation and evapotranspiration over 88 years in the eastern US deciduous forest, Int. J. Biometeorol., 42, 139–145, http://dx.doi.org/10.1007/s004840050097, doi:10.1007/s004840050097, 1999.

Wilson, K. B. and Baldocchi, D. D.: Seasonal and interannual variability of energy fluxes over a broadleaved temperate deciduous forest in North America, Agr. Forest Meteo-

rol., 100, 1–18, doi:10.1016/S0168-1923(99)00088-X, http://www.sciencedirect.com/science/article/B6V8W-3Y9G9YN-1/%2/a64d3b46065d636190187ce3df2a333a, 2000.

Wright, S. J. and Vanschaik, C. P.: Light and the Phenology of Tropical Trees, Am. Nat., 143, 192–199, 1994.

Yang, W. Z., Tan, B., Huang, D., Rautiainen, M., Shabanov, N. V., Wang, Y., Privette, J. L., Huemmrich, K. F., Fensholt, R., Sandholt, I., Weiss, M., Ahl, D. E., Gower, S. T., Nemani, R. R., Knyazikhin, Y., and Myneni, R. B.: MODIS leaf area index products: From validation to algorithm improvement, IEEE T. Geosci. Remote., 44, 1885–1898, 2006.

References

Aide, T.M. (1992). Dry season leaf production: An escape from herbivory. *Biotropica*, **24**, pp. 532–537.

Aono, Y. and Kazui, K. (2008). Phenological data series of cherry tree flowering in Kyoto, Japan, and its application to reconstruction of springtime temperatures since the 9th century. *International Journal of Climatology*, **28**, 905–914.

Aragao, L., Shimabukuro, Y.E., Santo, F. and Williams, M. (2005). Landscape pattern and spatial variability of leaf area index in Eastern Amazonia. *Forest Ecology and Management*, **211**, 240–256.

Aragao, L., Malhi, Y., Metcalfe, D.B., Silva-Espejo, J.E., Jimenez, E., Navarrete, D., Almeida, S., Costa, A.C.L., Salinas, N., Phillips, O.L., Anderson, L.O., Alvarez, E., Baker, T.R., Goncalvez, P.H., Huaman-Ovalle, J., Mamani-Solorzano, M., Meir, P., Monteagudo, A., Patino, S., Penuela, M.C., Prieto, A., Quesada, C.A., Rozas-Davila, A., Rudas, A., Silva, J.A. and Vasquez, R. (2009). Above- and below-ground net primary productivity across ten Amazonian forests on contrasting soils. *Biogeosciences*, **6**, 2759–2778.

Arain, M.A., Yuan, F. and Black, T.A. (2006). Soilplant nitrogen cycling modulated carbon exchanges in a western temperate conifer forest in canada. *Agricultural and Forest Meteorology*, **140**, 171 – 192, ¡ce:title¿The Fluxnet-Canada Research Network: Influence of Climate and Disturbance on Carbon Cycling in Forests and Peatlands¡/ce:title¿.

Arora, V.K. and Boer, G.J. (2005). A parameterization of leaf phenology for the terrestrial ecosystem component of climate models. *Global Change BIiology*, **11**, 39–59.

Asner, G.P. and Alencar, A. (2010). Drought impacts on the Amazon forest: the remote sensing perspective. *New Phytologist*, **187**, 569–578.

Asner, G.P., Scurlock, J.M.O. and A. Hicke, J. (2003). Global synthesis of leaf area index observations: implications for ecological and remote sensing studies. *Global Ecology and Biogeography*, **12**, 191–205.

Baldocchi, D., Falge, E., Gu, L., Olson, R., Hollinger, D., Running, S., Anthoni, P., Bernhofer, C., Davis, K.J., Evans, R., Fuentes, J., Goldstein, A., Katul, G., Law, B.E., Lee, Z., Malhi, Y., Meyers, T., Munger, J.W., Oechel, W., Paw U, K.T., Pilegaard, K., Schmid, H.P., Valentini, R., Verma, S., Vesala, T., Wilson, K.B. and Wofsy, S. (2001). FLUXNET: a new tool to study the temporal and spatial variability of ecosystem-scale carbon dioxide, water vapor, and energy flux densities. *Bulletin of the American Meteorological Society*, **82**, 2415–2434.

Baldocchi, D.D. and Wilson, K.B. (2001). Modeling CO_2 and water vapor exchange of a temperate broadleaved forest across hourly to decadal time scales. *Ecological Modelling*, **142**, 155 – 184.

Baret, F. and Guyot, G. (1991). Potentials and limits of vegetation indices for LAI and APAR assessment. *Remote Sensing of Environment*, **35**, 161 – 173.

Barkley, M.P., Palmer, P.I., De Smedt, I., Karl, T., Guenther, A. and Van Roozendael, M. (2009). Regulated large-scale annual shutdown of Amazonian isoprene emissions? *Geophysical Research Letters*, **36**.

Bauerle, W.L., Oren, R., Way, D.A., Qian, S.S., Stoy, P.C., Thornton, P.E., Bowden, J.D., Hoffman, F.M. and Reynolds, R.F. (2012). Photoperiodic regulation of the seasonal pattern of photosynthetic capacity and the implications for carbon cycling. *Proceedings of the National Academy of Sciences*.

Beck, P.S.A., Atzberger, C., Hogda, K.A., Johansen, B. and Skidmore, A.K. (2006). Improved monitoring of vegetation dynamics at very high latitudes: A new method using MODIS NDVI. *Remote Sensing of Environment*, **100**, 321–334.

Beuker, E. (1994). Adaptation to climatic changes of the timing of bud burst in populations of Pinus sylvestris L. and Picea abies (l.) Karst. *Tree Physiology*, **14**, 961–970.

Beven, K. and Freer, J. (2001). Equifinality, data assimilation, and uncertainty estimation in mechanistic modelling of complex environmental systems using the GLUE methodology. *Journal of Hydrology*, **249**, 11 – 29.

Bey, I., Jacob, D., Yantosca, R., Logan, J., Field, B., Fiore, A., Li, Q., Liu, H., Mickley, L. and Schultz, M. (2001). Global modeling of tropospheric chemistry with assimilated meteorology: Model description and evaluation. *Journal of Geophysical Research*, **106**, 23073–23095.

Bonal, D., Bosc, A., Ponton, S., Goret, J.Y., Burban, B., Gross, P., Bonnefond, J.M., Elbers, J., Longdoz, B., Epron, D., Guehl, J.M. and Granier, A. (2008). Impact of severe dry season on net ecosystem exchange in the neotropical rainforest of french guiana. *Global Change Biology*, **14**, 1917–1933.

Borchert, R. (1994). Soil and stem water storage determine phenology and distribution of tropical dry forest trees. *Ecology*, **75**, pp. 1437–1449.

Bounoua, L., Hall, F.G., Sellers, P.J., Kumar, A., Collatz, G.J., Tucker, C.J. and Imhoff, M.L. (2010). Quantifying the negative feedback of vegetation to greenhouse warming: A modeling approach. *Geophysical Research Letters*, **37**, L23701–.

Brando, P.M., Goetz, S.J., Baccini, A., Nepstad, D.C., Beck, P.S.A. and Christman, M.C. (2010). Seasonal and interannual variability of climate and vegetation indices across the Amazon. *Proceedings of the National Academy of Sciences*, **107**, 14685–14690.

Braswell, B.H., Sacks, W.J., Linder, E. and Schimel, D.S. (2005). Estimating diurnal to annual ecosystem parameters by synthesis of a carbon flux model with eddy covariance net ecosystem exchange observations. *Global Change Biology*, **11**, 335–355.

Brock, T.D. (1981). Calculating solar radiation for ecological studies. *Ecological Modelling*, **14**, 1 – 19.

Bustamante, M.M.C., Medina, E., Asner, G.P., Nardoto, G.B. and Garcia-Montiel, D.C. (2006). Nitrogen cycling in tropical and temperate savannas. In L.A. Martinelli and R.W. Howarth, eds., *Nitrogen Cycling in the Americas: Natural and Anthropogenic Influences and Controls*, 209–237, Springer Netherlands.

Caldararu, S., Palmer, P.I. and Purves, D.W. (2012). Inferring Amazon leaf demography from satellite observations of leaf area index. *Biogeosciences*, **9**, 1389–1404.

Caldararu, S., Palmer, P.I. and Purves, D.W. (2013). A global phenology model based on a carbon benefit approach. *Global Change Biology, Under review*.

Canadell, J., Ciais, P., Cox, P. and Heimann, M. (2004). Quantifying, understanding and managing the carbon cycle in the next decades. *Climatic Change*, **67**, 147–160.

Chave, J., Navarrete, D., Almeida, S., Alvarez, E., Aragao, L., Bonal, D., Chatelet, P., Silva-Espejo, J.E., Goret, J.Y., von Hildebrand, P., Jimenez, E., Patino, S., Penuela, M.C., Phillips, O.L., Stevenson, P. and Malhi, Y. (2010). Regional and seasonal patterns of litterfall in tropical South America. *Biogeosciences*, **7**, 43–55.

Chen, J., Menges, C. and Leblanc, S. (2005). Global mapping of foliage clumping index using multi-angular satellite data. *Remote Sensing of Environment*, **97**, 447 – 457.

Chen, J.M. and Cihlar, J. (1996). Retrieving leaf area index of boreal conifer forests using Landsat TM images. *Remote Sensing of Environment*, **55**, 153–162.

Chen, J.M., Rich, P.M., Gower, S.T., Norman, J.M. and Plummer, S. (1997). Leaf area index of boreal forests: Theory, techniques, and measurements. *Journal of Geophysical Research-Atmospheres*, **102**, 29429–29443.

Chen, J.M., Mo, G., Pisek, J., Liu, J., Deng, F., Ishizawa, M. and Chan, D. (2012). Effects of foliage clumping on the estimation of global terrestrial gross primary productivity. *Global Biogeochem. Cycles*, **26**, GB1019–.

Cheng-Hsuan, L., Kanamitsu, M., Roads, J.O., Ebisuzaki, W., Mitchell, K.E. and Lohmann, D. (2005). Evaluation of soil moisture in the ncep?ncar and ncep?doe global reanalyses. *Journal of Hydrometeorology*, **6**, 391 – 408.

Chmielewski, F..M.c.b. (2008). The International Phenological Gardens in Europe.

Chuine, I. (2000). A unified model for budburst of trees. *Journal of Theoretical Biology*, **207**, 337 – 347.

Chuine, I. and Cour, P. (1999). Climatic determinants of budburst seasonality in four temperate-zone tree species. *New Phytologist*, **143**, pp. 339–349.

Clark, D.B., Mercado, L.M., Sitch, S., Jones, C.D., Gedney, N., Best, M.J., Pryor, M., Rooney, G.G., Essery, R.L.H., Blyth, E., Boucher, O., Harding, R.J., Huntingford, C. and Cox, P.M. (2011). The joint uk land environment simulator (jules), model description - part 2: Carbon fluxes and vegetation dynamics. *Geoscientific Model Development*, **4**, 701–722.

Clark, J.E. (1936). The history of British phenology. *Quarterly Journal of the Royal Meteorological Society*, **62**, 19–24.

Clevers, J. (1989). Application of a weighted infrared-red vegetation index for estimating leaf area index by correcting for soil moisture. *Remote Sensing of Environment*, **29**, 25 – 37.

Cohen, W.B., Maiersperger, T.K., Turner, D.P., Ritts, W.D., Pflugmacher, D., Kennedy, R.E., Kirschbaum, A., Running, S.W., Costa, M. and Gower, S.T. (2006). MODIS land cover and LAI collection 4 product quality across nine sites in the western hemisphere. *IEEE T Geosci Remote*, **44**, 1843–1857.

Cramer, W., Bondeau, A., Woodward, F., Prentice, I., Betts, R., Brovkin, V., Cox, P., Fisher, V., Foley, J., Friend, A., Kucharik, C., Lomas, M., Ramankutty, N., Sitch, S., Smith, B., White, A. and Young-Molling, C. (2001). Global response of terrestrial ecosystem structure and function to CO_2 and climate

change: results from six dynamic global vegetation models. *Global Change Biology*, **7**, 357–373.

Crimmins, M.A. and Crimmins, T.M. (2008). Monitoring plant phenology using digital repeat photography. *Environmental management*, **41**, 949–958.

da Rocha, H.R., Goulden, M.L., Miller, S.D., Menton, M.C., Pinto, L., de Freitas, H.C. and Figueira, A. (2004). Seasonality of water and heat fluxes over a tropical forest in eastern Amazonia. *Ecological Applications*, **14**, S22–S32.

Daley, R. (1993.). Atmospheric data analysis.

Defila, C. and Clot, B. (2001). Phytophenological trends in Switzerland. *International Journal of Biometeorology*, **45**, 203–207, 10.1007/s004840100101.

dePury, D.G.G. and Farquhar, G.D. (1997). Simple scaling of photosynthesis from leaves to canopies without the errors of big-leaf models. *Plant Cell and Environment*, **20**, 537–557.

Dezzeo, N. and Chacon, N. (2006). Litterfall and nutrient input in undisturbed and adjacent fire disturbed forests of the Gran Sabana, Southern Venezuela. *Interciencia*, **31**, 894–899.

Doughty, C.E. and Goulden, M.L. (2008). Seasonal patterns of tropical forest leaf area index and CO_2 exchange. *Journal of Geophysical Research*, **113**.

El Maayar, M., Price, D.T., Black, T.A., Humphreys, E.R. and Jork, E. (2002). Sensitivity tests of the integrated biosphere simulator to soil and vegetation characteristics in a pacific coastal coniferous forest. *Atmosphere-Ocean*, **40**, 313–332.

Elser, J.J., Bracken, M.E., Cleland, E.E., Gruner, D.S., Harpole, W.S., Hillebrand, H., Ngai, J.T., Seabloom, E.W., Shurin, J.B. and Smith, J.E. (2007). Global analysis of nitrogen and phosphorus limitation of primary producers in freshwater, marine and terrestrial ecosystems. *Ecology Letters*, **10**, 1135–1142.

Farquhar, G.D., Caemmerer, S. and Berry, J.A. (1980). A biochemical model of photosynthetic CO_2 assimilation in leaves of c_3 species. *Planta*, **149**, 78–90, 10.1007/BF00386231.

Fischer, A. (1994). A model for the seasonal variations of vegetation indices in coarse resolution data and its inversion to extract crop parameters. *Remote Sensing of Environment*, **48**, 220 – 230.

Fisher, J.B., Badgley, G. and Blyth, E. (2012). Global nutrient limitation in terrestrial vegetation. *Global Biogeochem. Cycles*, **26**, GB3007–.

Fox, A., Williams, M., Richardson, A.D., Cameron, D., Gove, J.H., Quaife, T., Ricciuto, D., Reichstein, M., Tomelleri, E., Trudinger, C.M. and Wijk, M.T.V. (2009). The REFLEX project: Comparing different algorithms and implementations for the inversion of a terrestrial ecosystem model against eddy covariance data. *Agricultural and Forest Meteorology*, **149**, 1597 – 1615.

Friend, A.D., Arneth, A., Kiang, N.Y., Lomas, M., Ogée, J., Rödenbeck, C., Running, S.W., Santaren, J.d., Sitch, S., Viovy, N., Ian Woodward, F. and Zaehle, S. (2007). FLUXNET and modelling the global carbon cycle. *Global Change Biology*, **13**, 610–633.

Fyllas, N.M., Patino, S., Baker, T.R., Nardoto, G.B., Martinelli, L.A., Quesada, C.A., Paiva, R., Schwarz, M., Horna, V., Mercado, L.M., Santos, A., Arroyo, L., Jimenez, E.M., Luizao, F.J., Neill, D.A., Silva, N., Prieto, A., Rudas, A., Silviera, M., Vieira, I.C.G., Lopez-Gonzalez, G., Malhi, Y., Phillips, O.L. and Lloyd, J. (2009). Basin-wide variations in foliar properties of Amazonian forest: phylogeny, soils and climate. *Biogeosciences*, **6**, 2677–2708.

Gao, X., Huete, A.R., Ni, W. and Miura, T. (2000). Optical-biophysical relationships of vegetation spectra without background contamination. *Remote Sensing of Environment*, **74**, 609 – 620.

Gelfand, A.E. and Smith, A.F.M. (1990). Sampling-based approaches to calculating marginal densities. *Journal of the American Statistical Association*, **85**, 398–409.

Gelman, A. (2004). *Bayesian data analysis*. Texts in statistical science, Chapman & Hall, Boca Raton ; London, 2nd edn.

Gelman, A. and Rubin, D.B. (1992). Inference from iterative simulation using multiple sequences. *Statistical Science*, **7**, pp. 457–472.

Geman, S. and Geman, D. (1984). Stochastic relaxation, Gibbs distributions, and the Bayesian restoration of images. *Pattern Analysis and Machine Intelligence, IEEE Transactions on*, **PAMI-6**, 721 –741.

Gilks, W.R. (1996.). Markov chain Monte Carlo in practice edited by W.R. Gilks, S. Richardson and D.J. Spiegelhalter.

Goetz, S.J. and Prince, S.D. (1996). Remote sensing of net primary production in boreal forest stands. *Agricultural and Forest Meteorology*, **78**, 149–179.

Goulden, M.L., Miller, S.D., da Rocha, H.R., Menton, M.C., de Freitas, H.C., Figueira, A. and de Sousa, C.A.D. (2004). Diel and seasonal patterns of tropical forest CO_2 exchange. *Ecological Applications*, **14**, S42–S54.

Goward, S.N., Tucker, C.J. and Dye, D.G. (1985). North American vegetation patterns observed with the NOAA-7 advanced very high resolution radiometer. *Plant Ecology*, **64**, 3–14, 10.1007/BF00033449.

Graham, E.A., Mulkey, S.S., Kitajima, K., Phillips, N.G. and Wright, S.J. (2003). Cloud cover limits net CO_2 uptake and growth of a rainforest tree during tropical rainy seasons. *Proceedings of the National Academy of Sciences*, **100**, 572–576.

Grant, R., Barr, A., Black, T., Margolis, H., Dunn, A., Metsaranta, J., Wang, S., McCaughey, J. and Bourque, C. (2009). Interannual variation in net ecosystem productivity of canadian forests as affected by regional weather patterns a fluxnet-canada synthesis. *Agricultural and Forest Meteorology*, **149**, 2022 – 2039, ¡ce:title¿Special Section on Water and Carbon Dynamics in Selected Ecosystems in China¡/ce:title¿.

Gu, L., Post, W.M., Baldocchi, D., Andy Black, T., Verma, S.B., Vesala, T. and Wofsy, S.C. (2003). Phenology of vegetation photosynthesis. In M.D. Schwartz, H. Lieth and A. Kratochwil, eds., *Phenology: An Integrative Environmental Science*, vol. 39 of *Tasks for vegetation science 34*, 467–485, Springer Netherlands.

Guenther, A., Hewitt, C.N., Erickson, D., Fall, R., Geron, C., Graedel, T., Harley, P., Klinger, L., Lerdau, M., McKay, W.A., Pierce, T., Scholes, B., Steinbrecher, R., Tallamraju, R., Taylor, J. and Zimmerman, P. (1995). A global-model of natural volatile organic-compound emissions. *Journal of Geophysical Research-Atmospheres*, **100**, 8873–8892.

Guisan, A. and Thuiller, W. (2005). Predicting species distribution: offering more than simple habitat models. *Ecology Letters*, **8**, 993–1009.

Hanninen, H. (1990). Modelling bud dormancy release in trees from cool and temperate regions. *Acta Forestalia Fennica*, **213**, 1–47.

Hänninen, H., Häkkinen, R., Hari, P. and Koski, V. (1990). Timing of growth cessation in relation to climatic adaptation of northern woody plants. *Tree Physiology*, **6**, 29–39.

Hanson, P.J., Amthor, J.S., Wullschleger, S.D., Wilson, K.B., Grant, R.F., Hartley, A., Hui, D., Hunt, E.R., Jr, Johnson, D.W., Kimball, J.S., King, A.W., Luo, Y., McNulty, S.G., Sun, G., Thornton, P.E., Wang, S., Williams, M., Baldocchi, D.D. and Cushman, R.M. (2004). Oak forest carbon and water simulations: Model intercomparisons and evaluations against independent data. *Ecological Monographs*, **74**, 443–489.

Harper, A.B., Denning, A.S., Baker, I.T., Branson, M.D., Prihodko, L. and Randall, D.A. (2010). Role of deep soil moisture in modulating climate in the Amazon rainforest. *Geophysical Research Letters*, **37**, L05802.

Hastings, W.K. (1970). Monte Carlo sampling methods using Markov chains and their applications. *Biometrika*, **57**, 97–109.

Haxeltine, A. and Prentice, I.C. (1996a). Biome3: An equilibrium terrestrial biosphere model based on ecophysiological constraints, resource availability, and competition among plant functional types. *Global Biogeochem. Cycles*, **10**, 693–709.

Haxeltine, A. and Prentice, I.C. (1996b). A general model for the light-use efficiency of primary production. *Functional Ecology*, **10**, pp. 551–561.

Haxeltine, A., Prentice, I.C. and Creswell, D.I. (1996). A coupled carbon and water flux model to predict vegetation structure. *Journal of Vegetation Science*, **7**, 651–666.

Hayden, B.P. (1998). Ecosystem feedbacks on climate at the landscape scale. *Philosophical Transactions of the Royal Society of London. Series B: Biological Sciences*, **353**, 5–18.

Hijmans, R., Cameron, S., Parra, J., Jones, P. and Jarvis, A. (2005). Very high resolution interpolated climate surfaces for global land areas. *International Journal of Climatology*, **25**, 1965–1978.

Hikosaka, K. (2003). A model of dynamics of leaves and nitrogen in a plant canopy: An integration of canopy photosynthesis, leaf life span, and nitrogen use efficiency. *The American Naturalist*, **162**, pp. 149–164.

Hogg, E., Price, D. and Black, T. (2000). Postulated feedbacks of deciduous forest phenology on seasonal climate patterns in the western Canadian interior. *Journal of Climate*, **13**, 4229.

Holben, B., Kimes, D. and Fraser, R.S. (1986). Directional reflectance response in AVHRR red and near-IR bands for three cover types and varying atmospheric conditions. *Remote Sensing of Environment*, **19**, 213 – 236.

Holben, B.N. (1986). Characteristics of maximum-value composite images from temporal AVHRR data. *International Journal of Remote Sensing*, **7**, 1417–1434.

Hooper, D.U. and Johnson, L. (1999). Nitrogen limitation in dryland ecosystems: Responses to geographical and temporal variation in precipitation. *Biogeochemistry*, **46**, 247–293, 10.1007/BF01007582.

Hovis, W.A., Jr., Blaine, L.R. and Forman, M.L. (1970). Infrared reflectance of high altitude clouds. *Applied Optics*, **9**, 561–563.

Huemmrich, K.F., Black, T.A., Jarvis, P.G., McCaughey, J.H. and Hall, F.G. (1999). High temporal resolution NDVI phenology from micrometeorological radiation sensors. *Journal of Geophysical Research*, **104**, 27935–27944.

Huete, A. (1988). A soil-adjusted vegetation index (SAVI). *Remote Sensing of Environment*, **25**, 295 – 309.

Huete, A., Liu, H. and van Leeuwen, W. (1997). The use of vegetation indices in forested regions: issues of linearity and saturation. In *Geoscience and Remote Sensing, 1997. IGARSS '97. Remote Sensing - A Scientific Vision for Sustainable Development., 1997 IEEE International*, vol. 4, 1966 –1968 vol.4.

Huete, A., Didan, K., Miura, T., Rodriguez, E., Gao, X. and Ferreira, L. (2002). Overview of the radiometric and biophysical performance of the MODIS vegetation indices. *Remote Sensing of Environment*, **83**, 195 – 213.

Huete, A.R., Didan, K., Shimabukuro, Y.E., Ratana, P., Saleska, S.R., Hutyra, L.R., Yang, W.Z., Nemani, R.R. and Myneni, R. (2006). Amazon rainforests green-up with sunlight in dry season. *Geophysical Research Letters*, **33**.

Hutyra, L.R., Munger, J.W., Saleska, S.R., Gottlieb, E., Daube, B.C., Dunn, A.L., Amaral, D.F., de Camargo, P.B. and Wofsy, S.C. (2007). Seasonal controls on the exchange of carbon and water in an Amazonian rain forest. *Journal of Geophysical Research - Biogeosciences*, **112**.

IPCC (2001a). Climate change 2001 the scientific basis: contribution of Working Group I to the third assessment report of the Intergovernmental Panel on Climate Change.

IPCC (2001b). Contribution of Working Group II to the third assessment report of the Intergovernmental Panel on Climate Change. In J. McCarthy, O. Canziani, N. Leary, D. Dokken and K. White, eds., *Climate Change 2001: Impacts, Adaptations, and Vulnerability*, 1032, Cambridge University Press, New York.

Jackson, R.D. (1983). Spectral indices in N-space. *Remote Sensing of Environment*, **13**, 409 – 421.

Jain, A.K. and Yang, X. (2005). Modeling the effects of two different land cover change data sets on the carbon stocks of plants and soils in concert with CO_2 and climate change. *Global Biogeochem. Cycles*, **19**, GB2015–.

Jipp, P.H., Nepstad, D.C., Cassel, D.K. and Reis De Carvalho, C. (1998). Deep soil moisture storage and transpiration in forests and pastures of seasonally-dry Amazonia. *Climatic Change*, **39**, 395–412, 10.1023/A:1005308930871.

Jolly, W.M., Nemani, R. and Running, S.W. (2004). Enhancement of understory productivity by asynchronous phenology with overstory competitors in a temperate deciduous forest. *Tree Physiology*, **24**, 1069–1071.

Jones, M., Bay, C. and Nordenhall, U. (1997). Effects of experimental warming on arctic willows (Salix spp.): a comparison of responses from the Canadian High Arctic, Alaskan Arctic, and Swedish Subarctic. *Global Change Biology*, **3**, 55–60.

Ju, W., Chen, J.M., Black, T.A., Barr, A.G., Liu, J. and Chen, B. (2006). Modelling multi-year coupled carbon and water fluxes in a boreal aspen forest. *Agricultural and Forest Meteorology*, **140**, 136 – 151.

Justice, C., Vermote, E., Townshend, J., Defries, R., Roy, D., Hall, D., Salomonson, V., Privette, J., Riggs, G., Strahler, A., Lucht, W., Myneni, R., Knyazikhin, Y., Running, S., Nemani, R., Wan, Z., Huete, A., van Leeuwen, W., Wolfe, R., Giglio, L., Muller, J., Lewis, P. and Barnsley, M. (1998). The Moderate Resolution Imaging Spectroradiometer (MODIS): Land remote sensing for global change research. *IEEE TRANSACTIONS ON GEOSCIENCE AND REMOTE SENSING*, **36**, 1228–1249.

Kalnay, E., Kanamitsu, M., Kistler, R., Collins, W., Deaven, D., Gandin, L., Iredell, M., Saha, S., White, G., Woollen, J., Zhu, Y., Chelliah, M., Ebisuzaki, W., Higgins, W., Janowiak, J., Mo, K., Ropelewski, C., Wang, J., Leetmaa, A., Reynolds, R., Jenne, R. and Joseph, D. (1996). The NCEP/NCAR 40-year reanalysis project. *Bulletin of the American meteorological society*, **77**, 437–471.

Kanamitsu, M., Lu, C.H., Schemm, J. and Ebisuzaki, W. (2003). The predictability of soil moisture and near-surface temperature in hindcasts of the ncep seasonal forecast model. *J. Climate*, **16**, 510–521.

Kaufman, Y. and Tanre, D. (1992). Atmospherically resistant vegetation index (ARVI) for EOS-MODIS. *Geoscience and Remote Sensing, IEEE Transactions on*, **30**, 261 –270.

Keenan, T., Baker, I., Barr, A., Ciais, P., Davis, K., Dietze, M., Dragoni, D., Gough, C.M., Grant, R., Hollinger, D., Hufkens, K., Poulter, B., McCaughey, H., Raczka, B., Ryu, Y., Schaefer, K., Tian, H., Verbeeck, H., Zhao, M. and Richardson, A.D. (2012). Terrestrial biosphere model performance for inter-annual variability of land-atmosphere CO_2 exchange. *Global Change Biology*, **18**, 1971–1987.

Keskitalo, J., Bergquist, G., Gardestrm, P. and Jansson, S. (2005). A cellular timetable of autumn senescence. *Plant Physiology*, **139**, 1635–1648.

Kikuzawa, K. (1995). Leaf phenology as an optimal strategy for carbon gain in plants. *Canadian Journal of Botany-Revue Canadienne De Botanique*, **73**, 158–163.

Kilpelainen, A., Peltola, H., Rouvinen, I. and Kellomaki, S. (2006). Dynamics of daily height growth in Scots pine trees at elevated temperature and CO_2. *Trees*, **20**, 16–27.

Kirkpatrick, S., Gelatt, C.D. and Vecchi, M.P. (1983). Optimization by simulated annealing. *Science*, **220**, 671–680.

Kitajima, K., Mulkey, S. and Wright, S. (1997). Decline of photosynthetic capacity with leaf age in relation to leaf longevities for five tropical canopy tree species. *American Journal of Botany*, **84**, 702–708.

Klein, A.G., Hall, D.K. and Riggs, G.A. (1998). Improving snow cover mapping in forests through the use of a canopy reflectance model. *Hydrological Processes*, **12**, 1723–1744.

Kljun, N., Black, T., Griffis, T., Barr, A., Gaumont-Guay, D., Morgenstern, K., McCaughey, J. and Nesic, Z. (2006). Response of net ecosystem productivity of three boreal forest stands to drought. *Ecosystems*, **9**, 1128–1144.

Knorr, W., Kaminski, T., Scholze, M., Gobron, N., Pinty, B., Giering, R. and Mathieu, P.P. (2010). Carbon cycle data assimilation with a generic phenology model. *Journal of Geophysical Research*, **115**, G04017–.

Knyazikhin, Y., Miessen, G., Panfyorov, O. and Gravenhorst, G. (1997). Small-scale study of three-dimensional distribution of photosynthetically active radiation in a forest. *Agricultural and Forest Meteorology*, **88**, 215–239.

Knyazikhin, Y., J., G., Privette, J.L., Tian, Y., Lotsch, A., Zhang., Y., Wang, Y., Morisette, J.T., P.Votava, Myneni, R., Nemani, R.R. and Running, S.W. (1999). MODIS leaf area index (LAI) and fraction of photosynthetically active radiation absorbed by vegetation (FPAR) product (MOD15) algorithm theoretical basis document. *http://eospso.gsfc.nasa.gov/atbd/modistables*.

Korner, C. and Basler, D. (2010). Phenology Under Global Warming. *Science*, **327**, 1461–1462.

Kramer, K. (1994). Selecting a model to predict the onset of growth of Fagus sylvatica. *Journal of Applied Ecology*, **31**, pp. 172–181.

Krinner, G., Viovy, N., de Noblet-Ducoudr, N., Oge, J., Polcher, J., Friedlingstein, P., Ciais, P., Sitch, S. and Prentice, I.C. (2005). A dynamic global vegetation model for studies of the coupled atmosphere-biosphere system. *Global Biogeochem. Cycles*, **19**, GB1015–.

Kubiske, M. and Pregitzer, K. (1996). Effects of elevated CO_2 and light availability on the photosynthetic light response of trees of contrasting shade tolerance. *Tree Physiology*, **16**, 351–358.

Kucharik, C.J., Foley, J.A., Delire, C., Fisher, V.A., Coe, M.T., Lenters, J.D., Young-Molling, C., Ramankutty, N., Norman, J.M. and Gower, S.T. (2000). Testing the performance of a dynamic global ecosystem model: Water balance, carbon balance, and vegetation structure. *Global Biogeochem. Cycles*, **14**, 795–825.

Langenheim, J., Osmond, C., Brooks, A. and Ferrar, P. (1984). Photosynthetic responses to light in seedlings of selected Amazonian and Australian rainforest tree species. *Oecologia*, **63**, 215–224.

Lieberman, D. and Lieberman, M. (1984). The causes and consequences of synchronous flushing in a dry tropical forest. *Biotropica*, **16**, pp. 193–201.

Linkosalo, T. (2000). Mutual regularity of spring phenology of some boreal tree species: predicting with other species and phenological models. *Canadian Journal of Forest Research-Revue Canadienne De Recherche Forestiere*, **30**, 667–673.

Lips, J.M. and Duivenvoorden, J.F. (1996). Fine litter input to terrestrial humus forms in Colombian Amazonia. *Oecologia*, **108**, 138–150.

Liu, H.Q. and Huete, A. (1995). A feedback based modification of the NDVI to minimize canopy background and atmospheric noise. *Geoscience and Remote Sensing, IEEE Transactions on*, **33**, 457 –465.

Lloyd, D. (1990). A phenological classification of terrestrial vegetation cover using shortwave vegetation index imagery. *International Journal of Remote Sensing*, **11**, 2269–2279.

Ludeke, M.K.B., Ramge, P.H. and Kohlmaier, G.H. (1996). The use of satellite NDVI data for the validation of global vegetation phenology models: Application to the Frankfurt Biosphere Model. *Ecological Modelling*, **91**, 255–270.

Malhado, A.C.M., Costa, M.H., de Lima, F.Z., Portilho, K.C. and Figueiredo, D.N. (2009). Seasonal leaf dynamics in an Amazonian tropical forest. *Forest Ecology and Management*, **258**, 1161–1165.

Malhi, Y. and Grace, J. (2000). Tropical forests and atmospheric carbon dioxide. *Trends in Ecology and Evolution*, **15**, 332 – 337.

Malhi, Y., Nobre, A.D., Grace, J., Kruijt, B., Pereira, M.G.P., Culf, A. and Scott, S. (1998). Carbon dioxide transfer over a central Amazonian rain forest. *Journal of Geophysical Research*, **103**, 31593–31612.

Margary, I.D. (1926). The Marsham phenological record in Norfolk, 1736-1925, and some others. *Quarterly Journal of the Royal Meteorological Societ*, **22**, 27–54.

Margary, I.D. (1927). The effects of weather on plant life. broadcast talk no. 1. *Quarterly Journal of the Royal Meteorological Society*, **53**, 83–86.

Marsham, R.A. (1789). Indications of spring. *Philosophical Transactions of the Royal Society*, **79**, 145–156.

Maul, G. and Sidran, M. (1972). Atmospheric effects on remote sensing of sea-surface temperature from NOAA I satellite. *Transactions-American Geophysical Union*, **53**, 399–&.

McDowell, N., Pockman, W.T., Allen, C.D., Breshears, D.D., Cobb, N., Kolb, T., Plaut, J., Sperry, J., West, A., Williams, D.G. and Yepez, E.A. (2008). Mechanisms of plant survival and mortality during drought: why do some plants survive while others succumb to drought? *New Phytologist*, **178**, 719–739.

Medvigy, D., Wofsy, S.C., Munger, J.W., Hollinger, D.Y. and Moorcroft, P.R. (2009). Mechanistic scaling of ecosystem function and dynamics in space and time: Ecosystem demography model version 2. *Journal of Geophysical Research*, **114**, G01002–.

Meir, P., Grace, J. and Miranda, A.C. (2000). Photographic method to measure the vertical distribution of leaf area density in forests. *Agricultural and Forest Meteorology*, **102**, 105 – 111.

Menzel, A. (2000). Trends in phenological phases in Europe between 1951 and 1996. *International Journal of Biometeorology*, **44**, 76–81, 10.1007/s004840000054.

Menzel, A., Sparks, T.H., Estrella, N., Koch, E., Aasa, A., Ahas, R., Alm-kbler, K., Bissolli, P., Braslavsk, O., Briede, A., Chmielewski, F.M., Crepinsek, Z., Curnel, Y., Dahl, ., Defila, C., Donnelly, A., Filella, Y., Jatczak, K., Mge, F., Mestre, A., Nordli, ., Peuelas, J., Pirinen, P., Remiov, V., Scheifinger, H., Striz, M., Susnik, A., Van Vliet, A.J.H., Wielgolaski, F.e., Zach, S. and Zust, A. (2006). European phenological response to climate change matches the warming pattern. *Global Change Biology*, **12**, 1969–1976.

Metropolis, N., Rosenbluth, A.W., Rosenbluth, M.N., Teller, A.H. and Teller, E. (1953). Equation of state calculations by fast computing machines. *J Chem Phys*, **21**, 1087–1092.

Michaelides, S., Levizzani, V., Anagnostou, E., Bauer, P., Kasparis, T. and Lane, J. (2009). Precipitation: Measurement, remote sensing, climatology and modeling. *Atmospheric Research*, **94**, 512 – 533.

Miranda, E., Vourlitis, G., Priante, N., Priante, P., Campelo, J., Suli, G., Fritzen, C., Lobo, F. and Shiraiwa, S. (2005). Seasonal variation in the leaf gas exchange of tropical forest trees in the rain forest-savanna transition of the southern Amazon Basin. *Journal of Tropical Ecology*, **21**, 451–460.

Monson, R.K., Lerdau, M.T., Sharkey, T.D., Schimel, D.S. and Fall, R. (1995). Biological aspects of constructing volatile organic-compound emission inventories. *Atmospheric Environment*, **29**, 2989–3002.

Moore, K.E., Fitzjarrald, D.R., Sakai, R.K., Goulden, M.L., Munger, J.W. and Wofsy, S.C. (1996). Seasonal variation in radiative and turbulent exchange at a deciduous forest in Central Massachusetts. *Journal of Applied Meteorology*, **35**, 122–134.

Morin, X., Roy, J., Soni, L. and Chuine, I. (2010). Changes in leaf phenology of three European oak species in response to experimental climate change. *New Phytologist*, **186**, 900–910.

Morisette, J.T., Richardson, A.D., Knapp, A.K., Fisher, J.I., Graham, E.A., Abatzoglou, J., Wilson, B.E., Breshears, D.D., Henebry, G.M., Hanes, J.M. and Liang, L. (2008). Tracking the rhythm of the seasons in the face of global change: phenological research in the 21st century. *Frontiers in Ecology and the Environment*, **7**, 253–260.

Moulin, S., Kergoat, L., Viovy, N. and Dedieu, G. (1997). Global-scale assessment of vegetation phenology using NOAA/AVHRR satellite measurements. *Journal of Climate*, **10**, 1154–1170.

Myneni, R., Maggion, S., Iaquinta, J., Privette, J., Gobron, N., Pinty, B., Kimes, D., Verstraete, M. and Williams, D. (1995a). Optical remote sensing of vegetation: Modeling, caveats, and algorithms. *Remote Sensing of Environment*, **51**, 169 – 188.

Myneni, R.B., Hall, F.G., Sellers, P.J. and Marshak, A.L. (1995b). The interpretation of spectral vegetation indexes. *IEEE T Geosci Remote*, **33**, 481–486.

Myneni, R.B., Keeling, C.D., Tucker, C.J., Asrar, G. and Nemani, R.R. (1997). Increased plant growth in the northern high latitudes from 1981 to 1991. *Nature*, **386**, 698–702.

Myneni, R.B., Yang, W.Z., Nemani, R.R., Huete, A.R., Dickinson, R.E., Knyazikhin, Y., Didan, K., Fu, R., Juarez, R.I.N., Saatchi, S.S., Hashimoto, H., Ichii, K., Shabanov, N.V., Tan, B., Ratana, P., Privette, J.L., Morisette, J.T., Vermote, E.F., Roy, D.P., Wolfe, R.E., Friedl, M.A., Running, S.W., Votava, P., El-Saleous, N., Devadiga, S., Su, Y. and Salomonson, V.V. (2007). Large seasonal swings in leaf area of Amazon rainforests. *Proc Natl Acad Sci U S A*, **104**, 4820–4823.

Nepstad, D.C., de Carvalho, C.R., Davidson, E.A., Jipp, P.H., Lefebvre, P.A., Negreiros, G.H., da Silva, E.D., Stone, T.A., Trumbore, S.E. and Vieira, S. (1994). The role of deep roots in the hydrological and carbon cycles of Amazonian forests and pastures. *Nature*, **372**, 666–669.

Norby, R.J., Hartz-Rubin, J.S. and Verbrugge, M.J. (2003). Phenological responses in maple to experimental atmospheric warming and CO_2 enrichment. *Global Change Biology*, **9**, 1792–1801.

Osada, N., Takeda, H., Furukawa, A. and Awang, M. (2001). Leaf dynamics and maintenance of tree crowns in a Malaysian rain forest stand. *Journal of Ecology*, **89**, 774–782.

Parmentier, F.J.W., van der Molen, M.K., van Huissteden, J., Karsanaev, S.A., Kononov, A.V., Suzdalov, D.A., Maximov, T.C. and Dolman, A.J. (2011). Longer growing seasons do not increase net carbon uptake in the northeastern Siberian tundra. *Journal of Geophysical Research*, **116**, G04013–.

Parmesan, C. and Yohe, G. (2003). A globally coherent fingerprint of climate change impacts across natural systems. *Nature*, **421**, 37–42.

Phillips, O.L., Aragao, L.E.O.C., Lewis, S.L., Fisher, J.B., Lloyd, J., Lopez-Gonzalez, G., Malhi, Y., Monteagudo, A., Peacock, J., Quesada, C.A., van der Heijden, G., Almeida, S., Amaral, I., Arroyo, L., Aymard, G., Baker, T.R., Banki, O., Blanc, L., Bonal, D., Brando, P., Chave, J., de Oliveira, A.C.A., Cardozo, N.D., Czimczik, C.I., Feldpausch, T.R., Freitas, M.A., Gloor, E., Higuchi, N., Jimenez, E., Lloyd, G., Meir, P., Mendoza, C., Morel, A., Neill, D.A., Nepstad, D., Patino, S., Penuela, M.C., Prieto, A., Ramirez, F., Schwarz, M., Silva, J., Silveira, M., Thomas, A.S., Steege, H.t., Stropp, J., Vasquez, R., Zelazowski, P., Davila, E.A., Andelman, S., Andrade, A., Chao, K.J., Erwin, T., Di Fiore, A., C, E.H., Keeling, H., Killeen, T.J., Laurance, W.F., Cruz, A.P., Pitman, N.C.A., Vargas, P.N., Ramirez-Angulo, H., Rudas, A., Salamao, R., Silva, N., Terborgh, J. and Torres-Lezama, A. (2009). Drought sensitivity of the Amazon rainforest. *Science*, **323**, 1344–1347.

Piao, S., Ciais, P., Friedlingstein, P., Peylin, P., Reichstein, M., Luyssaert, S., Margolis, H., Fang, J., Barr, A., Chen, A., Grelle, A., Hollinger, D.Y., Laurila, T., Lindroth, A., Richardson, A.D. and Vesala, T. (2008). Net carbon dioxide losses of northern ecosystems in response to autumn warming. *Nature*, **451**, 49–52.

Piles, M., Camps, A., Vall-llossera, M., Corbella, I., Panciera, R., Rudiger, C., Kerr, Y. and Walker, J. (2011). Downscaling SMOS-derived soil moisture using MODIS visible/infrared data. *Geoscience and Remote Sensing, IEEE Transactions on*, **49**, 3156–3166.

Pinty, B. and Verstraete, M.M. (1992). GEMI: a non-linear index to monitor global vegetation from satellites. *Plant Ecology*, **101**, 15–20, 10.1007/BF00031911.

Pisek, J., Chen, J., Miller, J., Freemantle, J., Peltoniemi, J. and Simic, A. (2010). Mapping forest background reflectance in a boreal region using multiangle compact airborne spectrographic imager data. *Geoscience and Remote Sensing, IEEE Transactions on*, **48**, 499 –510.

Prentice, I.C., Cramer, W., Harrison, S.P., Leemans, R., Monserud, R.A. and Solomon, A.M. (1992). A global biome model based on plant physiology and dominance, soil properties and climate. *Journal of Biogeography*, **19**, pp. 117–134.

Prentice, I.C., Sykes, M.T. and Cramer, W. (1993). A simulation model for the transient effects of climate change on forest landscapes. *Ecological Modelling*, **65**, 51 – 70.

Price, J. (1993). Estimating leaf area index from satellite data. *Geoscience and Remote Sensing, IEEE Transactions on*, **31**, 727–734.

Rahman, M.M., Csaplovics, E. and Koch, B. (2005). An efficient regression strategy for extracting forest biomass information from satellite sensor data. *International Journal of Remote Sensing*, **26**, 1511–1519.

Raupach, M., Rayner, P., Barrett, D., DeFries, R., Heimann, M., Ojima, D., Quegan, S. and Schmullius, C. (2005). Model-data synthesis in terrestrial carbon observation: methods, data requirements and data uncertainty specifications. *Global Change Biology*, **11**, 378 – 397.

Rautiainen, M., Heiskanen, J. and Korhonen, L. (2012). Seasonal changes in canopy leaf area index and MODIS vegetation products for a boreal forest site in central Finland. *Boreal Environment Research*, **17**, 72–84.

Reaumur, R.A.F.d. (1753). Observations du thermometre, faites a paris pendant i'annee, compares avec celles qui ont ete faites sous la ligne, a l'lsle de France, a Alger et en quelques-unes de nos isles de l'Amerique. *Mmoires de l'Acadmie des Sciences*, **545**.

Reed, B.C., Brown, J.F., VanderZee, D., Loveland, T.R., Merchant, J.W. and Ohlen, D.O. (1994). Measuring phenological variability from satellite imagery. *Journal of Vegetation Science*, **5**, 703–714.

Reich, P.B. and Borchert, R. (1982). Phenology and ecophysiology of the tropical tree, Tabebuia neochrysantha (Bignoniaceae). *Ecology*, **63**, pp. 294–299.

Reich, P.B., Uhl, C., Walters, M.B., Prugh, L. and Ellsworth, D.S. (2004). Leaf demography and phenology in Amazonian rain forest: A census of 40 000 leaves of 23 tree species. *Ecological Monographs*, **74**, 3–23.

Repo, T., Hanninen, H. and Kellomaki, S. (1996). The effects of long-term elevation of air temperature and CO_2 on the frost hardiness of Scots pine. *Plant, Cell & Environment*, **19**, 209–216.

Rich, P.M., Clark, D.B., Clark, D.A. and Oberbauer, S.F. (1993). Long-term study of solar radiation regimes in a tropical wet forest using quantum sensors and hemispherical photography. *Agricultural and Forest Meteorology*, **65**, 107 – 127.

Richardson, A., Jenkins, J., Braswell, B., Hollinger, D., Ollinger, S. and Smith, M.L. (2007). Use of digital webcam images to track spring green-up in a deciduous broadleaf forest. *Oecologia*, **152**, 323–334, 10.1007/s00442-006-0657-z.

Richardson, A.D. and OḰeefe, J. (2009). *Phenology of Ecosystem Processes: Applications in Global Change Research*, chap. Phenological Differences Between Understory and Overstory: A Case Study Using the Long-Term Harvard Forest Records, 87 –117. Springer.

Richardson, A.D., Bailey, A.S., Denny, E.G., Martin, C.W. and O'Keefe, J. (2006). Phenology of a northern hardwood forest canopy. *Global Change Biology*, **12**, 1174 – 1188.

Richardson, A.D., Hollinger, D.Y., Dail, D.B., Lee, J.T., Munger, J.W. and Okeefe, J. (2009). Influence of spring phenology on seasonal and annual carbon balance in two contrasting New England forests. *Tree Physiology*, **29**, 321–331.

Richardson, A.D., Andy Black, T., Ciais, P., Delbart, N., Friedl, M.A., Gobron, N., Hollinger, D.Y., Kutsch, W.L., Longdoz, B., Luyssaert, S., Migliavacca, M., Montagnani, L., William Munger, J., Moors, E., Piao, S., Rebmann, C., Reichstein, M., Saigusa, N., Tomelleri, E., Vargas, R. and Varlagin, A. (2010). Influence of spring and autumn phenological transitions on forest ecosystem productivity. *Philosophical Transactions of the Royal Society B: Biological Sciences*, **365**, 3227–3246.

Richardson, A.D., Anderson, R.S., Arain, M.A., Barr, A.G., Bohrer, G., Chen, G., Chen, J.M., Ciais, P., Davis, K.J., Desai, A.R., Dietze, M.C., Dragoni, D., Garrity, S.R., Gough, C.M., Grant, R., Hollinger, D.Y., Margolis, H.A., McCaughey, H., Migliavacca, M., Monson, R.K., Munger, J.W., Poulter, B., Raczka, B.M., Ricciuto, D.M., Sahoo, A.K., Schaefer, K., Tian, H., Vargas, R., Verbeeck, H., Xiao, J. and Xue, Y. (2012). Terrestrial biosphere models need better representation of vegetation phenology: results from the north American carbon program site synthesis. *Global Change Biology*, **18**, 566–584.

Richardson, A.D., Keenan, T.F., Migliavacca, M., Ryu, Y., Sonnentag, O. and Toomey, M. (2013). Climate change, phenology, and phenological control of vegetation feedbacks to the climate system. *Agricultural and Forest Meteorology*, **169**, 156 – 173.

Richey, M. (2010). The evolution of Markov Chain Monte Carlo methods. *American Mathematical Monthly*, **117**, 383–413.

Riddoch, I., Lehto, T. and Grace, J. (1991). Photosynthesis of tropical tree seedlings in relation to light and nutrient supply. *New Phytologist*, **119**, pp. 137–147.

Roberts, J., Cabral, O., Costa, J., da, P., McWilliam, A.L., Sa, T. and de, A. (1996). *Amazonian Deforestation and Climate*, chap. An overview of the leaf area index and physiological measurements during ABRACOS, 287–306. John Wiley & Sons, Chichester.

Ryu, Y., Baldocchi, D.D., Kobayashi, H., van Ingen, C., Li, J., Black, T.A., Beringer, J., van Gorsel, E., Knohl, A., Law, B.E. and Roupsard, O. (2011). Integration of MODIS land and atmosphere products with a coupled-process model to estimate gross primary productivity and evapotranspiration from 1 km to global scales. *Global Biogeochem. Cycles*, **25**, GB4017–.

Sala, O.E., III, F.S.C., Armesto, J.J., Berlow, E., Bloomfield, J., Dirzo, R., Huber-Sanwald, E., Huenneke, L.F., Jackson, R.B., Kinzig, A., Leemans, R., Lodge, D.M., Mooney, H.A., Oesterheld, M., Poff, N.L., Sykes, M.T., Walker, B.H., Walker, M. and Wall, D.H. (2000). Global biodiversity scenarios for the year 2100. *Science*, **287**, pp. 1770–1774.

Saleska, S.R., Didan, K., Huete, A.R. and da Rocha, H.R. (2007). Amazon forests green-up during 2005 drought. *Science*, **318**, 612–612.

Samanta, A., Ganguly, S., Hashimoto, H., Devadiga, S., Vermote, E., Knyazikhin, Y., Nemani, R.R. and Myneni, R.B. (2010). Amazon forests did not green-up during the 2005 drought. *Geophysical Research Letters*, **37**, L05401.

Samanta, A., Knyazikhin, Y., Xu, L., Dickinson, R.E., Fu, R., Costa, M.H., Saatchi, S.S., Nemani, R.R. and Myneni, R.B. (2012). Seasonal changes in leaf area of Amazon forests from leaf flushing and abscission. *Journal of Geophysical Research*, **117**, G01015–.

Sanches, L., Valentini, C.M.A., Jnior, O.B.P., Nogueira, J.d.S., Vourlitis, G.L., Biudes, M.S., da Silva, C.J., Bambi, P. and Lobo, F.d.A. (2008). Seasonal and interannual litter dynamics of a tropical semideciduous forest of the southern Amazon Basin, Brazil. *Journal of Geophysical Research*, **113**.

Schaefer, K., Collatz, G.J., Tans, P., Denning, A.S., Baker, I., Berry, J., Prihodko, L., Suits, N. and Philpott, A. (2008). Combined Simple Biosphere/Carnegie-Ames-Stanford Approach terrestrial carbon cycle model. *Journal of Geophysical Research*, **113**, G03034–.

Schimel, D.S., House, J.I., Hibbard, K.A., Bousquet, P., Ciais, P., Peylin, P., Braswell, B.H., Apps, M.J., Baker, D., Bondeau, A., Canadell, J., Churkina, G., Cramer, W., Denning, A.S., Field, C.B., Friedlingstein, P., Goodale, C., Heimann, M., Houghton, R.A., Melillo, J.M., Moore, B., Murdiyarso, D., Noble, I., Pacala, S.W., Prentice, I.C., Raupach, M.R., Rayner, P.J., Scholes, R.J., Steffen, W.L. and Wirth, C. (2001). Recent patterns and mechanisms of carbon exchange by terrestrial ecosystems. *Nature*, **414**, 169–172.

Schöngart, J., Piedade, M.T.F., Ludwigshausen, S., Horna, V. and Worbes, M. (2002). Phenology and stem-growth periodicity of tree species in Amazonian floodplain forests. *Journal of Tropical Ecology*, **18**, pp. 581–597.

Schwartz, M.D. (1992). Phenology and springtime surface-layer change. *Monthly Weather Review*, **120**, 2570–2578.

Schwartz, M.D. (1998). Green-wave phenology. *Nature*, **394**, 839–840.

Schwartz, M.D. (1999). Advancing to full bloom: planning phenological research for the 21st century. *International Journal of Biometeorology*, **42**, 113–118.

Sellers, P., Berry, J., Collatz, G., Field, C. and Hall, F. (1992). Canopy reflectance, photosynthesis, and transpiration. III. a reanalysis using improved leaf models and a new canopy integration scheme. *Remote Sensing of Environment*, **42**, 187 – 216.

Sellers, P.J., Mintz, Y., Sud, Y.C. and Dalcher, A. (1986). A simple biosphere model (SIB) for use within general circulation models. *J. Atmos. Sci.*, **43**, 505–531.

Sellers, P.J., Tucker, C.J., Collatz, G.J., Los, S.O., Justice, C.O., Dazlich, D.A. and Randall, D.A. (1996). A revised land surface parameterization (sib2) for atmospheric gcms. part ii: The generation of global fields of terrestrial biophysical parameters from satellite data. *J. Climate*, **9**, 706–737.

Shabanov, N.V., Zhou, L.M., Knyazikhin, Y., Myneni, R.B. and Tucker, C.J. (2002). Analysis of interannual changes in northern vegetation activity observed in AVHRR data from 1981 to 1994. *IEEE Transactions on Geoscience and Remote Sensing*, **40**, 115–130.

Shabanov, N.V., Dong, H., Wenze, Y., Tan, B., Knyazikhin, Y., Myneni, R.B., Ahl, D.E., Gower, S.T., Huete, A.R., Aragao, L.E.O.C. and Shimabukuro,

Y.E. (2005). Analysis and optimization of the MODIS leaf area index algorithm retrievals over broadleaf forests. *Geoscience and Remote Sensing, IEEE Transactions on*, **43**, 1855–1865.

Sharpe, J. (1997). Leaf growth and demography of the rheophytic fern Thelypteris angustifolia (Willdenow) Proctor in a Puerto Rican rainforest. *Plant Ecology*, **130**, 203–212.

Sherry, R.A., Zhou, X., Gu, S., Arnone, J.A., Schimel, D.S., Verburg, P.S., Wallace, L.L. and Luo, Y. (2007). Divergence of reproductive phenology under climate warming. *Proceedings of the National Academy of Sciences*, **104**, 198–202.

Sitch, S., Smith, B., Prentice, I.C., Arneth, A., Bondeau, A., Cramer, W., Kaplan, J.O., Levis, S., Lucht, W., Sykes, M.T., Thonicke, K. and Venevsky, S. (2003). Evaluation of ecosystem dynamics, plant geography and terrestrial carbon cycling in the LPJ dynamic global vegetation model. *Glob Change BIiol*, **9**, 161–185.

Smith, T.M. (1997). *Plant functional types :their relevance to ecosystem properties and global change /edited by T.M. Smith, H.H. Shugart and F.I. Woodward.*. Cambridge University Press,, Cambridge :.

Sombroek, W. (2001). Spatial and temporal patterns of Amazon rainfall - consequences for the planning of agricultural occupation and the protection of primary forests. *Ambio*, **30**, 388–396.

Sombroek, W., Fearnside, P. and Cravo, M. (2000). Geographic assessment of carbon stored in Amazonian terrestrial ecosystems and their soils in particular. In Lal, R and Kimble, JM and Stewart, BA, ed., *Global Climate Change and Tropical Ecosystems*, 375–389, CRC PRESS-TAYLOR & FRANCIS GROUP, Boca Raton.

Sparks, T.H. and Menzel, A. (2002). Observed changes in seasons: an overview. *International Journal of Climatology*, **22**, 1715–1725.

Strong, A.E. (1974). Remote sensing of algal blooms by aircraft and satellite in lake erie and utah lake. *Remote Sensing of Environment*, **3**, 99–107.

Thompson, R. and Clark, R.M. (2008). Is spring starting earlier? *Holocene*, **18**, 95–104.

Thornton, P., Law, B., Gholz, H.L., Clark, K.L., Falge, E., Ellsworth, D., Goldstein, A., Monson, R., Hollinger, D., Falk, M., Chen, J. and Sparks, J. (2002). Modeling and measuring the effects of disturbance history and climate on carbon and water budgets in evergreen needleleaf forests. *Agricultural and Forest Meteorology*, **113**, 185 – 222, ¡ce:title¿FLUXNET 2000 Synthesis¡/ce:title¿.

Tucker, C.J. (1979). Red and photographic infrared linear combinations for monitoring vegetation. *Remote Sensing of Environment*, **8**, 127 – 150.

Van Wijk, M.T., Williams, M., Laundre, J.A. and Shaver, G.R. (2003). Interannual variability of plant phenology in tussock tundra: modelling interactions of plant productivity, plant phenology, snowmelt and soil thaw. *Glob Change BIiol*, **9**, 743–758.

Van Wijk, M.T., Clemmensen, K.E., Shaver, G.R., Williams, M., Callaghan, T.V., Chapin, F.S., Cornelissen, J.H.C., Gough, L., Hobbie, S.E., Jonasson, S., Lee, J.A., Michelsen, A., Press, M.C., Richardson, S.J. and Rueth, H. (2004). Long-term ecosystem level experiments at Toolik Lake, Alaska, and at Abisko, Northern Sweden: generalizations and differences in ecosystem and plant type responses to global change. *Global Change Biology*, **10**, 105–123.

Walker, M.D., Wahren, C.H., Hollister, R.D., Henry, G.H.R., Ahlquist, L.E., Alatalo, J.M., Bret-Harte, M.S., Calef, M.P., Callaghan, T.V., Carroll, A.B., Epstein, H.E., Jnsdttir, I.S., Klein, J.A., Magnsson, B., Molau, U., Oberbauer, S.F., Rewa, S.P., Robinson, C.H., Shaver, G.R., Suding, K.N., Thompson, C.C., Tolvanen, A., Totland, ., Turner, P.L., Tweedie, C.E., Webber, P.J. and Wookey, P.A. (2006). Plant community responses to experimental warming across the tundra biome. *Proceedings of the National Academy of Sciences of the United States of America*, **103**, 1342–1346.

Weng, E. and Luo, Y. (2011). Relative information contributions of model vs. data to short- and long-term forecasts of forest carbon dynamics. *Ecological Applications*, **21**, 1490–1505.

White, G. (1789). *The Natural History and Antiquities of Selborne in the County of Southampton: with Engravings, and an Appendix*. Benjamin White & Son, London.

White, M.A., Thornton, P.E. and Running, S.W. (1997). A continental phenology model for monitoring vegetation responses to interannual climatic variability. *Global Biogeochem. Cycles*, **11**, 217–234.

White, M.A., Running, S.W. and Thornton, P.E. (1999). The impact of growing-season length variability on carbon assimilation and evapotranspiration over 88 years in the eastern us deciduous forest. *International Journal of Biometeorology*, **42**, 139–145, 10.1007/s004840050097.

Wielicki, B., Barkstrom, B., Harrison, E., Lee, R., Smith, G. and Cooper, J. (1996). Clouds and the earth's radiant energy system (CERES): An earth observing system experiment. *Bulletin of the American Meteorological Society*, **77**, 853–868.

Williams, R.J., Myers, B.A., Muller, W.J., Duff, G.A. and Eamus, D. (1997). Leaf phenology of woody species in a North Australian tropical savanna. *Ecology*, **78**, pp. 2542–2558.

Wilson, K.B. and Baldocchi, D.D. (2000). Seasonal and interannual variability of energy fluxes over a broadleaved temperate deciduous forest in North America. *Agricultural and Forest Meteorology*, **100**, 1 – 18.

Wright, S.J. and Vanschaik, C.P. (1994). Light and the phenology of tropical trees. *American Naturalist*, **143**, 192–199.

Yang, W.Z., Tan, B., Huang, D., Rautiainen, M., Shabanov, N.V., Wang, Y., Privette, J.L., Huemmrich, K.F., Fensholt, R., Sandholt, I., Weiss, M., Ahl, D.E., Gower, S.T., Nemani, R.R., Knyazikhin, Y. and Myneni, R.B. (2006). MODIS leaf area index products: From validation to algorithm improvement. *IEEE T Geosci Remote*, **44**, 1885–1898.

Yates, H.W. (1970). A general discussion of remote sensing of the atmosphere. *Applied*, **9**, 1971–1971.

Zhang, X.Y., Friedl, M.A., Schaaf, C.B., Strahler, A.H., Hodges, J.C.F., Gao, F., Reed, B.C. and Huete, A. (2003). Monitoring vegetation phenology using MODIS. *Remote Sensing of Environment*, **84**, 471–475.